TECHNICAL TRANSACTIONS
CZASOPISMO TECHNICZNE

CHEMISTRY
CHEMIA

ISSUE 1-Ch (18)
ZESZYT 1-Ch (18)

YEAR 2014 (111)
ROK 2014 (111)

WYDAWNICTWO POLITECHNIKI KRAKOWSKIEJ

TECHNICAL TRANSACTIONS | CZASOPISMO TECHNICZNE

CHEMISTRY | CHEMIA

ISSUE 1-Ch (18) | ZESZYT 1-Ch (18)
YEAR 2014 (111) | ROK 2014 (111)

Pierwotną wersją każdego Czasopisma Technicznego jest wersja on-line
www.czasopismotechniczne.pl www.technicaltransactions.com

Chemistry Series
1-Ch/2014

TECHNICAL TRANSACTIONS | CZASOPISMO TECHNICZNE
CHEMISTRY | CHEMIA
1-Ch/2014

MONIKA GWADERA*, KRZYSZTOF KUPIEC*

BATCH ADSORPTION IN A FINITE VOLUME RESERVOIR – APPLICATION OF AN APPROXIMATE KINETIC MODEL

ADSORPCJA W ZBIORNIKU O OGRANICZONEJ OBJĘTOŚCI – ZASTOSOWANIE PRZYBLIŻONEGO MODELU KINETYCZNEGO

Abstract

The paper refers to the kinetics of batch adsorption in a perfect mixing reservoir. Systems with a linear adsorption equilibrium, spherical adsorbent pellets and mass transfer resistance in both phases are considered. An approximate kinetic model, based on approximation with the use of continued fractions, was used in calculations. It was found that the model gives results consistent with the exact solution.

Keywords: *adsorption kinetics*, *approximate kinetic equations*

Streszczenie

Artykuł dotyczy kinetyki adsorpcji okresowej w zbiorniku z idealnym mieszaniem. Rozważono układy z liniową równowagą adsorpcyjną, kulistymi ziarnami adsorbentu i z oporami przenoszenia masy występującymi w obu fazach. W obliczeniach wykorzystano przybliżony model kinetyczny oparty na aproksymacji ułamkami łańcuchowymi. Stwierdzono, że model ten daje wyniki zgodne z rozwiązaniem ścisłym.

Słowa kluczowe: *kinetyka adsorpcji*, *przybliżone równania kinetyczne*

* Ph.D. Eng. Monika Gwadera; Ph.D. Eng. Krzysztof Kupiec, prof. PK, Faculty of Chemical Engineering and Technology, Cracow University of Technology.

Nomenclature

Bi – Biot number
C – adsorbate concentration in the fluid phase [kg/m^3]
D_s – solid diffusivity [m^2/s]
K – adsorption equilibrium constant
L – characteristic linear dimension (radius for a sphere) [m]
m – mass [kg]
q_m – adsorbate concentration in solid phase [kg/kg]
Q – dimensionless concentration of the adsorbate in solid phase
t – time [s]
V – volume [m^3]
Y – dimensionless adsorbate concentration in fluid phase

Greek symbols

α – adsorbent load factor
η – dimensionless space coordinate
τ – dimensionless time

Indexes

0 – initial value
1 – pellet surface
– – average value

1. Introduction

Three different methods are used in order to conduct studies on adsorption kinetics in a liquid phase [1]. These methods are presented in Fig. 1.

In the first method (Fig. 1a), adsorbent pellets are put inside a reservoir containing a solution with the adsorbate. The content of the reservoir is stirred. In the case of the second method (Fig. 1b), the adsorbent is put in a mesh basket attached to a stirrer. The stirrer is rotated and a solution with the adsorbate is introduced into the reservoir. The third method (Fig. 1c) consists of putting an amount of adsorbent into a small column connected with the reservoir that contains the adsorbate. The reservoir is connected to the column by a closed loop. The contents of the loop are circulated and flow through the bed of the adsorbent with such a speed that the adsorption time is much greater than the residence time of adsorbate in the loop. In this way, the flow rate of the solution containing the adsorbate can be controlled so that the heat of the adsorption can be effectively removed and the process can be conducted under isothermal conditions.

In all cases, the saturation of pellets goes together with a reduction of the adsorbate concentration in the solution over time. This results from the finite volume of the solution (reservoir). Hence, the driving force of the process decreases because of two factors: the decreasing concentration of adsorbate in the solution; the increasing concentration

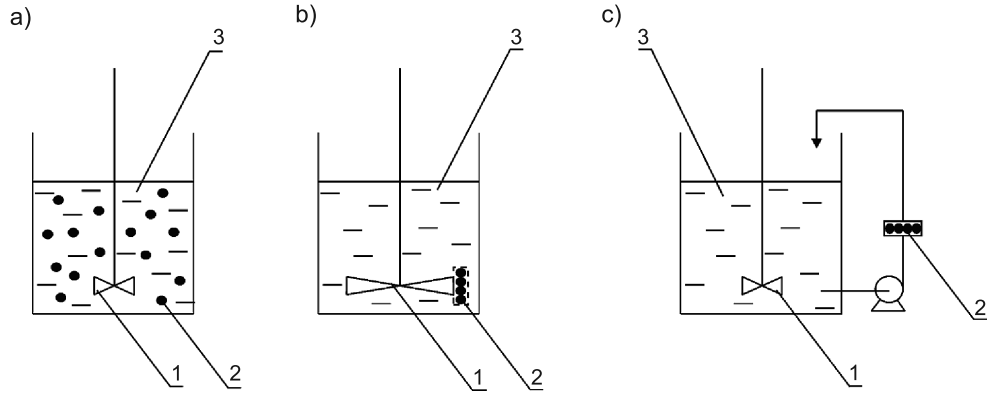

Fig. 1. Studies on adsorption kinetics: 1 – stirrer, 2 – adsorbent pellets, 3 – liquid solution containing an adsorbate

of adsorbate in the pellets. An extreme case is when the volume of the solution is infinitely large. In this case, the adsorbate concentration in the solution does not change over time.

For adsorption in a finite volume reservoir, the adsorbent load factor is the main parameter. It is defined in the following way:

$$\alpha = \frac{VC_0}{m_s q_{m0}} = \frac{V}{m_s K} \tag{1}$$

where:

- V – the volume of the solution,
- C_0 – initial concentration of the adsorbate in the solution;,
- m_s – mass of adsorbent pellets,
- q_{m0} – concentration of adsorbate in pellets in equilibrium with C_0,
- K – adsorption equilibrium constant ($= q_{m0}/C_0$).

When the solution volume is infinite, then $\alpha \to \infty$.

The aim of this work is to analyze the suitability of the application of the approximate kinetic model for adsorption in a finite volume reservoir. The results obtained on the basis of the approximate model presented in [2] and [3] were compared with the results of the exact analytical solution. Adsorption systems with linear equilibrium are considered in the paper. The presented analysis refers to spherical pellets.

2. Computation expressions

2.1. Equation of adsorption and diffusion

It is convenient to present the equation of adsorption and diffusion in the dimensionless form with the use of dimensionless quantities. The dimensionless concentration of the adsorbate in the pellet is defined in the following way:

$$Q = \frac{q_m}{q_{m0}} \tag{2}$$

The average concentration is defined analogically:

$$\bar{Q} = \frac{\bar{q}_m}{q_{m0}} \tag{3}$$

where:

$\bar{q}_m$ – concentration averaged over pellet volume.

The dimensionless space coordinate η is introduced:

$$\eta = \frac{x}{L} \tag{4}$$

and the dimensionless time τ:

$$\tau = \frac{D_s t}{L^2} \tag{5}$$

Symbol D_s in the foregoing definitions denotes solid diffusivity, and L – characteristic linear dimension (radius for a sphere). The equation of diffusion and adsorption has the form:

$$\frac{\partial Q}{\partial \tau} = \frac{\partial^2 Q}{\partial \eta^2} + \frac{2}{\eta} \cdot \frac{\partial Q}{\partial \eta} \tag{6}$$

For pellets that do not contain the adsorbate, the initial condition has the form:

$$\tau = 0, \quad Q = 0 \tag{7}$$

One of the boundary conditions refers to the symmetry of the pellet:

$$\eta = 0, \quad \frac{\partial Q}{\partial \eta} = 0 \tag{8}$$

The boundary condition for pellet surface takes the form:

$$\eta = 1, \quad \frac{\partial Q}{\partial \eta} = \mathrm{Bi}[Q_1^* - Q_1] \tag{9}$$

The value of Q_1^* is the solid dimensionless adsorbate concentration in equilibrium with the actual bulk concentration in liquid phase, Q_1 is a dimensionless concentration on the pellet surface, and Bi – Biot number.

2.2. Adsorbate balance in the fluid phase

When the reservoir with fluid and adsorbent pellets has finite volume, concentration of adsorbate in the solution changes during adsorption. Not only a balance equation for the adsorbate in solid phase, but also a balance equation in fluid phase should be taken into account in the model of the process. The equation has the form:

$$\frac{dY}{d\tau} = -\frac{1}{\alpha} \cdot \frac{d\bar{Q}}{d\tau} \tag{10}$$

where the dimensionless concentration in the fluid phase is defined in the following way:

$$Y = \frac{C}{C_0} \tag{11}$$

The initial condition for the fluid phase:

$$\tau = 0, \quad Y = 1 \tag{12}$$

The solution to equation (10) with initial conditions (7) and (12) have the form:

$$\alpha(1 - Y) = \bar{Q} \tag{13}$$

For $\tau \to \infty$, the concentrations of adsorbate in the pellet and the fluid are in equilibrium. According to the definition of dimensionless concentration, the following relationship is valid for linear equilibrium:

$$Q^* = Y \tag{14}$$

It results from equations (13) and (14) that:

$$\lim_{\tau \to \infty} Y = \lim_{\tau \to \infty} \bar{Q} = \frac{\alpha}{1 + \alpha} \tag{15}$$

2.3. Exact kinetic model

The results of numerical calculations were compared with results obtained from the analytical solution of the system of equations (6) and (10) with conditions (7), (8), (9) and (12). In this case, the analytical solution was given by Huang and Li [4]. The expression has the form:

$$Y = 1 - \frac{1}{1 + \alpha}\left[1 - \sum_{i=1}^{\infty} \frac{6\mathrm{Bi}^2(1 + \alpha)\exp(-\mu_i^2 \tau)}{\left(\frac{9}{\alpha} + \alpha\mu_i^2 + 9\right)\mathrm{Bi}^2 - (6 + \alpha)\mu_i^2 \mathrm{Bi} + \alpha\mu_i^4}\right] \tag{16}$$

where μ_i are consecutive positive roots of the algebraic equation:

$$\frac{\tan\mu}{\mu} = \frac{3\mathrm{Bi} - \alpha\mu^2}{(\mathrm{Bi} - 1)\alpha\mu^2 + 3\mathrm{Bi}} \tag{17}$$

Values of the roots μ_i depend on the parameter α and also on the Biot number. In order to determine the location of the first few roots for different combinations of the values of α and Bi, graphs of functions y_1 and y_2 presented in Fig. 2 were plotted. These functions are defined in the following way:

$$y_1 = \tan\mu \tag{18a}$$

$$y_2 = \frac{(3\mathrm{Bi} - \alpha\mu^2)\mu}{(\mathrm{Bi} - 1)\alpha\mu^2 + 3\mathrm{Bi}} \tag{18b}$$

The graph of function y_2 depends not only on the parameter α, but also on Bi. The abscissas of the intersections of functions y_1 and y_2 correspond to the solutions of equation (17), because the equality $y_1 = y_2$ is equivalent to this equation. Values of the first six roots of equation (17) are presented in Table 1.

Table 1

Values of solutions to equation (17)

α	Bi	μ_1	μ_2	μ_3	μ_4	μ_5	μ_6
1/9	5	4.3172	7.3235	10.0032	12.3015	14.8172	17.6935
	20	4.3344	7.4383	10.4685	13.4484	16.3765	19.2553
	100	4.3385	7.4596	10.5306	13.5867	16.6374	19.6864
	∞	4.3395	7.4645	10.5437	13.6133	16.6831	19.7565
1	5	3.3499	5.6845	8.4194	11.3837	14.4323	17.5171
	20	3.6411	6.4247	9.2826	12.2069	15.1802	18.1894
	100	3.7100	6.6329	9.6322	12.6749	15.7411	18.8207
	∞	3.7264	6.6814	9.7156	12.7927	15.8924	19.0049
9	5	2.6872	5.3866	8.3144	11.3398	14.4105	17.5049
	20	3.0939	6.0318	9.0156	12.0243	15.0532	18.0992
	100	3.2116	6.2736	9.3664	12.4680	15.5733	18.6807
	∞	3.2410	6.3353	9.4599	12.5928	15.7291	18.8672

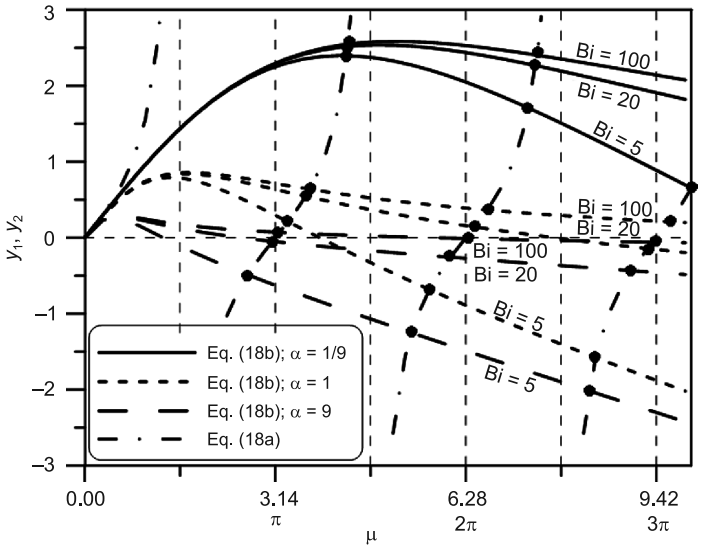

Fig. 2. Location of solutions to equation (17)

2.4. Approximate kinetic model

In order to describe transient mass (also heat) transfer, it is useful to use such an approximation that consists in elimination of a space coordinate in a body (pellet). The process is described with an ordinary differential equation and the resulting expression is called the approximate kinetic equation. The approximate model used in this paper is based on the use of the Laplace transformation for the diffusion equation, rearrangement of the solution to form a continued fraction and truncation of the obtained expression to such a number of terms that ensures the required accuracy. Such a model was presented for the first time by Lee and Kim [2] for systems without external resistance to mass transfer, and the model for systems with resistance in both phases was presented in work by the authors of this paper [3]. The considered approximate model refers to the basic shapes of pellets: infinite slab, infinite cylinder and sphere.

The main advantage of approximate kinetic equations is the fact that they are ordinary differential equations (not partial equations). This results in the reduction of the calculation time when compared to the exact calculations. This is important when a kinetic equation is solved repeatedly in a complex procedure.

In order to determine the adsorbate concentration in the pellet as a function of time with the use of the approximate kinetic equation, the following system of equations must be solved [3]:

$$\dot{\mathbf{x}} = \mathbf{d}^{-1}\mathbf{A}\mathbf{x} + \mathbf{d}^{-1}\mathbf{b}Q_1^* \tag{19}$$

where vectors $\dot{\mathbf{x}}, \mathbf{x}$ and $\mathbf{b}$ are defined in the following way:

$$\dot{\mathbf{x}} = \begin{bmatrix} \dot{x}_1 & \dot{x}_2 & \dots & \dot{x}_n \end{bmatrix}^T \tag{20}$$

$$\mathbf{x} = \begin{bmatrix} x_1 & x_2 & \dots & x_n \end{bmatrix}^T \tag{21}$$

$$\mathbf{b} = \begin{bmatrix} 3 & 3 & \dots & 3 \end{bmatrix}^T \tag{22}$$

Elements of matrix $\mathbf{A}$ are defined as:

$$A_{ij} = -p_i q_j \quad \text{for} \quad j > i \tag{23a}$$

$$A_{ij} = -p_j q_j \quad \text{for} \quad j < i \tag{23b}$$

$$A_{ij} = -p_i q_i \quad \text{for} \quad j = i \tag{23c}$$

where p_i and q_i have the forms:

$$p_i = 2i^2 + i \tag{24}$$

$$q_i = 4i + 1 \tag{25}$$

$$d_{ij} = \frac{q_j}{\mathrm{Bi}} \quad \text{for} \quad j \neq i \tag{26a}$$

$$d_{ij} = 1 + \frac{q_j}{\mathrm{Bi}} \quad \text{for} \quad j = i \tag{26b}$$

The number of equations (19) is the order of approximation; the higher the order is, the higher the accuracy of the approximation.

Average dimensionless concentration of adsorbate in an adsorbent pellet after time τ is defined by the following equation [2]:

$$\bar{Q} = \mathbf{q}\mathbf{x} \tag{27}$$

where:

$$\mathbf{q} = [q_1 \quad q_2 \quad \cdots \quad q_n] \tag{28}$$

Substituting $Q_1^* = Y$ into (19) and considering equation (13) one gets:

$$\dot{\mathbf{x}} = \mathbf{d}^{-1}\mathbf{A}\mathbf{x} + \mathbf{d}^{-1}\mathbf{b}\left(1 - \frac{\bar{Q}}{\alpha}\right) \tag{29}$$

After transformation, it was obtained that:

$$\dot{\mathbf{x}} = \mathbf{d}^{-1}\left(\mathbf{A} - \frac{1}{\alpha}\mathbf{b}\mathbf{q}\right)\mathbf{x} + \mathbf{d}^{-1}\mathbf{b} \tag{30}$$

The following initial condition is required to solve the system of equations (30):

$$\tau = 0, \quad \mathbf{x} = 0 \tag{31}$$

This condition refers to the pellet that does not contain the adsorbate at the beginning of the process. As a result of solving system (30), a vector function $\mathbf{x}(\tau)$ is obtained. On the basis of relation (27) the scalar function $\bar{Q}(\tau)$ is determined.

The algorithm was as follows. Elements of matrix **A** and vectors **b**, **q** and **d** were determined for given values of Bi and *n*. Then the system of equations (30) with initial condition (31) is solved. Finally, the function $\bar{Q}(\tau)$ was obtained from formula (27).

3. Results of calculations

Comparison of results obtained with the use of the approximate and exact kinetic models for adsorption in a finite volume reservoir with mass transfer resistance in both phases is presented in Fig. 3a, b and c. Solid lines refer to the approximate model. Dots denote values found with the use of the exact solution. The figures present results for different values of parameter α.

Concentrations in the fluid phase decrease, while in the pellets, they increase. After some time, the system reaches equilibrium and the dimensionless concentrations become equal to each other. Values of dimensionless equilibrium concentrations in both phases depend on the values of α. For instance, for Fig. 3a that refers to $\alpha = 1/9$, it is easy to calculate from formula (15) that for $\tau \to \infty$, it is $Y = \bar{Q} = \dfrac{1/9}{1+1/9} = 0.1$.

It can be seen from the figures that the greater value the Biot number has, the faster the system reaches equilibrium. It results from this fact that for a given value of diffusivity

in a pellet, a smaller value of external resistance corresponds to greater Bi. The reduction of the external resistance, while the internal one is constant, results in the decrease of the total resistance to mass transfer.

It can also be seen from these figures that the approximate model gives results very similar to the exact results. Some deviations can be observed only for a high Biot number, a low adsorbent load factor and short adsorption times.

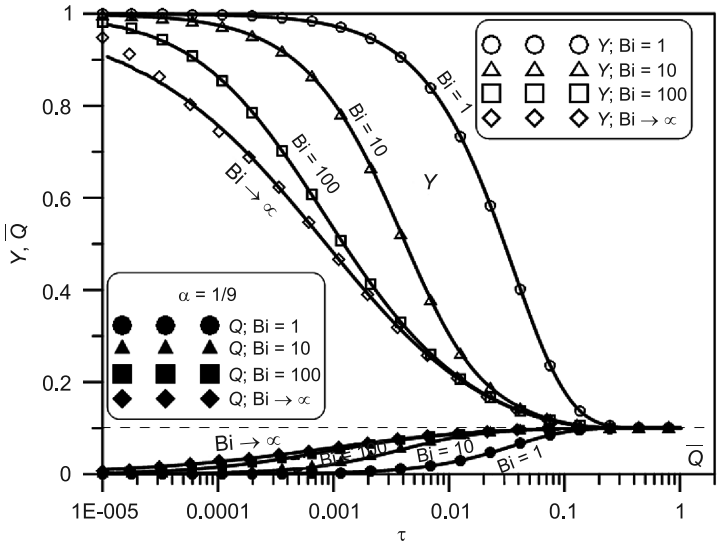

Fig. 3a. Adsorption in a finite volume reservoir for $\alpha = 1/9$

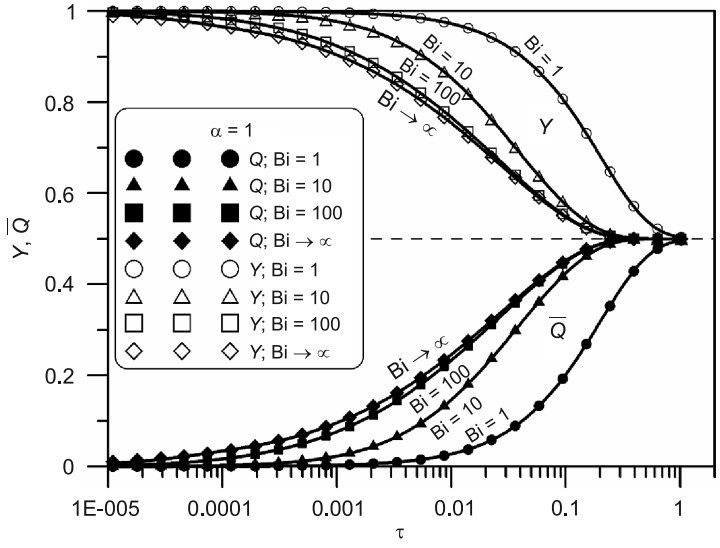

Fig. 3b. Adsorption in a finite volume reservoir for $\alpha = 1$

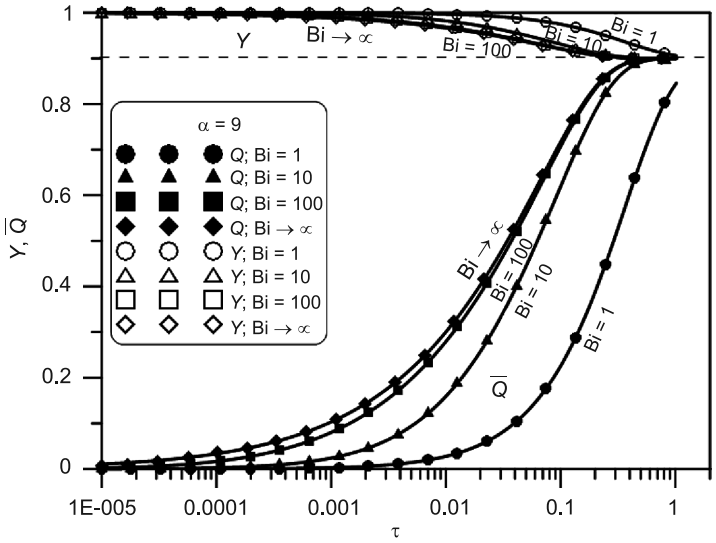

Fig. 3c. Adsorption in a finite volume reservoir for $\alpha = 9$

The agreement between values obtained on the basis of the approximate and exact models confirms that the approximate model based on the continued fractions approximation can be used in the design and modeling of batch adsorption in a reservoir.

4. Conclusions

The approximate model for adsorption kinetics based on continued fractions is much more convenient to use than exact models based on solutions in the form of an infinite series. The obtained results do not differ much from the results obtained with the use of the exact methods.

The project was funded by The National Science Centre (Poland) on the basis of the decision No. DEC-2011/03/N/ST8/04634.

References

[1] Do D.D., *Adsorption Analysis: Equilibria and Kinetics*, ICP 1998.

[2] Lee J., Kim D.H., *Simple high-order approximations for unsteady-state diffusion, adsorption and reaction in a catalyst: a unified method by a continued fraction for slab, cylinder and sphere geometries*, Chemical Engineering Journal, 173, 2011, 644-650.

[3] Kupiec K., Gwadera M., *Approximation for unsteady state diffusion and adsorption with mass transfer resistance in both phases*, Chemical Engineering and Processing, 65, 2013, 76-82.

[4] Huang T-C., Li K-Y., *Ion-exchange kinetics for calcium radiotracer in a batch system*, Industrial and Engineering Chemistry Fundamentals, 12, 1973, 50-55.
[5] Crank J., *The Mathematics of Diffusion*, Clarendon Press, Oxford, 1975.
[6] Suzuki M., *Adsorption Engineering*, Elsevier 1990.
[7] Carslaw H.S., Jaeger J.C., *Conduction of Heat in Solids*, Clarendon Press, Oxford, 1959.
[8] Petrus R. at al., *Wymiana masy w układzie ciało stałe-ciecz*, OWPR Rzeszów 1998.

TECHNICAL TRANSACTIONS | CZASOPISMO TECHNICZNE
CHEMISTRY | CHEMIA
1-Ch/2014

WITOLD JANICZEK*

A SIMPLIFIED MODEL OF THE ABSORPTIVE--REGENERATIVE PROCESS IN THE TECHNOLOGY OF NITRIC ACID PRODUCTION

UPROSZCZONY MODEL PROCESU ABSORPCYJNO--REGENERACYJNEGO W TECHNOLOGII KWASU AZOTOWEGO

Abstract

This paper presents a method of calculating the physical absorption of low concentrated gaseous nitrogen oxides in liquid nitric acid solutions. This absorption is used in the absorptive-regenerative process (AR process) to reduce the nitrogen oxide content in the exhaust gas from nitric acid plants. This method consists of the calculation of the effectiveness of the absorption in dependence on the liquid/gas ratio, the number of theoretical shelves adequate to the absorption system and other parameters of the process. The paper presents some results of calculations based on, for example, the accepted values of the initial parameters of the process. Conclusions formulated in this paper result from the calculations and concern the rational formation of the AR process as a whole and especially, the stage of regeneration.

Keywords: *nitric acid*, *nitrogen oxides*, *exhaust gas*, *physical absorption*, *regeneration*

Streszczenie

Przedstawiono sposób obliczenia procesu fizycznej absorpcji nisko stężonych tlenków azotu w wodnym roztworze kwasu azotowego, służący w tzw. procesie absorpcyjno-regeneracyjnym („proces AR") do zmniejszenia strat azotu związanego w gazie wylotowym z instalacji produkcyjnych kwasu azotowego. Sposób polega na obliczeniu wydajności absorpcji w zależności od stosunku gaz/ciecz, liczby półek teoretycznych jakim odpowiada układ absorpcyjny i pozostałych parametrów procesu. Przedstawiono wyniki obliczeń na przykładowo założonych wartościach parametrów wyjściowych. Wnioski wynikają z przedstawionych obliczeń dla racjonalnego ukształtowania procesu AR zwłaszcza dla etapu regeneracji.

Słowa kluczowe: *kwas azotowy*, *tlenki azotu*, *gaz wylotowy*, *absorpcja fizyczna*, *regeneracja*

* Doc. Ph.D. Witold Janiczek, Emeritus, Institute of Inorganic Chemistry and Technology, Faculty of Chemical Engineering and Technology, Cracow University of Technology.

1. Introduction

Under the absorptive-regenerative process (AR process) in the technology of nitric acid production, one understands a method of increasing the efficiency of nitric oxide absorption whilst at the same time, reducing losses of bound nitrogen in exhaust gases by subjecting exhaust gases to absorption in a nitric acid solution of an appropriately chosen concentration in which nitric oxides are 'physically' absorbed. The solution containing the dissolved nitric oxides then undergoes a change to a regenerative operation consisting of the removal of the dissolved nitrogen oxides (by any method), and at the same time, restoring the ability of the solution to absorb nitrogen oxides. After this, the solution returns to the absorption stage.

For the first time, the essential idea of the AR process was shown in Polish patent Nr 51804 applied in 1963 [1] and two substantially identical papers [2–3]. A wide summary of these papers was published in Brit. Chem. Eng. [4]. The scheme of the AR process idea quoted there is shown on Fig. 1.

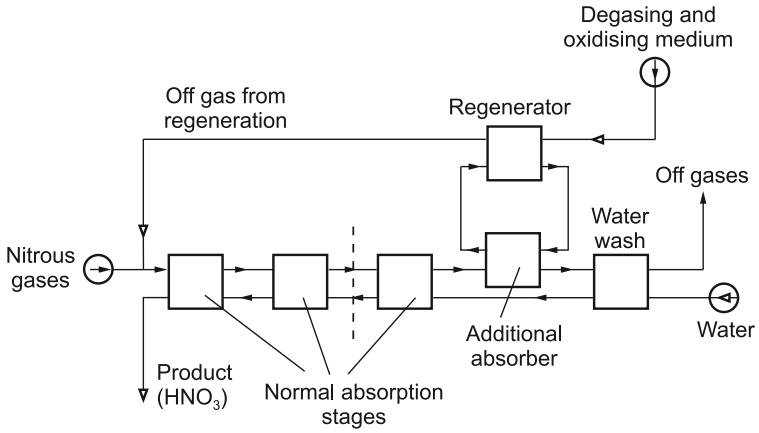

Fig. 1. Idea scheme of the AR process quoted in Brit. Chem. Eng. [18], copied from Polish papers [16, 17]. The inscriptions are replaced by English ones

In the following years, many publications and patent descriptions appeared concerning different varieties of the AR process and methods of its realization [5–21], as well some its theoretical bases [22–27].

This paper presents a simplified calculation method of the absorption stage of the AR process, the results of which seem to throw significant light on the AR process in general. The calculations are preceded by a presentation of the detailed composition of diluted nitrogen oxides standing in chemical equilibrium with a nitric acid water solution of a given concentration.

2. Detailed composition of the gas phase containing dilute nitric oxides standing in chemical equilibrium with the nitric acid solution

In the absorption stage of the AR process, the dilute nitrogen oxides are in contact with the nitric acid solution of a given concentration which is significantly higher than that occurring in the final stages of the traditional absorption process. The cause of this is that, although we call it 'physical' absorption, it is a complex process: dilute nitrogen oxides consisting mainly of NO must be oxidized at the cost of nitric acid, the absorbed NO occurs in the liquid phase mainly as NO_2, N_2O_4 or nitrous acid HNO_2.

Fig. 2 is a diagram showing the detailed composition of diluted gaseous nitrogen compounds in equilibrium with a 30% solution of nitric acid as a function of its total content (including HNO_3) in the gas phase. A similar diagram for the composition of diluted gaseous nitrogen compounds in equilibrium with a 55% HNO_3 solution is easy to calculate, but is of no real significance for further reasoning and will not be shown here.

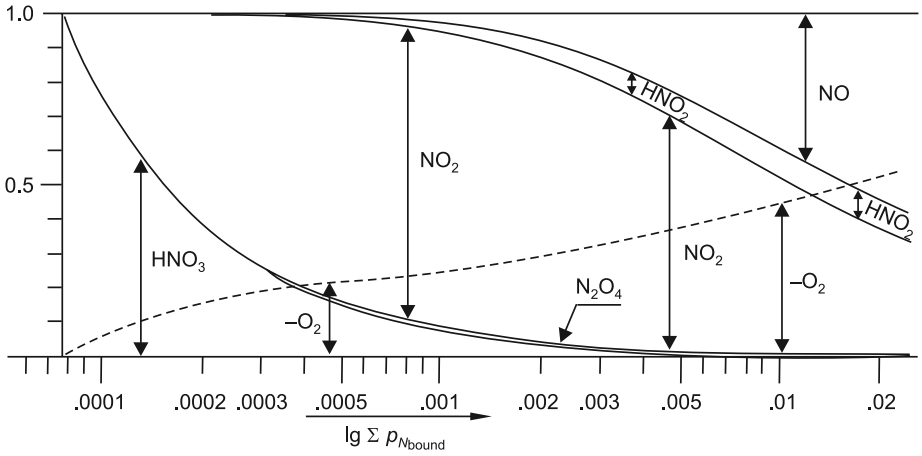

Fig. 2. Shows in a little demonstrative manner the detailed composition of diluted gaseous nitrogen oxides in equilibrium with 30% HNO_3 solution at 30°C. The sum of vapor pressures of all nitrogen compounds (including P_{HNO_3}) are marked in a logarithmic scale on the horizontal axis. Vertical distances between the curves relate to the part of a given compound in fractions of unity. The partial pressure of a given compound is received by multiplying the sum of partial vapor pressures red from the horizontal scale with its share red on the vertical scale. The broken line relates to the 'oxygen demand' that is the partial pressure of O_2 which would be needed to oxidize all nitrogen compounds to derivatives of N_2O_5

The following data was accepted for the calculations:

For reactions in the gas phase, for $T = 30°C$ (303 K), the following values of equilibrium constants were accepted:

$2\,NO \leftrightarrow N2O4$	$K_p = 5.325$	[28–29]
$NO + NO_2 \leftrightarrow N_2O_3$	$K_p = 0.394$	[30–32]

$$NO + NO_2 + H_2O \leftrightarrow 2\ HNO_2 \qquad K_P = 1.246 \qquad [33–34]$$

For the equilibrium between the gas phase and the HNO_3 solution at 30°C, the data in Table 1 was accepted.

Table 1

Concentration of the HNO_3 solution, %	30	55
Density, g/cm^3	1.18	1.339
'Partial equilibrium constant', $K_2 = (p_{NO}/(p_{NO2})^3$	30200.0	75.9
Vapor pressure of water, bars	0.03173	0.01626
Vapor pressure of HNO_3, bars	0.0000773	0.001104

The value of the K_2 constant is the subject of many publications [33, 35–42]. Considerable disagreements are caused by a difficulty to analytically distinguish between the different nitrogen compounds. A special publication is devoted to this problem [43]. Vapor pressures of H_2O and HNO_3 were taken from partially extrapolated Taylor's data [44]. A diagram of the gaseous nitrogen oxides in equilibrium with HNO_3 is shown on Fig. 2

3. Calculation of the absorption stage in the AR process

The calculations and their results presented below present some practical aspects of the 'physical' absorption of nitrogen oxides having essential significance for the reasonable design of the AR process as a whole. The calculations are based on determining the number of theoretical shelves necessary for gaining the desired effectiveness of the absorption in dependence of other parameters in the process.

The 'theoretical shelf' is a definite notion in the field of chemical engineering. It does not mean that in a filled tower to a theoretical shelf suits still one and the same segment of the filling. That depends on many process parameters, such as pressure, velocity of the gas phase, density of the liquid supply and others. Nevertheless, defining the effectiveness of the absorption as a function of the number of the theoretical shelves is sensible and it allows for a better understanding of the specifics of the process.

In the calculations, the following assumptions and dates were accepted:

Instead of converting the absorbed nitric oxides to a given nitrogen compound such as NO_2 or HNO_2, in order to determine their amount in the liquid phase, a substitute parameter was used – the demand for oxygen, expressed in the number of moles of O_2 stoichiometrically needed to oxidize all lower oxidized nitrogen compounds to a derivative of N_2O_5[1]). This parameter will be symbolized here with the letter *S*. A similar parameter for the gas phase, which is the oxygen demand for oxidizing NO and NO_2 to N_2O_5, follows from the following stoichiometric equations:

[1] In [45] appears a description of a separate determination of N_2O_3, NO_2 and HNO_2 in the liquid phase. The author proposed to the editorial of this journal a publication assuming this method as totally wrong, but the editorial replied evasively.

$$NO + 0.75\ O_2 = NO_{2.5}$$
$$NO_2 + 0.25\ O_2 = NO_{2.5}$$

From which results the oxygen demand in the gas phase symbolized here by the letter Z:

$$Z = 0.75\ NO + 0.25\ NO_2 \quad (1)$$

Evidently, the oxygen demands in both phases S and Z must be balanced within each theoretical shelf.

A scheme of balance equations of the absorption system composed of N theoretical shelves is presented in Fig. 3.

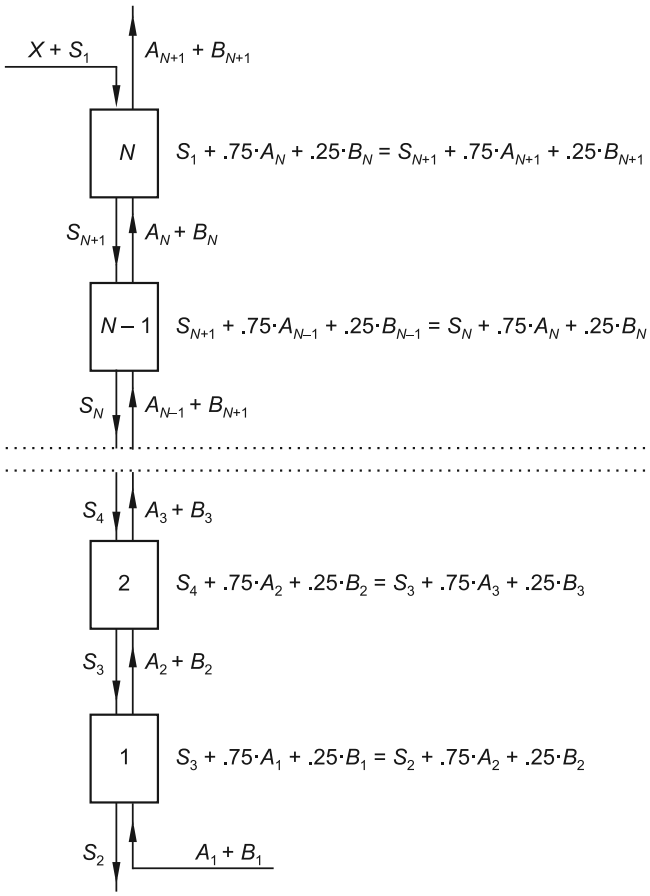

Fig. 3. Balance scheme of an absorption stage composed of N theoretical shelves. A balance equation of the 'oxygen demand' is given for each symbol of the shelf. At phases flowing from one shelf to another, the balance constituent of the phase is given. The letters have following meanings: A – the number of NO moles in the gas phase, B – the number of NO_2 moles in the gas phase, S – the oxygen demand in the liquid phase in one mole of O_2. Further comments and supplements are to be found in the text

In order to be able to use the balance of oxygen demands in both phases for calculating the absorption as a whole, they are complemented with dependencies between the oxygen demands S and Z and the NO and NO_2 contents in the gas phase A and B one rests on the following assumptions and simplifications:

1) Considering the small quantity of exchanged compounds in comparison to the size of both phases, small changes of sizes of both phases resulting from the process are neglected and their sizes remain constant. Due to the intense circulation of the nitric acid solution, its concentration in the quite absorption stage remains constant. For the same reason, the temperature in the quite system also remains constant.
2) The partial pressures p_{NO} and p_{NO_2} are agreeing with the so called 'partial equilibrium constant' of the reaction:

$$3\ NO_2 + H_2O \leftrightarrow 2HNO_3 + NO$$

$$K_2 = p_{NO}/(p_{NO_2})^3 \tag{2}$$

The value of K_2 depends on the concentration of the nitric acid solution with which the gaseous phase is in equilibrium and on the temperature.

Taking into account

$$p_{NO} = P\cdot(A/L) \text{ and } p_{NO_2} = P\cdot(B/L), \tag{3}$$

where P = total pressure and L = number of moles of the gaseous phase, one gets:

$$B = ((A \cdot L^2)/(K_2 \cdot P^2))^{1/3} \tag{4}$$

3) Between the values of S and Z exists a dependence similar to Henry's law

$$S/V_C = f \cdot Z/V_G$$

That is:

$$S = f \cdot Z \cdot (V_C/V_G). \tag{5}$$

where V_C and V_G mean the volumes of the liquid or the gas phases, and f is a proportional coefficient meaning the multiplicity of the gas phase volume to the liquid phase volume by which the oxygen demands in both phases are the same, while

$$V_C = X/d, \tag{6}$$

where X is the amount of the nitric acid solution in one kg falling for L moles of the gas phase while d is its density in g/cm^3.

The volume of the gas phase is expressed by the equation:

$$V_G = (L \cdot T \cdot 22.4)/(273 \cdot P) \tag{7}$$

where L is the number of moles in the gas phase, T is the absolute temperature and P is the total pressure.

Currently, only an approximate value of coefficient f is known. Data from paper [2], as well as an approximate extrapolation of Bode's data [46], and own unpublished fragmentary research, for T = 30°C and 30% acid, the value of f = 30 and for a 55% acid solution, the value of f = 40 was accepted. Specifying coefficient f for different temperatures and acid concentrations requires careful laboratory examination. It is assumed that the values of the coefficient f accepted here are sufficiently close to the real

values in order to show the problem of a reasonable formation of the absorption stage in the AR process.

4) As nitrogen compounds in the gas phase, only NO and NO_2 are taken into account. All other compounds, such as HNO_2, N_2O_4 etc., are considered to be composed of the two first named here and were eventually neglected.
5) All gaseous compounds behave as ideal gases.

According to the definition of the theoretical shelf, phases leaving the shelf are in mutual equilibrium. In order to avoid mistakes about the balance on Fig. 3, both phases leaving the shelf are marked with the same number. Taking into account the dependencies resulting from equations (1)–(4), (6) and (7) and putting the values to equation (5), one gets finally:

$$S = (X \cdot (f \cdot 273 \cdot P)/(d \cdot T \cdot L \cdot 22.4)) \cdot (0.75 \cdot A + 0.25 \cdot (L^2 \cdot A \cdot K_{2-1} \cdot P^{-2})^{1/3}) \quad (8)$$

Inserting equations (4) and (8) into the set of equations presented on the balance scheme on Fig. 3, the coefficient values, and other values accepted for a given account we get a set of equations, allowing the calculating at accepted of the content of nitrogen oxides in exhaust gases after the absorption stage. ($A_{N+1} + B_{N+1}$) being a function of the number of theoretical shelves corresponding to the absorber system and of the supply of nitric acid solution at a given supply of L moles inlet gas By comparing that with the initial nitrogen oxide content ($A_1 + B_1$), the efficiency of the absorption in % can be calculated.

The absorption in a system with very numerous or an unlimited number of shelves is calculated separately. In such a situation as shown in Fig. 4, the entering gas is in equilibrium with the liquid phase leaving the absorption system in accordance with equation (5):

$$S_2/V_C = f \cdot (0.75 \cdot A_1 + 0.25 \cdot B_1)/V_G \quad (9)$$

Inserting the formula for S_2 into the balance equation in Fig. 4:

$$S_2 = X \cdot (0.75 \cdot A_1 + 0.25 \cdot B_1) \cdot 273 \cdot f \cdot P/(22.4 \cdot d \cdot L \cdot T) \quad (10)$$

Observing the dependence between B_2 and A_2 according to equation (4):

$$B_2 = ((A_2 \cdot L^2)/(K_2 \cdot P^2))^{1/3} \quad (11)$$

and inserting values of terms composed of parameters which are constant in a given series of calculations:

$$G_1 = L^2/(K_2 \cdot P^2) \text{ and } G_2 = (273 \cdot f \cdot P)/(22.4 \cdot d \cdot L \cdot T) \quad (12)$$

Finally, the balance equation for an absorbing system with an unlimited number of theoretical shelves is as follows:

$$S_1 + 0.75A_1 + 0.75B_1 = X \cdot (0.75A_1 + B_1) \cdot G_2 + 0.25 \cdot (A_2 \cdot G_1)^{1/3} \quad (13)$$

In equation (13), the only unknowns (A_2, B_2) will be calculated according to A_2, indentified with equation (11). From these two items of data, one gets the content of nitrogen oxides in the gas leaving the absorption stage, whilst at the same time, the effectiveness of the process as a function of X. This is the highest permissible effectiveness which can be attained by a given liquid/gas ratio improving the absorption system.

In the calculations below, the following initial parameters and some combinations of them have been accepted:

Pressure: 1.013 respectively 7.093 bars.

Temperature: 30°C (303 K), the same in all cases.

The initial content of nitrogen oxides in the entering gas: 10 respectively 2 moles $NO + NO_2$ per 1000 moles of gas (1% respectively 0.2% vol.). In all cases it is assumed that the nitrogen oxides at the entry are exclusively in the form of NO. This is of no significance because the balance equations (see Fig. 3) are not related to the content of nitrogen oxides but to the 'oxygen demand'. The calculation with an assumed 3% NO_2 at the entry would give the same result as in the case of an assumed 1% NO. The concentration of the circulating solution of nitric acid is assumed to be constant in the whole system: 30% or 55% by weight.

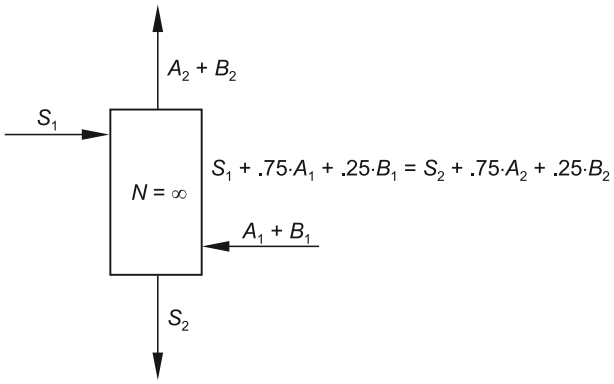

Fig. 4. Scheme of an absorption system with an unlimited number of theoretical shelves. Further explanations are presented in the text

The results of the calculations are presented below in graphic form. For better transparency and comparability, the same quantity of gas was assumed for all calculations: 1000 moles ($L = 1000$). Figs. 5–7 show concentrations of nitrogen oxides in moles $NO + NO_2$ per 1000 moles of gas leaving the absorption stage as a function of the liquid/gas ratio (X kg HNO_3 solution per 1000 moles of gas) and the number of theoretical shelves presented by the absorption system. For all three graphics, the common initial conditions are: the total pressure $P = 1.013$ bars; the inflowing gas contains nitric oxides only in form of NO ($B_1 = 0$); the HNO_3 solution given to the absorber contains no lower oxidized nitrogen compounds ($S_1 = 0$). Graphics illustrating similar dependencies under the pressure of 7.091 bars are presented in Figs. 8–12. For place saving reasons, in the graphic subscriptions the initial conditions are marked by following symbols: t: °C, P: bars; A: moles NO; B: moles NO_2; S: oxygen demand of the liquid phase in moles O_2; M: concentration of the circulating nitric acid solution in weight %% of HNO_3. Axis X stands for the liquid/gas ratio in kg HNO_3 per 1000 moles gas, axis Y stands for the number of $NO + NO_2$ moles in 1000 moles of gas leaving the absorption stage.

A review of the graphs in Figs. 5–7 justifies the following remarks and conclusions:

– The runs of curves presenting concentrations of nitrogen oxides in gases leaving the absorption stage are similar to each other in all three cases. The runs of curves for a given number of shelves (up to five), the curves for an unlimited number of shelves

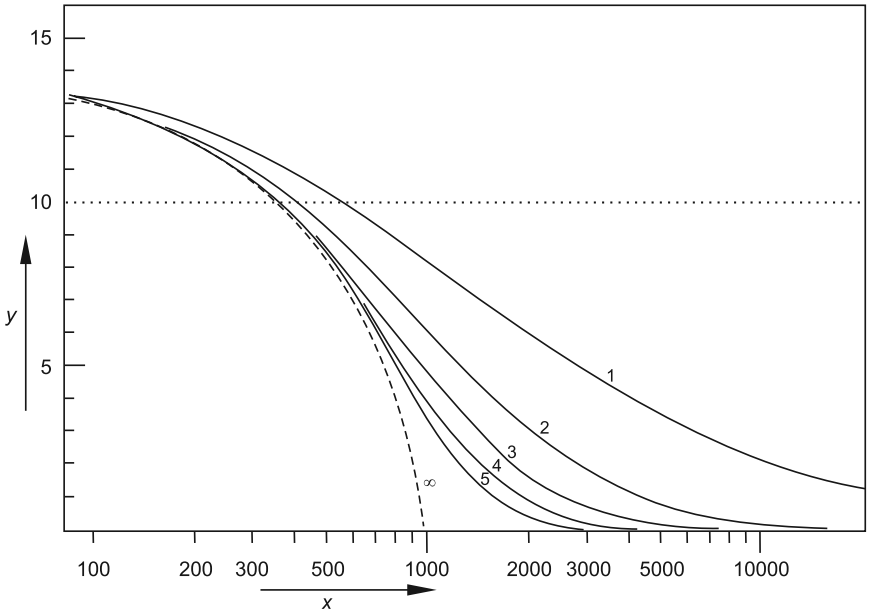

Fig. 5. Nitric oxide concentrations in gas leaving the absorption stage. Initial conditions: T = 30°C (303 K); P = 1.013 bar; A_1 = 10; B_1 = 0; M = 30%; S_1 = 0. Continuous lines present the results for absorbing systems appropriating successively to 1, 2, 3, 4 and 5 theoretical shelves. The broken line corresponds to an absorbing system with an unlimited number of theoretical shelves (the entering gas is in equilibrium with the nitric acid solution leaving the absorption stage). The dotted horizontal line shows the level of the initial content of NO + NO_2

(broken lines) and their mutual positions seem to be logical and convincing. Curves for shelve numbers greater than five will increasingly approach the curve for an unlimited number of shelves.

– In all three presented cases, the content of nitrogen oxides in gas leaving the absorption stage as a function of the liquid/gas ratio are passing fluently from the area in which the nitrogen oxides content is higher than initial to the area in which it is lower than initial. The cause of this is simple: in all presented cases, only NO in the entering gas phase is assumed. In the efflux gas from the traditional nitric acid plants, there is normally an excess of NO in comparison to NO_2. At low liquid/gas ratios, the amount of HNO_3 is sufficient to oxidize a large proportion of the NO to NO_2, but is too little to absorb it. The increase of nitrogen oxide content at low liquid/gas ratios is higher when using a 55% nitric acid solution as opposed to when using one of 30%.
– From the presented examples, it follows that having a sufficiently effective absorption system (corresponding to an adequate number of theoretical shelves) and having at one's disposal a nitric acid solution with no oxygen demand, it is possible to remove nitrogen oxides from the gas phase to any low level. The theoretical border is the vapor pressure of HNO_3, but this ingredient is easy to remove with the final water wash (see Fig. 1).

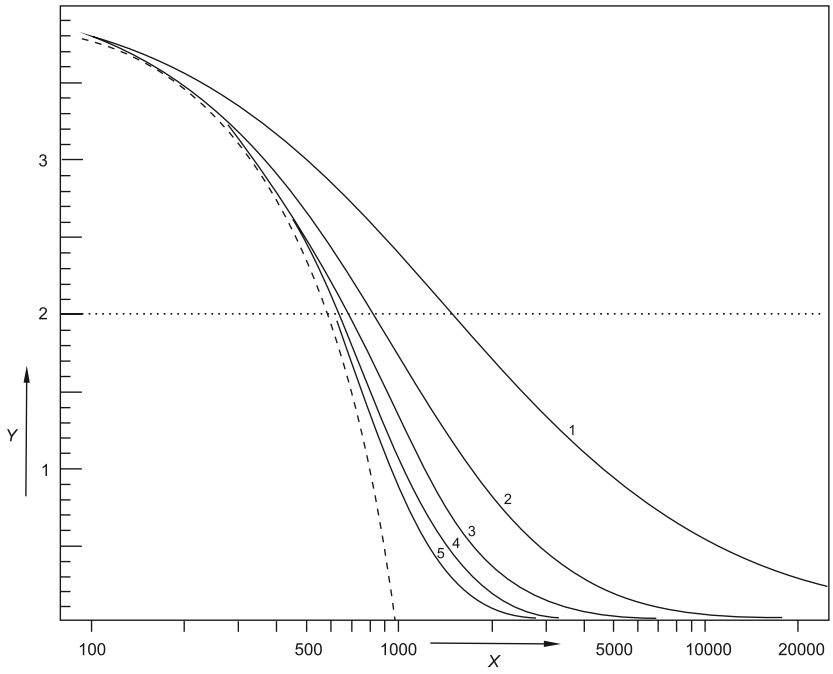

Fig. 6. Nitric oxide concentrations in gas leaving the absorption stage. Initial conditions: $A_1 = 2$. All other parameters are the same as in Fig. 5. The level of 0.2% vol. of nitric oxides in the tail gas is not typical for a non-pressure nitric acid process. Such an initial condition was only chosen for the purpose of comparability. The high similarity with the graph in Fig. 5 is as a result of the fivefold extended scale of the *Y*-axis

The effectiveness of the absorption stage highly depends on pressure. Fig. 9 shows the comparison of two cases differing only in pressure. From this graph, it could be read that for removing 90% nitrogen oxides from the gas containing an initial 0.2% NO in an absorbing system, adequate to five theoretical shelves under the atmospheric pressure 1600 kg of 30% nitric acid solution is needed, whereas under the pressure of 7.09 bars for the same result only 230 kg of this solution per 1000 moles of gas are sufficient.

What is interesting about the absorption systems which are adequate for several theoretical shelves is the shape of the gas composition after each shelf in a sequence, depending on the liquid/gas ratio. In order to present this, two extreme cases were chosen – the absorption of gas with 1% NO under atmospheric pressure using a 30% solution of nitric acid compared with the absorption of gas with a content of 0.2% NO under higher pressure (7.093 bars) using a 55% solution of nitric acid. Both cases are shown in Fig. 9 and 10.

Neither graph is fully comparable because all three values of X shown in Fig. 9 are lying in the ‘effective’ area. At the lower liquid/gas ratios, which are not shown here, appears the phenomenon of increasing the content of nitrogen oxides and not its lowering as a result of double function of nitric acid as an absorbing and oxidizing agent. A different situation is shown on Fig. 10 where the range of *X* values is wider and the increase in the nitrogen oxide

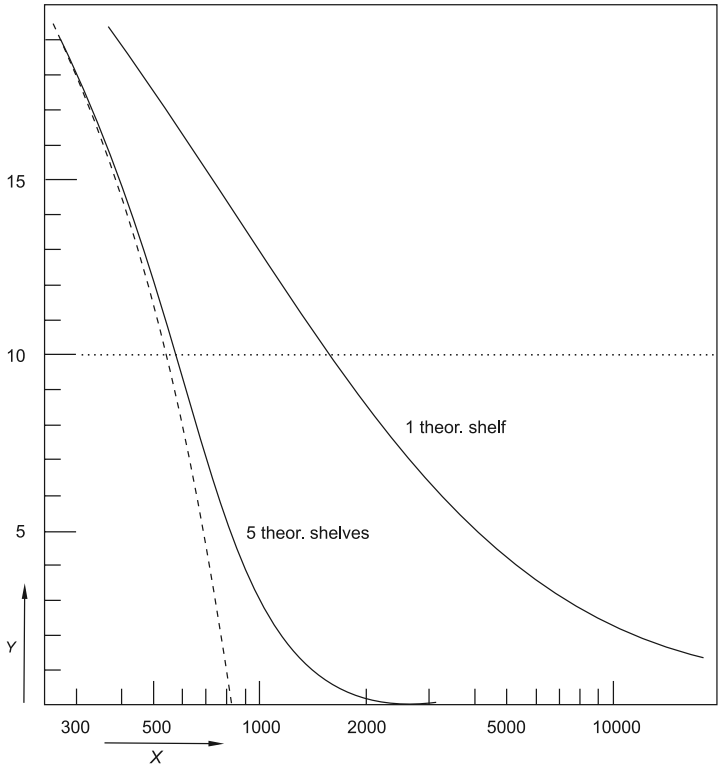

Fig. 7. Concentration of nitric oxides in gas leaving the absorption stage. Initial conditions: P = 1.013 bar; A_1 = 10; M = 55% HNO_3. Curves for two, three and four theoretical shelves are not shown

content at lower X values is quite distinct. The case of X = 200 on Fig.10 shows that even if the absorption after five theoretical shelves is effective (about 90%), a significant increase in the nitrogen oxide content in the gas phase can appear after the first shelve. It is also remarkable that if in the case presented in Fig. 10 one assumed 0.6% NO_2 instead of 0.2% NO ($A_1 = 0, B_1 = 6$) in the entering gas, the image would remain the same – only the horizontal line of initial NO_X would lie on level 6 instead of 2. A similar image would appear on Fig. 9. The reason for this is that balancing the oxygen demand by one mole of NO counts as much as balancing the oxygen demand by three moles of NO_2, please check that I've not accidentally changed the intended meaning whereas as a loss of bound nitrogen, both oxides count equally. Fig 11 presents a comparison of the absorption of nitrogen oxides in two nitric acid solutions of different concentrations under identical conditions.

On the graph in Fig. 11, for the growing liquid/gas ratio, both pairs of curves are passing from the area of increasing to the area of decreasing content of nitrogen oxides in the gas phase. The increase of nitrogen oxide content is distinctly bigger in the case of 55% HNO_3 than in the case of the 30% solution; passing to the decreasing area demands a twice higher liquid/gas ratio. Both curves are crossing. By further increase of X, the superiority

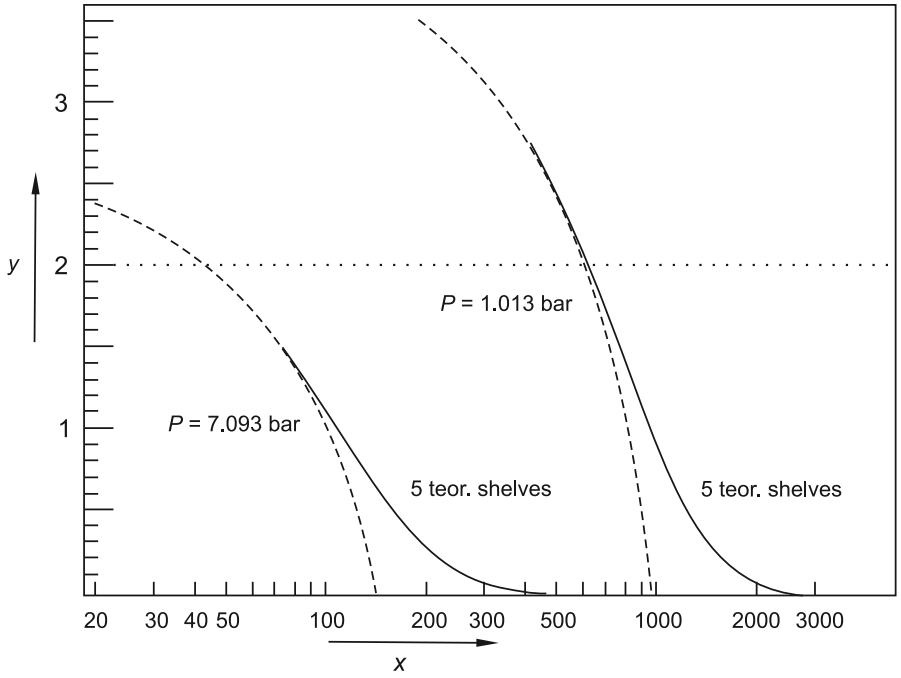

Fig. 8. Comparison of nitric oxide concentration in gas leaving the absorption stage under atmospheric pressure and under higher pressures. Common conditions: T = 303 K; $A_1 = 2$; $B_1 = 0$; $S_1 = 0$; M = 30%. The absorption system is adequate for five theoretical shelves (continuous lines), broken lines correspond to an unlimited number of theoretical shelves. The right pair of curves relates to the atmospheric pressure, the left pair relates to a pressure of 7.093 bars

of the 55% solution becomes higher and the co compensation of these superiority demands an about 30% bigger supply of the weaker solution.

In the examples given above, it was always assumed that the nitric acid solution put to absorption is free from any lower oxidized nitrogen compounds ($S_1 = 0$), which means, it is ideally. Such an assumption is not fully realistic. A non-fully accomplished regeneration must be taken into account. Fig. 12. shows a comparison of the absorption of nitrogen oxides by using both a fully and a non-fully regenerated HNO_3 solution.

The assumed oxygen demand of 0.0005 moles O_2 per kg of solution corresponds to the traditionally calculated manner 0.109 g NO_2 per litre. At a circulation of X = 400 kg per 1000 moles of gas, that would correspond to a regeneration degree of 90%. Increasing the supply of the nitric acid solution showing a given oxygen demand one cannot achieve a total removing of nitrogen oxides from the gas phase. In the example shown above, assuming a stable value of S_1, the content of NO_X would at increasing circulation establish on ca. 0.015% vol., which regarding the industrial conditions, could be recognized as a very good achievement. However, it is unknown how an increasing circulation would change the value of S_1 – no certain assumptions can be made regarding this.

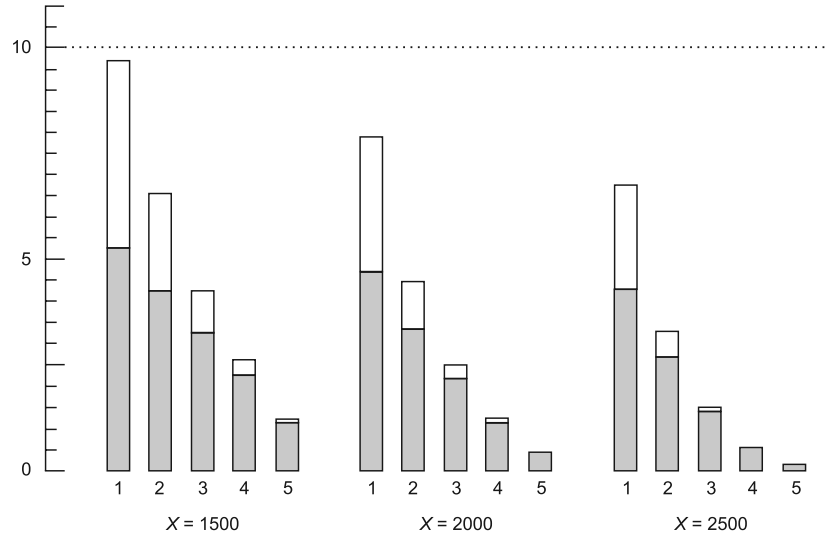

Fig. 9. Nitrogen oxide content after each shelf in an absorption system adequate to five theoretical shelves. Initial conditions: T = 303 K; P = 1.013 bars; M = 30%; A_1=10 (1% vol.); B_1 = 0; S_1 = 0. The height of the numbered bars is the measure of the nitrogen oxide content after each shelf (shelf numbers are given below the bars). The dotted parts of piles stand for NO_2, no dotted parts stand for NO. The values of X indicate kg of nitric acid solution per 1000 moles of gas

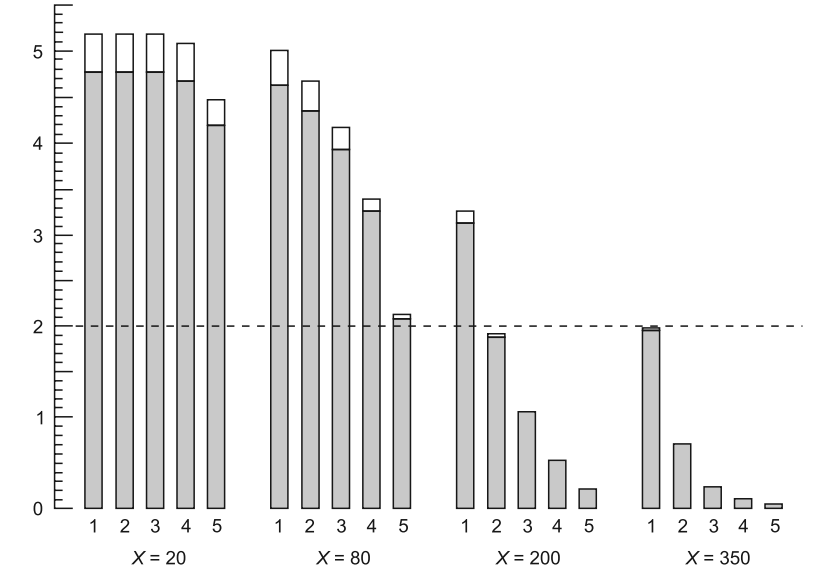

Fig. 10. Nitrogen oxide content after each shelf in an absorption system adequate to five theoretical shelves. Initial conditions: T = 303 K; P = 7.093 bars; M = 55%; A_1 = 2 (0.2% vol.); B_1 = 0, S_1 = 0. For further explanation, see Fig. 9

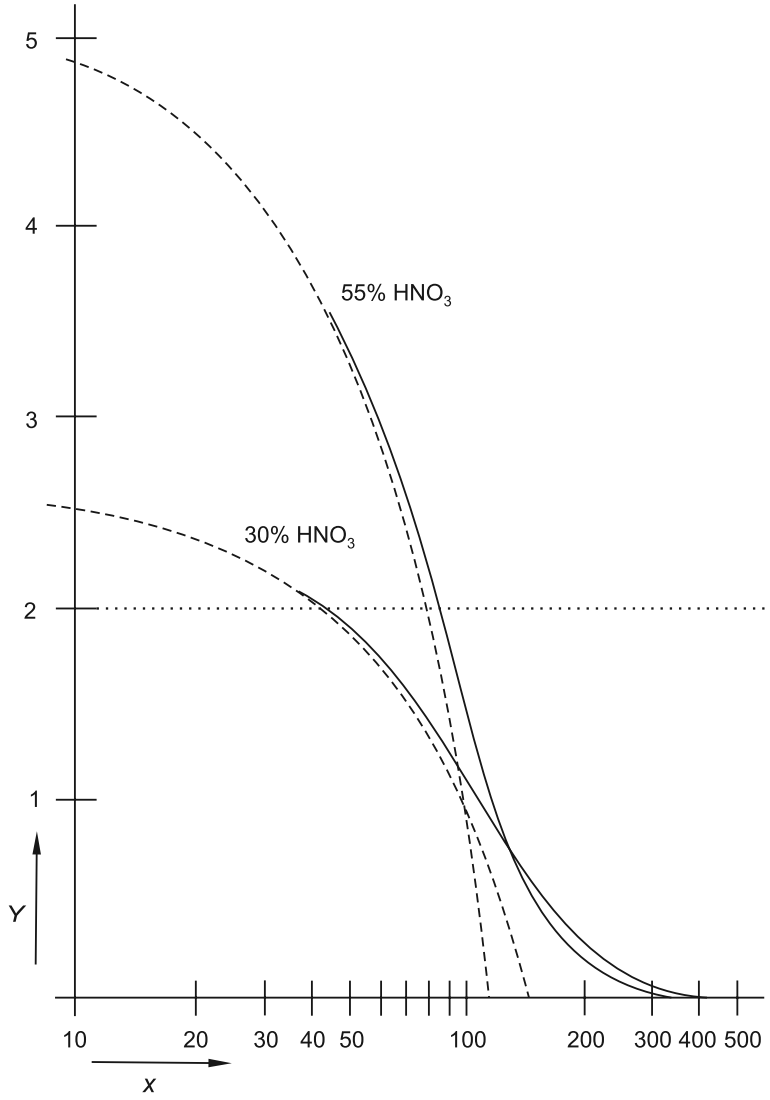

Fig. 11. Comparison of nitrogen oxide content in gases after absorption in nitric acid solutions of two different concentrations – 30% and 55%. Common conditions: T = 303 K (30°C); P = 7.093 bars; A_1 = 2; B_1 = 0; S_1 = 0. Both continuous lines relate to nitric oxide content after absorption in a system adequate to five theoretical shelves; broken lines relate to a system with an unlimited number of shelves

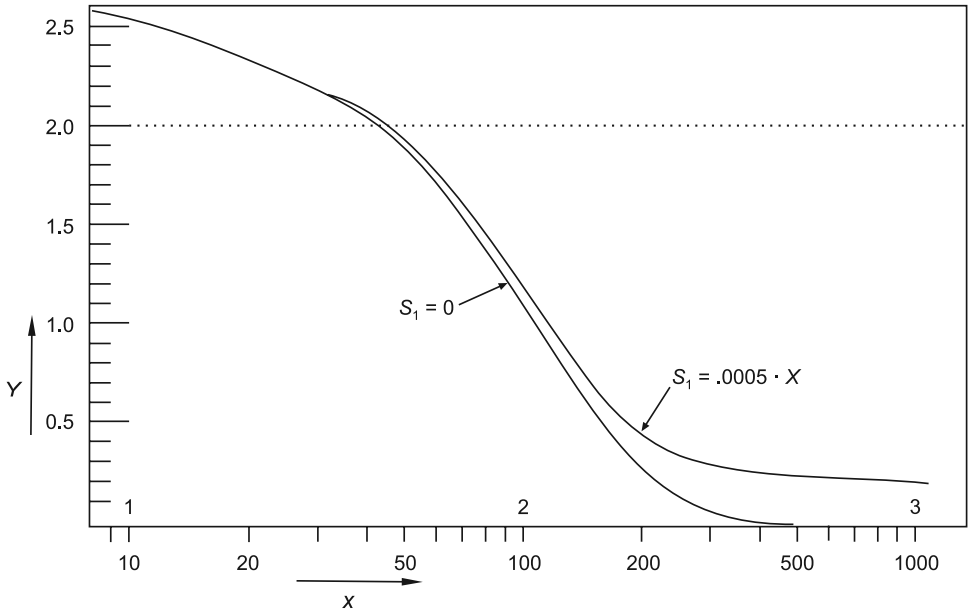

Fig. 12. Comparison of nitrogen oxide content in the gas phase after absorption in a 30% HNO_3 solution free of dissolved nitrogen oxides ($S_1 = 0$) with nitrogen oxide content in the gas phase after absorption in a solution showing an oxygen demand of 0.0005 moles of O_2 per kg of solution ($S_1 = 0.0005 \cdot X$). Common conditions: $T = 30°C$; $P = 7.093$ bars; $A_1 = 2$; $B_1 = 0$; $M = 30\%$. All curves were calculated for a system adequate to five theoretical shelves

4. Conclusions

The results of calculating the absorption stage in the AR process presented above provide in total, a coherent and logical picture. Having rationally constructed absorption equipment at one's disposal enables the application of a sufficient high liquid/gas ratio. It is in principle, possible to reduce the nitrogen oxides from the outlet gas to any low level. However, the essential condition for this is as follows: the nitric acid added at the absorption stage cannot contain dissolved nitrogen oxides (the oxygen demand must be $S_1 = 0$). The effectiveness of the AR process as a whole thus mainly depends on the effectiveness of the regeneration of the HNO_3 solution. An additional conclusion follows from this: absorption can be effectively made at a fairly broad range of concentrations of the nitric acid solution. Thus, the choice of this concentration should be made regardless of the optimization of the absorption, but with regard to optimizing its regeneration.

5. Remarks

The regeneration of the nitric acid solution containing absorbed nitrogen oxides consists of their removal and in this way, restoring the initial ability of the solution with regard to

absorbing nitrogen oxides. The stage of absorption is relatively transparent. It consists of two elements: of the absorption as such, and of the NO/NO_2 ratio dictated by the concentration of the nitric acid solution contacting with the gas phase. In comparison to that, the stage of regeneration is not so obvious. Methods of regeneration can be quite different. Under these methods two main categories can be distinguished:

1. 'Physical' removal of the dissolved nitrogen oxides using their significant fugitiveness in comparison to two other main components of the solution (H_2O and HNO_3) and
2. Oxidation of the absorbed nitrogen oxides, for instance according to summaric equations:

$$4NO_2 + O_2 + 2H_2O = 4HNO_3 \qquad \text{or} \qquad 2HNO_2 + O_2 = 2\ HNO_3$$

Both categories of methods, if effective and tolerating expenses related to it, are useful. Different combinations of both main directions are possible too. Physical regeneration can consist of 'boiling away' or 'blowing through' with gas or of combining both measures. The 'boiling away' approach demands a significant energy expense and extended heat exchangers, which increases costs. For 'blowing through' only the so called 'second air' can be used, which accounts for not more than 30% of the total gas volume and is needed for bleaching the product, therefore, its use demands a significant raising of temperature. An interesting (but, in the author's opinion, a not very attractive) example is the 'Bolme' process [14–15]. In that process, outlet gas nitrogen oxides are absorbed in nitric acid of the same concentration as that of the product which circulates between absorption and regeneration by 'blowing through' at high temperature. The circulation is fed by the raw product from the rich end of the traditional absorption line, an appropriate part of the regenerated solution is led off as ready product.

The second direction, which is regeneration by oxidization, is more diversified. Air as an oxidant is rather unuseful. A possible method for its use is shown in a Polish patent [1]. It is a combination of oxidization and 'blowing through', but its applicability is limited to multi-tower, non-pressure systems. Oxygen is more useful - its consumption does not significantly exceed the stoichiometric one, but a near complete removal of the nitrogen oxides from the solution (decreasing its oxygen demand to almost zero) would need sizable, thus expensive regenerators.

For years, much attention was paid to hydrogen peroxide H_2O_2 as a strong oxidizer of nitrogen oxides in the liquid phase [6, 11, 20, 21] – it can be used as an exclusive or as a supplementary oxidizer. Hydrogen peroxide is certainly very effective as an oxidizer, as a low fugitive substance can be introduced directly to the solution guided to the absorption. However, there is no information about its industrial realizations.

In last years interest is directed to ozone O_3 as an intensifying factor of the process of converting nitrogen oxides into nitric acid. Intensive research works on its application in nitric acid technology are led in Polish industrial and high school research institutions. The papers concerning these works [47–53] are distinguished by a high theoretical level, but an image of technological realization of their results is not shown.

The author of this thesis dares to express his conviction that the introduction of ozone into the technology of nitric acid production will bring about significant technical and economical, as well as ecological, progress.

References

[1] Polish Patent No. 51804, appl. 23.04.1963, *Method of producing nitric acid.*

[2] Janiczek W., Błasiak E., Karolewicz S., Gajewski A., *New prospects in the technology of nitric acid producing*, Przemysł Chemiczny, Vol. 48, 1, 1967, 28-31.

[3] Janiczek W., *Neue Aussichten in der Technologie der Salpeter-säureherstellung*, Chemische Technik, Vol. 19, 5, 1967, 269-282.

[4] Anonim, *Off-gas treatment at nitric acid plants*, Brit. Chem. Eng. Proc. Rev., 1967, 55.

[5] Mayland B.J., *Improve nitric acid processes*, Hydrocarbon Processing, 1972, 141-144.

[6] Japanese Patent No. 4 815 766, *N-oxide removal from exhaust gas*, 18 February 1973.

[7] Mayland B.J., Heinze R.C., *Continuous Catalytic Absorption For NOx Emission Control*, Chemical Engineering Progress, Vol. 69, 1973, 75-76.

[8] Anonim, *Oxidative tail gas scrubbing technique increases nitric acid plant product yield*, Nitrogen, Vol. 93, 1975, 47-48.

[9] Roudier L. et al., *Nitric Acid Recovery from Waste Nitrous Gases by the COFAZ Process Fertilizer Nitrogen*, The British Sulphur Corporation, London 1981/82, 561-569.

[10] Roland L.D., *Some Processes for the Treatment of Liquid and Gaseous Effluents in Nitrogen Fertilizer Production*, Studies in Environmental Sci., Vol. 19, 1982, 369-374.

[11] Patent USA No. 4 419 333, *Process for removal of nitrogen oxides* (16.07.1982).

[12] Mayland B.J., Roland L.D., *Nitrogen oxides emission control CDL/VITOK enhanced absorption process*, Fourth International Conference on Chemistry for Environmental Protection, Toulouse, France 1983, 605-612.

[13] Freitag W., Maurer R., *Developments in Nitric Acid Plants*, The Fertilizer Society, London, 01.12.1983.

[14] Busik J.R, Foster K.E., *Nitric Acid Plant Inspection Guide*, National Service Center for Environmental Publications (NSCEP), 1984, 25-50.

[15] USA Patent No. 4 562 052, *Process for the removal of nitrogen oxides from nitric acid plant tail gas*, Appl. 1984.

[16] Roiron, *How to Solve the Problem of NO_X Pollution from Nitric Acid Plants*, Brochure of Rhone – Poulenc, ed. by Nitrogen, 1986.

[17] Anonym: *NO_X Abatement Systems for Nitric Acid Plants*, Nitrogen, Vol. 171, 1988, 25-34.

[18] Kozłowski K., Wilk M., *Possible improvements of the absorption stage in nitric acid plants* (in Polish), Materials of Polish Forum Diminution of Nitrogen Oxides Content in Industrial off Gases, Puławy, Poland, 1988, 65-102.

[19] Polish patent No.166366, *Method and installation for reduction of the nitrogen oxides emission arised in industrial processes* (in Polish), Property of Beco Eng. Co. USA Priority 1989.

[20] Thomas D., Vanderschuren J., *The absorption-oxidation of NO_X with hydrogen peroxide for the treatment of tail gases*, Chem. Eng. Science, Vol. 51, 1996, 2649-54.

[21] Thomas D., Vanderschuren J., *Modeling of NO_X Absorption into Nitric Acid Solutions Containing Hydrogen Peroxide*, Industrial and Eng. Chemistry Research, Vol. 36, 1997, 3315--3322.

[22] Kristew I., Dimow W., *Absorption of low concentrated and low oxidized nitrogen oxides in nitric acid solutions* (in Rus.), Bulgarian Academy of science, Communications of the Departament of Chemistry, Vol. VIII, 3, 1975, 469-478.

[23] Tereszczenko L.J., Kucza M.I.,. Panow W.P., Zubow W.W., *The equilibrium of nitrogen oxides with nitric acid solutions*, Zhurnal Prikl. Chim., Vol. 52, 3, 1979, 1743-1747.

[24] Lefers J.B., de Boks F.C., van den Bleek C.M., van den Berg R.J., *The Oxidation and Absorption of Nitrogen Oxides in Nitric Acid in Relation to the Tail Gas Problem of Nitric Acid Plants*, Chemical Engineering Science, Vol. 35, 1980, 145-153.

[25] Carla G., Pigford R., *Absorption of Nitric Oxide in Nitric Acid and Water*, Industrial Eng. Chem. Fundamentals, Vol. 22, 1983, 329-335.
[26] Weisweiler W.W., Thiemann K.M., Scheibler E., Wiegand K.W., *Absorption of NO_2/N_2O_4 in nitric acid*, Chem. Eng. Technol., Vol. 13, 1, 1990, 91-97.
[27] Weisweiler W.W., Thieman K.M., Scheibler E., Wiegand K.W., *Absorption of Nitric Oxide in Dilute Nitric Acid*, Chem. Engng. and Technol., Vol. 14, 1991, 270-274.
[28] Vosper A.J., *Dissociation of dinitrogen tetroxide in the gaseous phase*, Journal of the Chemical Society, 1970, 625-627.
[29] Seshadri D.N., Vistanath D.S., Kuloor N.R., *Thermodynamic properties of the System $N_2O_4 = 2NO_2 = 2NO + O_2$*, AICHE Journal, Vol. 16, 3, 1970, 420-425.
[30] Abel E., Proisl J., *Über das Gleichgewicht zwischen Stickstoff-Monoxyd, -Dioxyd und –Trioxyd*, Zeitschrift für Elektrochemie, 35, Vol. 9, 1929, 712-715.
[31] Beattie I.R., Bell S.W., *Dinitrogen Trioxide. Part I. Stability in the Gaseous Phase*, Journal of Chemical Society, 1957, 1681-1686.
[32] Beattie I.R., Bell S.W., Vosper A.J., *Dinitrogen Trioxide, Part II and III*, Journal of Chemical Society, 1960, 4796-4802.
[33] Karawajew M.M., Skworcow I.G.A., *The equilibrium at the formation of the nitric acid in the gaseous phase* (in Rus.), Zhurnal Fiz. Chimii, Vol. 35, 5, 1962, 1072-1074.
[34] Waldorf J.M., Babb A.L., *Vapor phase equilibrium of NO, NO_2, H_2O and HNO_2*, The Journal of Chemical Physics, Vol. 39, No. 2. 1963, 432-435.
[35] Burdick C.L., Freed E.S., *The equilibrium between nitric oxide, nitrogen peroxide and aqueous solutions of nitric acid*, Journal of American Chemical Society, Vol. 43, 1921, 518-530.
[36] Chambers F.S., Sherwood T.K., *Absorption of Nitrogen dioxide by aqueous solutions*, Ind. and Eng. Chem., Vol. 29, 1937, 1415-1422.
[37] Pogrebnaja W.L., Usow A.P., Baranow A.W., Maczigin A.A., *The solubility of oxygen in nitric acid solutions* (Rus.), Chimija i Chim. Tiechnologija, vol. 17, 1971, 16-20.
[38] Theobald H., *Messungen zum Gleichgewicht Salpetersäure/nitrose Gase*, Chemie – Ingenieur – Technik, Vol. 40, 15, 1968, 763-764.
[39] Pozin M.E., Kopylew B.A., Tereszczenko L.J., Bielczenko G.W., *A method of computing the equilibrium composition of gaseous phase contaning nitrogen oxides in equilibrium with liquid solutions of nitric acid* (in Rus.), Zhurn. Prikl. Chim., 1963, 14-24.
[40] Sproesser W.C., Taylor G.B., *Vapor Pressures of Aqueous Solutions of Nitric Acid*, Journal of American Chemical Society, Vol. 43, 1921, 1782-1787.
[41] Wilson G.L., Miles F.D., *The Partial Pressures of Nitric Acid – Water Mixtures from 0–20°C*, Transactions of the Faraday Society, Vol. 35, 1940, 356-363.
[42] Tereszczenko L.J., Panow W.P., Pozin M.E., *The equilibrium between nitrogen oxides and nitric acid solutions*, Zhurn. Prikl. Chim., Vol. 41, 3, 1968, 487-492.
[43] Klemenc A., *Zur Kenntnis der Salpetersäure. Methoden zur Gasanalyse im System $N_2 – NO – NO_2 – N_2O_4 – N_2O_3 – HNO_2 – HNO_3$*, Monatshefte f. Chemie, Vol. 83, 2, 1952, 334-345.
[44] Taylor G.B., *Vapor Pressure of Aqueous Solutions of Nitric Acid*, Industrial and Engineering Chemistry, Vol. 17, 1925, 633-635.
[45] Semel G.V., *Bestimmung von N_2O_3, NO_2 und HNO_2 in Salpetersäure*, Chemie–Ingenieur–Technik, Vol. 38, 1966, 888-889.
[46] Bode H., *Über die Salpetersäurereduction durch Stickoxyd 1. Gleichgewicht*, Zeitschr. Anorg. U. Allgem. Chem., Vol. 195, Issue 1, 1931, 195-200.
[47] Jaroszyńska-Wolińska J., *Ozone application to a two stage NO removal from waste gases*, Polish Journal of Chemical Technology, Vol. 4, 2002, 5-7.

[48] Miller J.S., Wilk M., Chacuk A., Ledakowicz S., *Ozonation of nitrous acid in aqueous nitric acid solutions*, IOA 17th World Ozone Congress – Strasbourg, France, 2005.
[49] Chacuk A., Miller J.S., Wilk M., Ledakowicz S., *Intensification of nitrous acid oxidation*, Chemical Engineering Science, Vol. 62, 2007, 7446-7453.
[50] Skalska K., Ledakowicz S., Wilk M., Miller J.S., *Oxidation of NO_X in flue gases by ozone and UV radiation*, XXIII Photochemistry Symposium IUPAC, Ferrara, Italy 2010.
[51] Skalska K., Miller J.S, Ledakowicz S., *Trends in NO_X abatement: A review*, Science of the Total Environment, Vol. 408, 2010, 3976-3899.
[52] Ledakowicz S., Skalska K., Miller J.S., Wilk M., *Nitrogen oxides ozonation as a metod for NO_X emission abatement*, World Congress and Exhibition IOA IUVA,Paris, France 2011.
[53] Skalska K., Miller J.S., Ledakowicz S., *Kinetic model of NO_X ozonation and its experimental verification*, Chemical Engineering Science, Vol. 66, 2011, 3386-3391.

TECHNICAL TRANSACTIONS | **CZASOPISMO TECHNICZNE**
CHEMISTRY | CHEMIA
1-Ch/2014

TADEUSZ KOMOROWICZ*, KRZYSZTOF KUPIEC*, ANETA MÓŁKA*

THE APPLICATION OF NOVEL ORGANIC DEEMULSIFIERS FOR THE SEPARATION OF OIL-IN-WATER EMULSIONS

ZASTOSOWANIE NOWYCH DEEMULGATORÓW ORGANICZNYCH DO ROZDZIAŁU EMULSJI OLEJ-WODA

Abstract

The paper summarizes the results of tests of separation of oil-in-water emulsions with the application of novel organic deemulsifiers. Fresh and used emulsions of different concentrations were tested. The manipulated variables were: the concentration of oil in the emulsion; the concentration and amount of deemulsifier solution; the temperature. The results of these tests are presented graphically.

Keywords: *separation of oil-in-water emulsions*, *organic deemulsifiers*

Streszczenie

W artykule przedstawiono wyniki przeprowadzonych badań rozdziału emulsji olej-woda z zastosowaniem nowych deemulgatorów organicznych. Badano rozdział emulsji świeżej i przepracowanej w zależności od stężenia emulsji, stężenia i ilości roztworu deemulgatora oraz temperatury. Wyniki badań zilustrowano na wykresach

Słowa kluczowe: *rozdział emulsji olej-woda*, *deemulgatory organiczne*

* Ph.D. Eng. Tadeusz Komorowicz; Ph.D. Eng. Krzysztof Kupiec, prof. PK; M.Sc. Eng. Aneta Mółka; Faculty of Chemical Engineering and Technology, Cracow University of Technology.

Symbols

C_d – concentration of deemulsifier in mixture [dm^3/dm^3]
C_e – concentration of oil in emulsion sample [dm^3/dm^3]
C_m – concentration of oil in mixture [dm^3/dm^3]
m – slope of straight line
X_{vd} – volume of deemulsifier solution to volume of emulsion sample ratio [dm^3/dm^3]

1. Introduction

Various branches of industry generate oily waste water in the form of oil-in-water emulsions. Highly stable oil-in-water emulsions are often used in metal machining as emulsive cutting fluids. These emulsions are prepared from concentrates (soluble oil fluids) and are used in a diluted form (usual concentrations vary from 3 to 10% of oil). Soluble oil fluids consist mainly of a base mineral oil and emulsifiers to help produce stable emulsions. They also contain a variety of additives, e.g. rust inhibitors, bactericides.

The problem of utilizing used oil-in-water emulsions, particularly from machining processes, is of great importance because the quantity of these emulsions in Poland reaches 100.000 tons per year [1] and the 'producers' of these emulsions are spread all over Poland. In compliance with the Polish Act on Wastes [2], there is no option to dump these emulsions into the waste water treatment system. On the other hand, it is not profitable to transport the emulsions to a central point of processing because of the high water content in them. The emulsions have to be separated into their oil and water phases on the spot. The oil phase can be then transported to a recovery plant or can be burnt. The water phase can be recycled or diluted and discharged.

To separate oil-in-water emulsions into oil and water phases, various methods can be applied [3, 4] such as: thermal (vaporization); adsorptive methods; mechanical methods (micro and ultrafiltration); electrochemical methods (electrocoagulation and electrophoresis); chemical methods (with the use of salts, acids or deemulsifiers).

In this paper, investigations on the separation of some emulsive cutting fluids into their oil and water phases by means of various novel organic deemulsifiers have been described. The deemulsifiers are cation copolymers of polyamins with formula weights ranging from 75.000 to 200.000. Some types of this kind of organic deemulsifiers were tested by the authors in previous research [1, 5].

2. Range of investigations

Both fresh and used oil-in-water emulsions were used in the investigations. Fresh emulsions were prepared on a base of Emulgol ES-12 – a concentrate manufactured by Orlen Oil [6]. This concentrate is an amber-coloured transparent liquid. It consists mainly of lubricating oils, hydrocarbons $C_{20} - C_{50}$ and a neutral base oil. As a result of blending it with water in various proportions, very stable milky emulsions arise. The concentrations

of the tested fresh emulsions were 2, 5 and 8% by volume of oil. An unknown used emulsion was also tested.

For the separation of emulsions, the 1, 2 and 3% by volume aqueous solutions of the following organic deemulsifiers manufactured by SNF Floerger SA (France) were tested: FL 4340; FL 4820; FL 2565; FL 2949; EM 840TRM. The deemulsifiers were dense and viscous white liquids (except for yellow in the case of FL 4340) [7].

The investigations were carried out using 50 cm^3 volume samples of emulsions in 100 cm^3 capacity flasks at 20°C. Into each sample, small portions of solutions of deemulsifiers were added step by step. After each step, the flasks were shaken and the results of separation were observed. The tests were finished when a complete separation had taken place. In the investigations, two identical samples were used simultaneously. In the first sample the over-emulsification was reached in order to catch the sharpness of separation in the second. The final observations were made after 24 hours.

In order to determine the effect of temperature on separation, some tests were also carried out for 2% oil emulsions at 50°C.

The purity of the water phase after separation was determined on the basis of its chemical oxygen demand (COD).

The number of tests was as follows:
- 45 tests of separation of fresh emulsions at 20°C,
- 10 tests of separation of fresh emulsions at 50°C,
- 10 tests of separation of used emulsion at 20°C,
- 1 test of water phase purity.

3. Results of investigations

3.1. Results of separation of emulsions at 20°C

The results of separation, showing the quantities of deemulsifiers needed for separation of 50 cm^3 emulsion samples, were collected in tables and depicted in graphs. In this paper, it is placed only one table for deemulsifier FL 4820 at 20°C (Table 1). The particular columns of this table contain:
- the concentration of oil in the tested emulsion sample,
- the concentration of the tested deemulsifier solution,
- the volume of deemulsifier needed for separation (both the volume of the added deemulsifier solution and the calculated volume of raw deemulsifier),
- descriptions of water and oil phases (colour, form).

The results of Table 1 show that separation usually occurs in a certain range of deemulsifier to emulsion ratio. The graphs showing the lower and the upper separation limits for ES-12 emulsion samples for each concentration of the tested deemulsifier solution are shown in Fig. 1. The *Y*-axis presents the ratio of definite deemulsifier solution volume to the emulsion sample volume. The area between the lower (minimum) and upper (maximum) separation limits represents the area of the two-phase mixture. Instead of three areas for each deemulsifier (one area for each applied concentration), it is possible to graphically show (Fig. 2) the separation range in the form of one area where the *X* and *Y*-axes describe

the concentration of oil and the concentration of pure deemulsifier respectively in the tested mixture (water from deemulsifier solution dilutes the oil in sample). The table in Fig. 2 gives the values of the slopes of the straight lines. The gentler the slope, the smaller the amount of deemulsifier needed for separation.

Table 1

Exemplary results of separation of fresh emulsion ES-12 (50 cm^3) with use of deemulsifier FL 4820 at 20°C after 24 h

Concentration of emulsion [% v/v]	Concentration of deemulsifier [% v/v]	Volume of deemulsifier [cm^3] (separation range)		Description of	
		solution	raw deemulsifier	water phase	oil phase
2	1	6.5–6.8	0.065–0.068	clear, colourless	white, thin
	3	2.0–2.8	0.060–0.840		
	5	1.1-1.6	0.055–0.080		
5	1	27.7	0.277		cream-coloured, thin
	3	7.3–10.0	0.219–0.300		white, thin
	5	4.3–5.8	0.215–0.290		
8	1	no separation			
	3	12.5–15.0	0.375–0.450	clear, colourless	cream-coloured, thin
	5	8.5	0.425		

3.2. The effect of temperature on separation

Some selected results of the effect of temperature on separation quality are given in Table 2.

Table 2

Exemplary comparison of selected results of separation of 2% fresh emulsion ES-12 (50 cm^3) with use of deemulsifier FL 4820 at 20°C and 50°C after 24 h

Deemulsifier		Required volume of deemulsifier solution		Description of	
kind	concentration [% v/v]	20°C	50°C	water phase	oil phase
FL 4820	1	6.5–6.8	3.1–4.2	clear, colourless	cream, thin
	5	1.1–1.6	0.8–0.9	clear, colourless	cream, thin

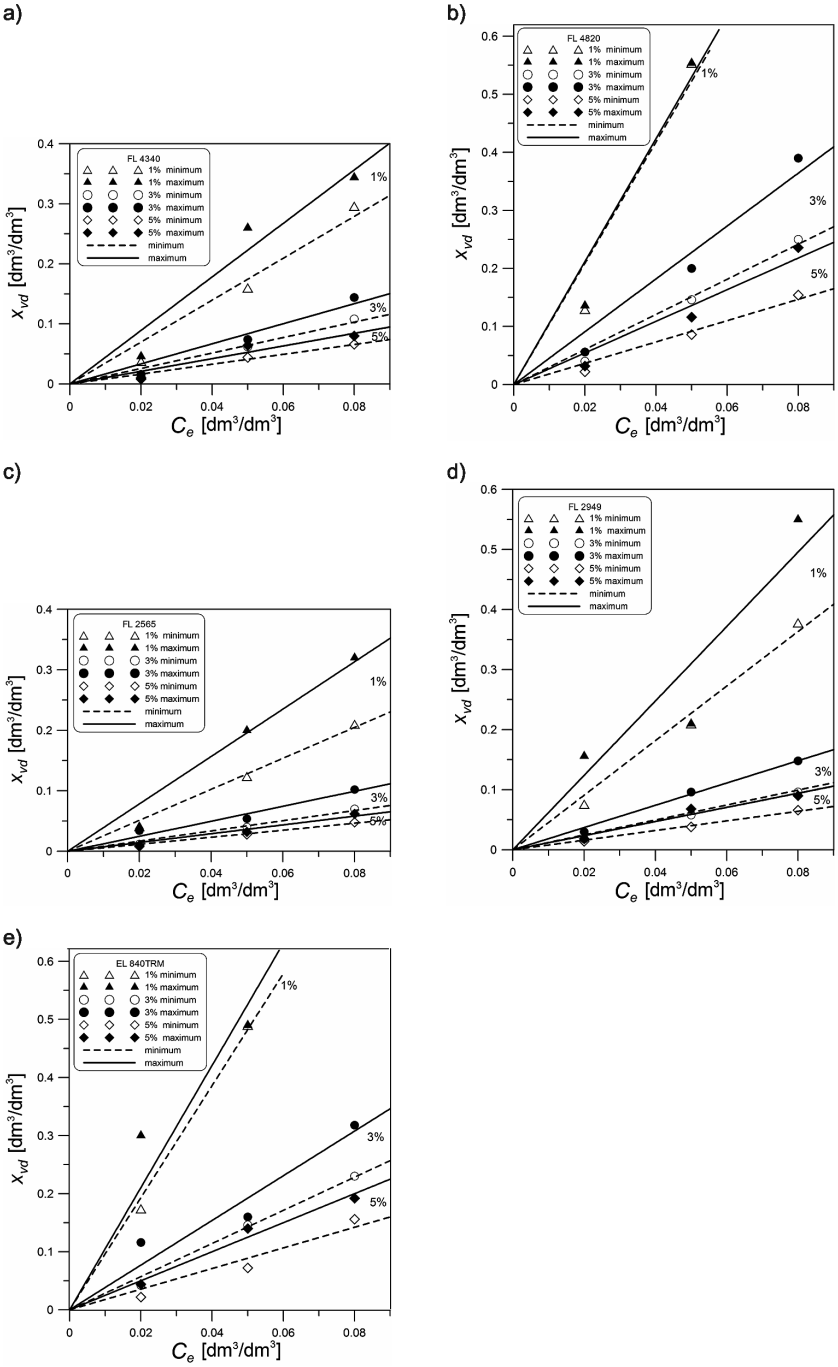

Fig. 1. Lower and upper separation limits for selected concentrations of deemulsifiers

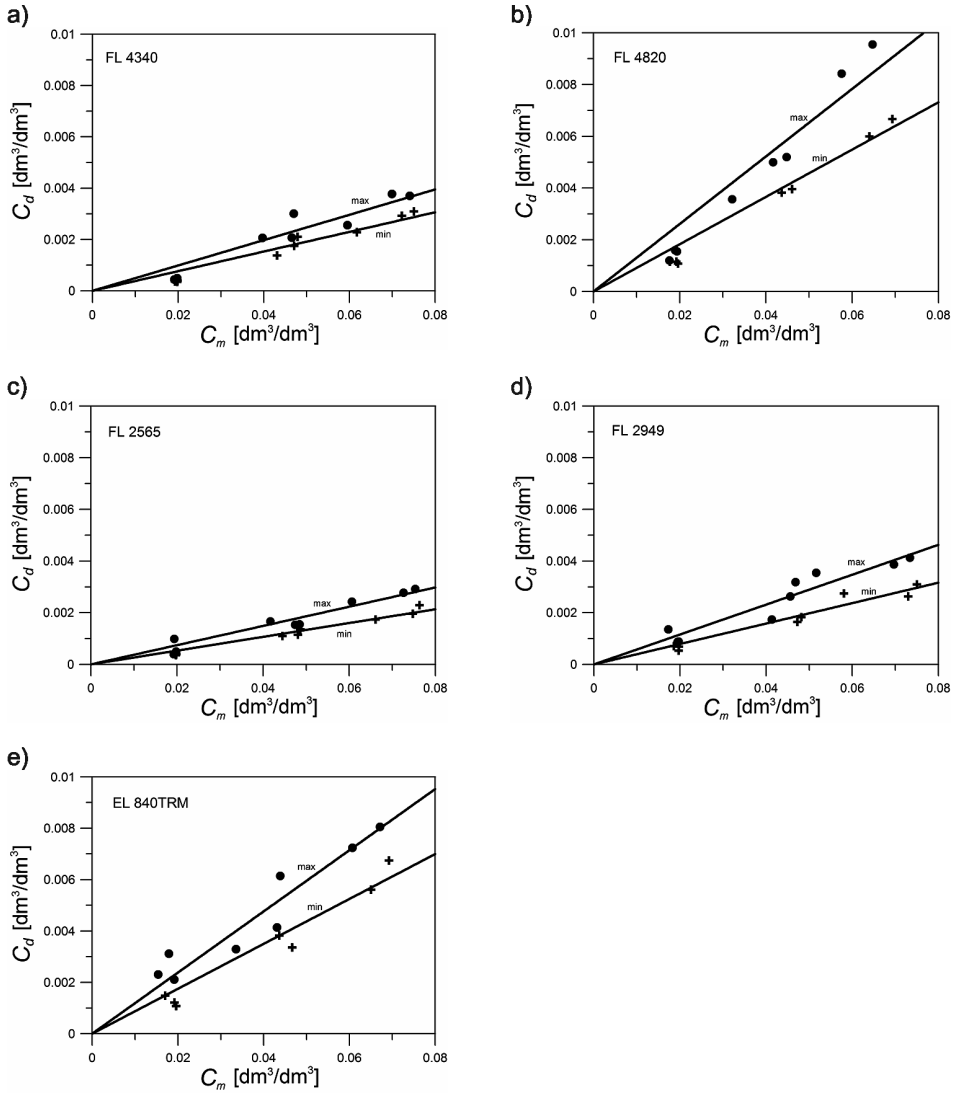

Slope of the straight lines (above)

m	FL 4340	FL 4820	FL 2565	FL 2949	EL 840TRM
minimum value	0.0383	0.0914	0.0267	0.0395	0.0874
maximum value	0.0494	0.1305	0.0372	0.0578	0.1191

Fig. 2. General lower and upper separation limits for each deemulsifier

Graphs showing the effect of temperature on quantity of deemulsifier needed for separation of 2% oil emulsion are presented in Fig. 3.

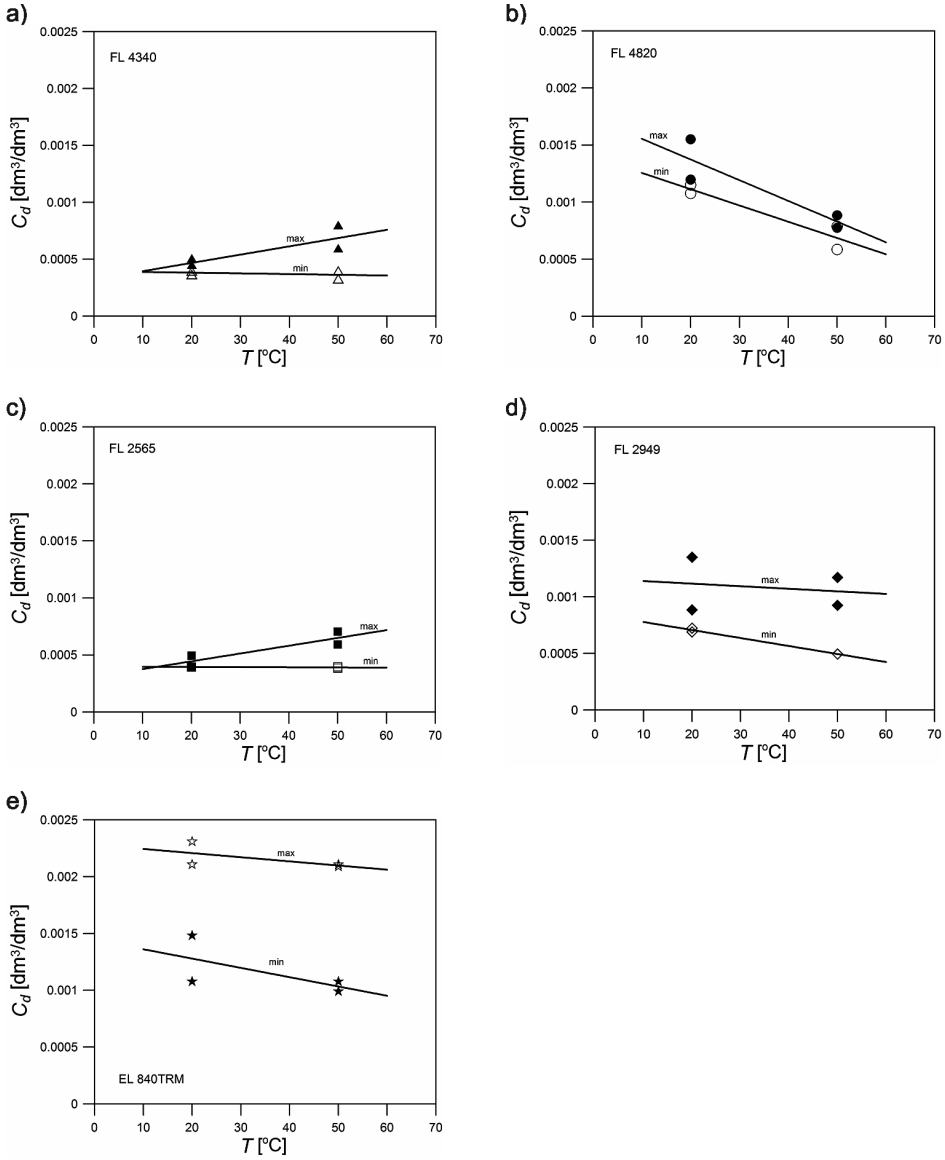

Fig. 3. Effect of temperature on quantity of deemulsifier (lower and upper limits) needed for the separation of 2% emulsion

3.3. Purity of water phase

For the testing of water phase purity, a sample of water phase obtained as a result of separation of the used emulsion with the aid of a 5% solution of deemulsifier FL 4820 was chosen. The water phase was light-yellow and turbid. Its value of COD (Chemical Oxygen Demand) was equal to 11.950 mgO_2/dm^3.

4. Conclusions

On the basis of the obtained results of these investigations, the following conclusions have been formulated below.

- From among the five tested organic deemulsifiers, the best results of separation, taking into account both the amount and the separation quality, were obtained for FL 4340 and FL 2565. Compared to other deemulsifiers, the quantity of them needed for separation was the smallest. When FL 4340 was used, the fresh emulsion separated into a clear, colourless water phase and a thin oil phase. In the case of FL 2565, the quality of separation was worse. The worst results were obtained for EM 840TRM – the separation of both fresh and used emulsions required large volumes. Additionally, the water phase was always turbid.
- The graphs depicting the quantities of the deemulsifier solutions needed for the separation of emulsions show the following relationships:
  - the higher the concentration of the deemulsifier solution, the smaller the volume needed for the separation of the emulsion of the definite oil concentration,
  - the higher the concentration of oil in the emulsion, the larger the volume of deemulsifier of a definite concentration needed for emulsion separation.
- Temperature considerably affects the separation efficiency, but the effect of temperature on separation is irregular. Usually, at higher temperatures the area of separation (the range of deemulsifier concentrations in the separated mixture) is larger.
- Generally, separation efficiency is time dependent. The longer the separation time, the sharper the separation and the clearer the water phase.
- The measure of the purity of the water phase is the index of Chemical Oxygen Demand (COD). If this exceeds the maximum permissible value of 125 mg O_2/dm^3 [8], the water phase has to be treated before being drained off. Usually, this treatment is necessary.

The method of the separation of oil-in-water emulsions with the use of organic deemulsifiers is possible for practical realization and can find widespread industrial application. The advantages of this method are low capital and power costs. Equipment necessary for the method's realization in industrial processes consists mainly of a storage tank for used emulsion, a mixer, a deemulsifier feeder and storage tanks for the oil and water phases. The total operating costs depend on the price of the deemulsifier. One inconvenience of this method is the necessity to select the kind and quantity of deemulsifier for each batch of used emulsion.

References

[1] Komorowicz T., Magiera J., Pacholarz M., Papka L., *Badania rozdziału emulsji olej-woda z zastosowaniem deemulgatorów*, Czasopismo Techniczne, 1-Ch/2007.

[2] Ustawa o odpadach z dn.14 grudnia 2012 roku, Dz. U. Nr 21 z 2013 r.

[3] Kąkol M., *Utylizacja przepracowanych cieczy chłodząco-smarujących*, Paliwa, Oleje i Smary w Eksploatacji, Nr 70, 2000.

[4] Komorowicz T., Magiera J., *Zatężanie zużytych emulsji olejowych w procesie ultrafiltracji okresowej*, Czasopismo Techniczne, 5-M/2003.

[5] Komorowicz T., *Deemulgatory organiczne w ochronie środowiska*, Inżynieria i Ochrona Środowiska, T. 10, Nr 10, 2007.

[6] Orlen Oil, *Katalog produktów*, 2011 (http://www.orlenoil.pl).

[7] NF Floerger S.A. (France), Catalogue of products, 2011.

[8] Rozporządzenie Ministra Środowiska z dn. 28 stycznia 2009 r., Dz. U. Nr 27, poz. 169 z 2009 r.

TECHNICAL TRANSACTIONS | CZASOPISMO TECHNICZNE
CHEMISTRY | CHEMIA
1-Ch/2014

JOANNA KUC*, ADAM GROCHOWALSKI*

METHODS FOR THE DETERMINATION OF HEXABROMOCYCLODODECANE IN FOOD

METODY OZNACZANIA HEKSABROMOCYKLODODEKANU W ŻYWNOŚCI

A b s t r a c t

Methods of sample preparation with a particular emphasis on extraction and purification techniques are described. Gas and liquid chromatography techniques applied for the determination of hexabromocyclododecane are presented. Issues relating to the determination of this compound in food samples are discussed.

Keywords: *BFRs*, *HBCD*, *food analysis*, *GC-MS*, *LC-MS*

S t r e s z c z e n i e

Omówiono metody przygotowania próbek do analizy ze szczególnym uwzględnieniem technik ekstrakcji i oczyszczania próbek. Zaprezentowano techniki chromatografii gazowej i cieczowej stosowane do oznaczania heksabromocyklododekanu. Przedyskutowano problemy oznaczania tego związku w próbkach żywności.

Słowa kluczowe: *BFRs*, *HBCD*, *analiza żywności*, *GC-MS*, *LC-MS*

* M.Sc. Eng. Joanna Kuc, Ph.D. D.Sc. Eng. Ass. Prof. Adam Grochowalski, Department of Analytical Chemistry, Department of Chemical Engineering and Technology, Cracow University of Technology.

Abbreviations and symbols

CAS	–	Chemical Abstract Service
EINECS	–	European Inventory of Existing Commercial Chemical Substances
ESI	–	electrospray ionization
GC-MS	–	gas chromatography coupled to mass spectrometry
LC-MS	–	liquid chromatography coupled to mass spectrometry
LOD	–	limit of detection
m/*z*	–	mass-to-charge
MS	–	mass spectrometry
PBT	–	persistent, bioaccumulative and toxic
POPs	–	persistent organic pollutants
PS	–	polystyrene
REACH	–	Registration, Evaluation, Authorisation and Restriction of Chemicals
S/N	–	signal-to-noise
SRM	–	single reaction monitoring
QA/QC	–	Quality Assurance and Quality Control

1. Introduction

Hexabromocyclododecane (HBCD) is a cycloaliphatic bromide which has been produced through the bromination of cis,trans,trans-1,5,9-cyclododecatriene since the 1960s and it's the most commonly used brominated flame retardant (BFR) [1, 2]. The technical product of HBCD consists of three predominant isomers: α-, β- and γ-HBCD among 16 possible stereoisomers: 6 diastereomeric pairs of enantiomers and 4 meso forms [3, 4]. The structures of the α-, β- and γ-HBCD isomers are shown in Fig. 1. The presence of traces of two minor diastereomers, δ- and ε-HBCD in the technical HBCD product, has also been reported [5].

HBCD inhibits ignition and combustion processes by interfering with the free radical mechanism in the gas phase during the combustion process [6, 7].

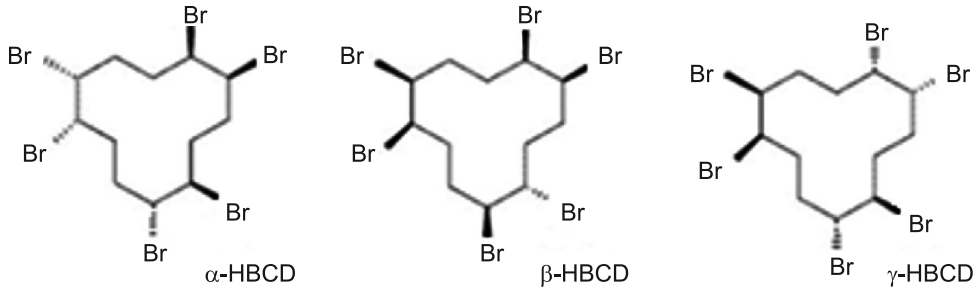

Fig. 1. Structures of α-, β- and γ-HBCD isomers

HBCD is a white solid substance produced in high quantities and it is commercially available under two names, corresponding to CAS and EINECS numbers [8–10].

Table 1

Identification of a commercial product of HBCD

1,2,5,6,9,10-Hexabromocyclododecane	
CAS No	3194-55-6
EINECS No	221-695-9

Hexabromocyclododecane	
CAS No	25637-99-4
EINECS No	247-148-4

Major diastereoisomers CAS No	
α-HBCD	134237-50-6
β-HBCD	134237-51-7
γ-HBCD	134237-52-8

Trade names
Cyclododecane, hexabromo; HBCD; Bromkal 73-6CD; Nikkafainon CG 1; Pyroguard F 800; Pyroguard SR 103; Pyrovatex 3887; Great Lakes CD-75; Dead Sea Bromine Group Ground FR 1206 I-LM;

HBCD is used mainly in expanded (EPS) and extruded (XPS) polystyrene foams which are applied as thermal insulation panels in the building industry [11–13]. The presence of HBCD in PS foams leads to significant improvements in the fire behavior of these materials. In case of exposure to a fire source, the foam shrinks rapidly, what results in a reduced possibility of ignition [14]. HBCD is also added to polymer matrices for cotton containing textile mixtures – this is used in the production of upholstery textiles such as furniture, wall coverings and draperies [15–17]. Some researches indicate the use of HBCD in high impact polystyrene (HIPS) applied in electrical and electronic equipment [7, 16, 18]. HBCD is not covalently bound to materials, and it can therefore be released from the product into the environment during the production, processing, and storage of waste containing this compound [15]. HBCD is considered to be persistent, bioaccumulative and toxic (PBT) and has been recently proposed for inclusion in the Protocol on POPs of the Stockholm Convention [7–9, 26, 27]. In the European Union, HBCD is identified as a Substance of Very High Concern (SVHC) under REACH [10] according to which, after 21 August 2015 only authorized applications of HBCD will continue to be allowed. Directive 67/548/EEC classifies HBCD as very toxic to aquatic organisms, causing long--term adverse effects in the aquatic environment. HBCD is also hazardous to unborn children and breastfed babies [7–9].

The wide use of HBCD has led to widespread contamination of this compound in different biotic and abiotic environmental compartments [16, 28–31] and in humans [32, 33]. The level of HBCD is studied in fish most frequently, due to their high position in the food chain and their ability to absorb high concentrations of contaminants. A relatively high

concentration of HBCD in fish is observed [24, 34-39]. At present, none of the alternative flame retardants are considered to be a suitable replacement for HBCD in PS foams [7], therefore, the monitoring of this contaminant and its determination in food is highly advisable.

Table 2

Physicochemical properties of HBCD

Property	Value	References
Chemical formula	$C_{12}H_{18}Br_6$	–
Molecular mass (g/mol)	641.7	–
Boiling point (°C)	Decomposes at >190°C	[20]
Melting point (°C)	175–195	[11]
	179–181°C (α-HBCD) 170–172°C (β-HBCD) 207–209°C (γ-HBCD)	[2]
Density (kg/m³) (25°C)	2403	[21]
Vapour pressure (Pa) (21°C)	$6.3 \cdot 10^{-5}$	[22]
Water solubility (mg/L) (20°C)	4.88×10^{-2} (α-HBCD) 1.47×10^{-2} (β-HBCD) 2.08×10^{-3} (γ-HBCD)	[23]
Log Kow (octanol-water partition coefficient) (25°C)	5.81	[24]
	5.07 ± 0.09 (α-HBCD) 5.12 ± 0.09 (β-HBCD) 5.47 ± 0.10 (γ-HBCD)	[25]

2. Methods for the determination of HBCD in food

Methods of HBCD analysis are similar to those of POPs. These methods have been well developed over the past several years and are commonly used as a reference in research [40]. The selection of suitable sample preparation methods is an important element in HBCD determination in food samples. Whilst sample preparation is a crucial element of every analytical methodology, it is also the principal source of errors. Food sample preparation is most commonly a multi-step and time-consuming process. Particular care must be taken to avoid sample contamination. The amount of sample used for analysis depends primarily on the expected level of contamination and the sensitivity of the available detection

techniques. Every step of the analytical procedure requires attention and monitoring to ensure high reliability of results (QA/QC) [41]. The typical procedure for the determination of HBCD in food samples is shown in Fig. 2.

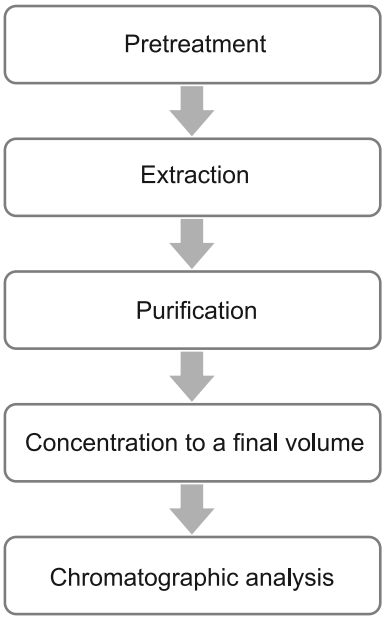

Fig. 2. Scheme of typical procedure for the determination of HBCD in food samples

Pretreatment of solid or semi-solid food samples includes washing, removal of irrelevant matter, mass reduction and drying. Mass reduction is carried out by using a mortar, homogenizer, automatic grinder or high-speed blender. Drying of the sample is most frequently carried out by vacuum methods in a freeze-dryer (lyophilizer) [42].

2.1. Extraction methods

For the determination of organic compounds, the essential step of sample treatment is extraction with an appropriate organic solvent or a mixture of solvents. Extraction techniques are most often used for the isolation and enrichment of analytes in food and environmental samples. Conventional Soxhlet extraction is a primary option for HBCD determination, as well as for other organic food contaminants – this has been well summarized [43–46]. The need to decrease the time of extraction and solvent consumption has resulted in the introduction of other extraction methods, e.g. accelerated solvent extraction (ASE) [47], supercritical fluid extraction (SFE) [48], microwave-assisted extraction (MAE) [49], and ultrasound-assisted extraction (UAE) [50]. The major advantage of these techniques is the possibility of extracting multiple samples simultaneously. ASE (DIONEX, Thermo Scientific) [51] is a pressurized fluid extraction (PFE) technique carried out under increased pressure and at higher temperatures, this results in a short extraction time and more favorable

kinetics of extraction [52]. In SFE, the fluid introduced into the sample exhibit solubilities similar to organic solvents [53]. MAE is typically carried out in a sealed Teflon vessel (a bomb) at high temperatures. A variety of solvents may be used [54–55]. To perform UAE, the sample is placed in a glass or metal vessel and inserted into an ultrasonic bath [56–57].

2.2. Clean-up methods

The co-extraction of interfering matrix components is an inherent difficulty in the extraction of food samples. It is therefore necessary to apply additional purification methods. The most commonly used clean-up methods are: gel permeation chromatography (GPC); dialysis with semipermeable membranes (SPM); multi-layer silica gel column [42]. GPC, also known as size exclusion chromatography (SEC), is an effective technique for the separation of components in a solution, based on their molecular size (hydrodynamic volume) [58]. GPC is often used for polymer analysis, however, this technique is also useful in analytical chemistry for separation of analyte from lipids. The authors [37, 45, 59] indicated that GPC does not sufficiently remove the lipids from food samples, therefore, other sample purification steps are required. For this purpose, treatment with modified silica gel [59, 60] or florisil [61] has been applied after GPC clean-up. The application of SPM as a clean-up technique for high fat food samples is based on dialysis [62, 63] and is a simple approach for analyte isolation. The future purification witch silica gel is required [63].

2.3. Detection methods

Both gas chromatography (GC) and liquid chromatography (LC) methods were used for the determination of HBCD. However, the separation of isomers is possible only by using LC [64–66]. Determination of individual HBCD isomers by GC is not feasible due

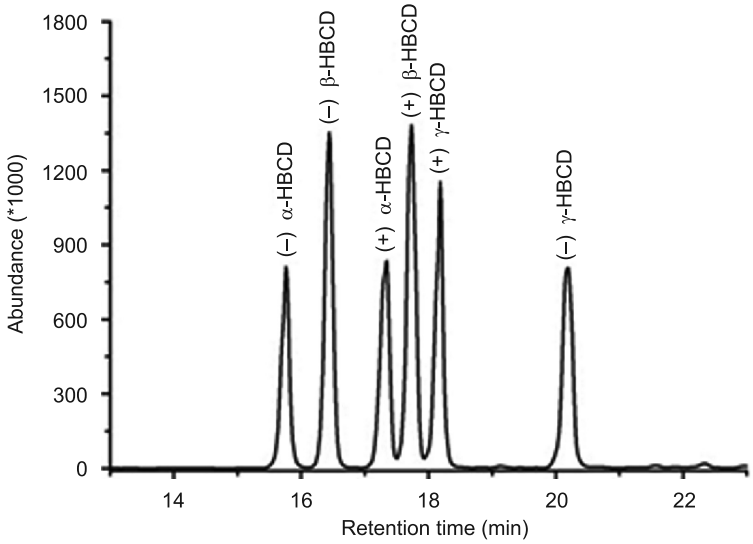

Fig. 3. LC-MS chromatogram of the (±)α-HBCD, (±)β-HBCD and (±)γ-HBCD enantiomers [60]

to the thermal inter-conversion of HBCD isomers at 160°C [20], decomposition of this compound at 240°C [67] and partial breakdown in dirty GC systems [68].

The research of two inter-laboratory studies for comparison of GC-MS and LC-MS application for HBCD determination shown no statistically significant differences between results obtained with both methods [66]. Exemplary chromatogram of the HBCD enantiomers is shown in Fig. 3.

A sensitive LC-MS method coupled with ESI ionization source with LOD of 4–6 pg for γ-HBCD standard solution had been developed [70] and subsequently optimized [34] resulting in LOD of 0.5 pg for γ-HBCD standard solution and 5 pg for fish extracts. With this method, a SRM transition of deprotonated molecular ion [M–H]− (*m*/*z* 640.6) to bromine ion [Br]− (*m*/*z* 79 and 81) was observed. However, inability of monitoring of this transition using a single quadrupole MS was noticed [71], which is due to the cut--off value of the instrument is higher than daughter ion m/z ratio. Although the decreased response at *m*/*z* 676.7 [M + Cl H]− originating from a chlorine adduct was reported [71], the authors [63] applied ion monitoring based on two SRM transitions simultaneously – the quantitative [M + Cl–H]− → [M–H]− and the confirmative [M–H]− → [Br]−, resulting with S/N ratio ≥ 3 and 1 pg/g fresh weight of fish tissue for individual HBCD isomers and more than 0.997 for the correlation factors of the linear regression line for both the quantitative and confirmative SRM transitions.

3. Conclusions

A dramatic growth in HBCD production and usage is observed. Therefore, the levels of this compound in the environment have increased. Due to the fact that HBCD is a potential hazard to aquatic environments and humans, the monitoring of this contaminant in the environment and food chain is highly advisable.

Most of the analytical methods for food sample preparation and the determination of HBCD are similar to those of POPs. Typically, HBCD is extracted from the sample, the extract is then purified and concentrated. The final analysis is most frequently done by LC-MS techniques coupled with an ESI ion source. The GC-MS technique may also be applied, however, separation of HBCD isomers is only possible by using LC-MS.

Currently, the challenge for researchers is to reduce the time-consuming procedures and solvent consumption. This is achieved by developing new or modifying existing analytical methods.

References

[1] Marvin C.H., Tomy G.T., Armitage J.M., Arnot J.A., McCarty L., Covaci A., Palace V., *Hexabromocyclododecane: Current understanding of chemistry, environmental fate and toxicology and implications for global management*, Environmental Science & Technology, vol. 45, 2011, 8613-8623.

[2] Smith K., Liu C-H., El-Hiti G.A., Kang G.S., Jonas E., Clement S.G., Checquer A.D., Howarth O.W., Hursthouse M.B., Coles S.J., *An extensive study of bromination of cis, trans-1,5,9-cyclododecatriene: product structures and conformations*, Organic & Biomolecular Chemistry, vol. 3, 2005, 1880-1892.

[3] Heeb N.V., Schweizer W.B., Kohler M., Gerecke A.C., *Structure elucidation of hexabromocyclododecanes – a class of compounds with a complex stereochemistry*, Chemosphere, vol. 61, 2005, 65-73.
[4] Heeb N.V., Schweizer W.B., Mattrel P., Haag R., Gerecke A.C., Kohler M., Schmid P., Zennegg M., Wolfensberger M., *Solid-state conformations and absolute configurations of (+) and (–) α-, β-, and γ-hexabromocyclododecanes (HBCDs)*, Chemosphere, vol. 68, 2007, 940-950.
[5] Arsenault G., Konstantinov A., Marvin C.H., MacInnis G., McAlees A., McCrindle R., Riddell N., Tomy G.T., Yeo B., *Synthesis of the two minor isomers, delta- and epsilon-1,2,5,6,9,10-hexabromocyclododecane, present in commercial hexabromocyclododecane*, Chemosphere, vol. 68, 2007, 887-92.
[6] Troitzsch J., *Overview of flame retardants*, Chimica Oggi/Chemistry Today, vol. 16, 1998, 1-19.
[7] Priority Existing Chemical Assessment Report No. 34 Hexabromocyclododecane, Sydney 2012.
[8] TemaNord 2008:520. Hexabromocyclododecane as a possible global POP, Copenhagen 2007.
[9] Proposal for Harmonised Classification and Labelling Based on the CLP Regulation (EC) No 1272/2008, Annex VI, Part 2. Hexabromocyclododecane, Swedish Chemicals Agency 2009.
[10] ECHA European Chemical Agency. Doc:ED/67/2008, *Inclusion of substances of very high concern in candidate list*, Helsinki, 28 October 2008.
[11] ACCBFRIP American Chemistry Council Brominated Flame Retardant Industry Panel, 2005, *HPV data summary and test plan for hexabromocyclododecane (HBCD)*, CAS No. 3194556, 20 December 2001, Updated March 2005, Arlington (VA).
[12] BSEF Bromine Science and Environmental Forum. Factsheet, Brominated Flame Retardant, Hexabromocyclododecane, October 2012.
[13] EUMEPS Healthy building with EPS, Belgium, August 2002.
[14] EUMEPS Behavior of EPS in case of fire, Belgium, August 2002.
[15] de Wit C.A., *An overview of brominated flame retardants in the environment*, Chemosphere, vol. 46, 2002, 583-624.
[16] Remberger M., Sternbeck J., Palm A., Kaj L., Strömberg K., Brorström-Lundén E., *The environmental occurrence of hexabromocyclododecane in Sweden*, Chemosphere, vol. 54, 2004, 9-21.
[17] Kajiwara N., Sueoka M., Ohiwa T., Takigami H., *Determination of flame-retardant hexabromocyclododecane diastereomers in textiles*, Chemosphere, vol. 74, 2009, 1485-1489.
[18] Vilaplana F., Karlsson P., Ribes-Greus A., Ivarsson P., Karlsson S., *Analysis of brominated flame retardants in styrenic polymers: Comparison of the extraction efficiency of ultrasonication, microwave-assisted extraction and pressurised liquid extraction*, Journal of Chromatography A, vol. 1196–1197, 2008, 139-146.
[19] de Wit C.A., Herzke D., Vorkamp K., *Brominated flame retardants in the Arctic environment – trends and new candidates*, Science of the Total Environment, vol. 408, 2010, 2885-2918.
[20] Peled M., Scharia R., Sondack D., *Thermal rearrangement of hexabromocyclododecane (HBCD)*, [in] Advances in Organobromine Chemistry II. Ed., Desmurs J-R., Gérard B. and Goldstein MJ. Elsevier, Amsterdam 1995, 92-99.
[21] Great Lakes Chemical Corporation, *Material Safety Data Sheet. Great Lakes CD-75-P, CD-75PM and CD-75PC*, West Lafayette (IN): Great Lakes Chemical Corporation. MSDS Number: 00177. Effective Date: 10/14/2005.
[22] Stenzel J.I., Nixon W.B., *Hexabromocyclododecane (HBCD): Determination of the vapor pressure using a spinning rotor gauge*, Wildlife international Ltd. 1997, Easton, Maryland. 439C-117, pp. 44.

[23] EBFRIP European Brominated Flame Retardant Industry Panel. 2004a, *Determination of water solubility of hexabromocyclododecane (HBCD) using a generator column method*, Easton (MD): Wildlife International, Ltd. Project No. 439C-138.

[24] Veith G.D., DeFoe D.L., Bergstedt B.V., *Measuring and estimating the bioconcentration factor of chemicals in fish*, Journal of the Fisheries Research Board of Canada, vol. 36, 1979, 1040-1048.

[25] Hayward S.J., Lei Y.D., Wania F., *Comparative evaluation of three HPLC-based KOW estimation methods for highly hydrophobic organic compounds: polybrominated diphenyl ethers and hexabromocyclododecane*, Environmental Toxicology and Chemistry, vol. 25, 2006, 2018-2027.

[26] EUROPEAN CENTRE FOR ENVIRONMENT AND HEALTH BONN OFFICE *Hazard assessment: five substances proposed for POPs protocol of CLRTAP*, 13th Meeting of the Task Force on Health in Bonn, April 2010.

[27] ECB – SUMMARY FACT SHEET PBT WORKING GROUP – PBT LIST NO. 58, *Results of the evaluation of the PBT/VPVB properties of hexabromocyclododecane*, 1st Draft, March, 2008.

[28] Alaee M., Arias P., Sjödin A., and Bergman A., *An overview of commercially used brominated flame retardants, their applications, their use patterns in different countries/regions and possible modes of release*, Environment International, vol. 29, 2003, 683-689.

[29] Covaci A., Gerecke A.C., Law R.J., Voorspoels S., Kohler M., Heeb N.V., Leslie H., Allchin C.R., and De Boer J., *Hexabromocyclododecanes (HBCDs) in the environment and humans: a review*, Environmental Science & Technology, vol. 40, 2006, 3679-3688.

[30] de Wit C.A., Alaee M., Muir D.C.C., *Levels and trends of brominated flame retardants in the Arctic*, Chemosphere, vol. 64, 2006, 209.

[31] Kohler M., Zennegg M., Bogdal C., Gerecke A.C., Schmid P., Heeb N.V., Sturm M., Vonmont H., Kohler H.P., Giger W., *Temporal trends, congener patterns, and sources of octa-, nona-, and decabromodiphenyl ethers (PBDE) and hexabromocyclododecanes (HBCD) in Swiss lake sediments*, Environmental Science & Technology, vol. 42, 2008, 6378- 6384.

[32] Thomsen C., Froshaug M., Broadwell S.L., Becher G., *Brominated flame retardants in breast milk from Norway*, Organohalogen Compound, vol. 67, 2005, 509-512.

[33] Thomsen C., Stigum H., Froshaug M., Broadwell S.L., Becher G., Eggesbo M., *Determinants of brominated flame retardants in breast milk from a large scale Norwegian study*, Environment International, vol. 36, 2010, 68-74.

[34] Janak K., Covaci A., Voorspoels S., Becher G., *Hexabromocyclododecane in marine species from the Western Scheldt Estuary: diastereoisomer- and enantiomer-specific accumulation*, Environment Science & Technology, vol. 39, 2005, 1987-1994.

[35] Law R.J., Herzke D., Harrad S., Morris S., Bersuder P., Allchin C.R., *Levels and trends of HBCD and BDEs in the European and Asian environments with some information for other BFRs*, Chemosphere, vol. 73, 2008, 223-241.

[36] Shaw S.D., Berger M.L., Brenner D., Kannan K., Lohmann N., Papke O., *Bioaccumulation of polybrominated diphenyl ethers and hexabromocyclododecane in the northwest Atlantic marine food web*, Science of the Total Environment, vol. 407, 2009, 3323-3329.

[37] Nakagawa R., Murata S., Ashizuka Y., Shintani Y., Hori T., Tsutsumi T., *Hexabromocyclododecane determination in seafood samples collected from Japanese coastal areas*, Chemosphere, vol. 81, 2010, 445-452.

[38] Rawn D.F.K., Sadler A., Quade S.C., Sun W.F., Lau B.P., Kosarac I., Hayward S., Ryan J.J., *Brominated flame retardants in Canadian chicken egg yolks*, Food Additive & Contaminants: part A, vol. 28, 2011, 807-815.

[39] Hu D., Hu X., Li J., Wang P., Guo S., *Determinations of hexabromocyclododecane (HBCD) isomers in plastic products from china by LC-MS/MS*, Journal of Liquid Chromatography & Related Technologies, vol. 35, 2012, 558-572.
[40] Xu W., Wang X., Cai Z., *Analytical chemistry of the persistent organic pollutants identified in the Stockholm Convention: A review*, Analytica Chimica Acta, vol. 790, 2013, 1-13.
[41] Namieśnik J., *Jakość wyników analitycznych*, [in] *Ocena i kontrola jakości wyników pomiarów analitycznych*, Wydawnictwo Naukowo-Techniczne, Warszawa 2007.
[42] Curren M.S.S., King J.W., *Chapter 25: Sampling and sample preparation for food analysis*, [in] *Comprehensive Analytical Chemistry XXWIZ*, J. Pawliszyn (Ed.) 2002 Elsevier Science B.V.
[43] Luque de Castro M.D., Priego-Capote F., *Soxhlet extraction: Past and present panacea*, Journal of Chromatography A, vol. 1217, 2010, 2383-2389.
[44] US EPA (1996), Method 3540C: soxhlet extraction.
[45] Frederiksen M., Vorkamp K., Svensmark B., *Method development for simultaneous analysis of HBCD, TBBPA, and dimethyl-TBBPA in marine biota from Greenland and the Faroe Islands*, International Journal of Environmental Analytical Chemistry, vol. 87, 2007, 1095-1109.
[46] Hu X., Hu D., Song Q., Li J., Wang P., *Determinations of hexabromocyclododecane (HBCD) isomers in channel catfish, crayfish, hen eggs and fish feeds from China by isotopic dilution LC-MS/MS*, Chemosphere, vol. 82, 2011, 698-707.
[47] US EPA (2007). Method 3545A: pressurized fluid extraction (PFE).
[48] US EPA (2007). Method 3562: supercritical fluid extraction of polychlorinated biphenyls (PCBs) and organochlorine pesticides.
[49] US EPA (2007). Method 3546: microwave extraction.
[50] US EPA (2007). Method 3550C: ultrasonic extraction.
[51] Accelerated Solvent Extraction (ASE®) Sample Preparation Techniques for Food and Animal Feed Samples, Technical Note 209, DIONEX, ThermoSc.
[52] Haukås M., E.Mariussena, Ruus A., Tollefsen K.E., *Accumulation and disposition of hexabromocyclododecane (HBCD) in juvenile rainbow trout (Oncorhynchus mykiss)*, Aquatic Toxicology, vol. 95, 2009, 144-151.
[53] Altwaiq A., Wolf M., van Eldik R., *Extraction of brominated flame retardants from polymeric waste material using different solvents and supercritical carbon dioxide*, Analytica Chimica Acta, vol. 491, 2003, 111-123.
[54] Eskilsson C.S., Björklund E., *Analytical-scale microwave-assisted extraction*, Journal Chromatography A, vol. 902, 2000, 227-250.
[55] Ganzler K., Salgo A., Valko K., *Microwave Extraction: A Novel Sample Preparation Method for Chromatography*, Journal of Chromatography, vol. 371, 1986, 299-306.
[56] Tadeo J.L., Sánchez-Brunete C., Albero B., García-Valcárcel A.I., *Application of ultrasound--assisted extraction to the determination of contaminants in food and soil samples*, Journal of Chromatography A, vol. 1217, 2010, 2415-2440.
[57] Luque-Garcia J.L., Luque de Castro M.D., *Ultrasound: a powerful tool for leaching*, Trends in Analytical Chemistry, vol. 22, 2003, 41-47.
[58] Moore J.C., *Gel permeation chromatography. I. A new method for molecular weight distribution of high polymers*, Journal of Polymer Science, vol. 2, 1964, 835-843.
[59] Kuc J., Grochowalski A., *Isolation of hexabromocyclododecane from fat matrix using size exclusion chromatography*, Czasopismo Techniczne, 2-Ch/2012.
[60] Gómara B., Lebrón-Aguilar R., Quintanilla-Lópezb J.E., González M.J., *Development of a new method for the enantiomer specific determination of HBCD using an ion trap mass spectrometer*, Analytica Chimica Acta, vol. 605, 2007, 53-60.
[61] Esslinger S., Becker R., Jung C., Schröter-Kermani C., Bremser W., Nehls I., Chemosphere, vol. 83, 2011, 161-167.

[62] Bergqvist P.-A., Strandberg B., Bergek S., Rappe C., *Lipid reduction during the analyses of PCDDs, PCDFs and PCBs in environmental samples using semipermeable membrane technique*, Organohalogen Compounds, 11, 1993, 41-44.

[63] Kuc J., Grochowalski A., Mach S., Placha D., *Level of hexabromocyclododecane isomers in the tissue of selected commonly consumed fish in Central European countries*, Acta Chromatografica DOI:10.1556/AChrom.26.2014.4.1 online preview.

[64] Schecter A., Szabo D.T., Miller J., Gent T.L., Malik-Bass N., Petersen M., Paepke O., Colacino J.A., Hynan L.S., Harris T.R., Malla S., Birnbaum L.S., *Hexabromocyclododecane (HBCD) Stereoisomers in U.S. Food from Dallas, Texas*, Environ Health Perspective, vol. 120, 2012, 1260-1264.

[65] Frederiksen M., Vorkamp K., Bossi R., Svensmark B., *Analysis of HBCD and TBBPA by GC-MS versus LC-MS-MS – indications of systematic differences in obtained results*, 4th International Symposium On Flame Retardants BRF2007, Amsterdam, Netherlands 2007.

[66] Haug L.S., Thomsen C., Liane V.H., and Becher G., *Comparison of GC and LC determinations of hexabromocyclododecane in biological samples – results from two interlaboratory comparison studies*, Chemosphere, vol. 71, 2008, 1087-1092.

[67] Barontini F., Cozzani V., Cuzzola A., Petarca L., *Investigation of hexabromocyclododecane thermal degradation pathways by gas chromatography/mass spectrometry*, Rapid Communication of Mass Spectrometry, vol. 15, 2001, 690-698.

[68] Covaci A., Voorspoels S., de Boer J., *Determination of brominated flame retardants, with emphasis on polybrominated diphenyl ethers (PBDEs) in environmental and human samples – A review*, Environment International, vol. 29, 2003, 735-756.

[69] Guerra P., Eljarrat E., Barceló D., *Determination of halogenated flame retardants by liquid chromatography coupled to mass spectrometry*, Trends in Analytical Chemistry, vol. 30, 2011, 842-855.

[70] Budakowski W., Tomy G., *Congener-specific analysis of hexabromocyclododecane by high-performance liquid chromatography/electrospray tandem mass spectrometry*, Rapid Communication of Mass Spectrometry, vol. 17, 2003, 1399-1404.

[71] Morris S., Bersuder P., Allchin C.R., Zegers B., Boon J.P., Leonards P.E.G., de Boer J., *Determination of the brominated flame retardant, hexabromocyclododecane in sediment and biota by liquid chromatography electrospray ionisation mass spectroscopy*, Trends in Analytical Chemistry, vol. 25, 2006, 343-349.

TECHNICAL TRANSACTIONS | **CZASOPISMO TECHNICZNE**
CHEMISTRY | CHEMIA
1-Ch/2014

BEATA KWASEK*, DARIUSZ BOGDAŁ*

THE USE OF HYALURONIC ACID IN THE TREATMENT OF OSTEOARTHRITIS OF KNEE CARTILAGE

ZASTOSOWANIE KWASU HIALURONOWEGO W LECZENIU CHOROBY ZWYRODNIENIOWEJ STAWU KOLANOWEGO

Abstract

The aim of this paper is to describe the possibilities of the therapeutic use of hyaluronic acid (HA) in the treatment of osteoarthritis of knee cartilage. This work provides an overview of the literature relating to the structure of hyaluronic acid, its properties and important functions of the human body. Moreover, the construction of the articular cartilage in the knee joint, including events leading to its degeneration, is presented. Viscosupplementation is a treatment for osteoarthritis involving several intra-articular injections of HA at specific time intervals. This treatment results in an increased lubricity, viscosity and elasticity of articular cartilage. Since HA is found naturally in the human body, viscosupplementation improves the biomechanical conditions of the joint whilst minimizing the side-effects of treatment. Hyaluronic acid occurs naturally in a linear form, but for many applications, chemical modifications are necessary. Thanks to this property, it remains in the body long enough to produce the desired therapeutic effect. Modification processes, in particular the cross-linking of HA, increase the mechanical properties of knee cartilage. HA is an example of a new kind of tissue engineering scaffold that is bioactive in both full-length and degraded forms. In turn, hydrogel scaffolds with interpenetrating polymeric network (IPN) gels can simulate the structure of the native extracellular matrix of cartilage tissue.

Keywords: *hyaluronic acid, knee cartilage, osteoarthritis, viscosuplementation, interpenetrating polymer network (IPNs), scaffolds*

Streszczenie

Celem badań jest przedstawienie możliwości terapeutycznego zastosowania kwasu hialuronowego w leczeniu choroby zwyrodnieniowej chrząstki stawu kolanowego. Praca zawiera przegląd literatury dotyczący struktury kwasu hialuronowego, jego właściwości oraz ważnych funkcji jakie pełni w ludzkim organizmie, ponadto budowy chrząstki stawowej w stawie kolanowym oraz czynników prowadzących do jej degeneracji. Wiskosuplementacja jest metodą leczenia osteoporozy polegającą na dostawowych wstrzyknięciach tego biopolimeru w określonych odstępach czasu oraz kilkakrotnych powtórzeniach. Leczenie zwiększa lepkość oraz elastyczność chrząstki stawowej, która jest lepiej odżywiana. Wiskosuplementacja poprawia warunki biomechaniczne stawu, co więcej kwas hialuronowy występuje naturalnie w organizmie człowieka, w ten sposób pomaga zminimalizować skutki uboczne leczenia. W naturalnej postaci kwas hialuronowy występuje w postaci liniowej, ale w wielu zastosowaniach konieczna jest jego modyfikacja chemiczna. Dzięki tej właściwości pozostaje w organizmie na tyle długo, aby wywołać pożądany efekt terapeutyczny. Procesy modyfikacji, w szczególności sieciowanie kwasu hialuronowego zwiększa właściwości mechaniczne materiału. Badania potwierdzają, że hydrożelowe rusztowania z wzajemnie przenikającymi się sieciami polimerowymi (IPNs) mogą symulować strukturę natywną macierzy zewnątrzkomórkowej chrząstki.

Słowa kluczowe: *kwas hialuronowy*, *chrząstka kolanowa*, *osteoporoza*, *wiskosuplementacja*, *IPNs, rusztowania*

* Prof. Ph.D. Eng. Dariusz Bogdał, M.Sc. Eng. Beata Kwasek, Chair of Biotechnology and Physical Chemistry, Faculty of Chemical Engineering and Technology, Cracow University of Technology.

1. Introduction

Hyaluronic acid (HA) is a polysaccharide composed of repeating disaccharide units containing D-glucuronic acid and N-acetyl-D-glucosamine alternating β-(1-4) and β-(1-3) glycosidic bonds (Fig. 1).

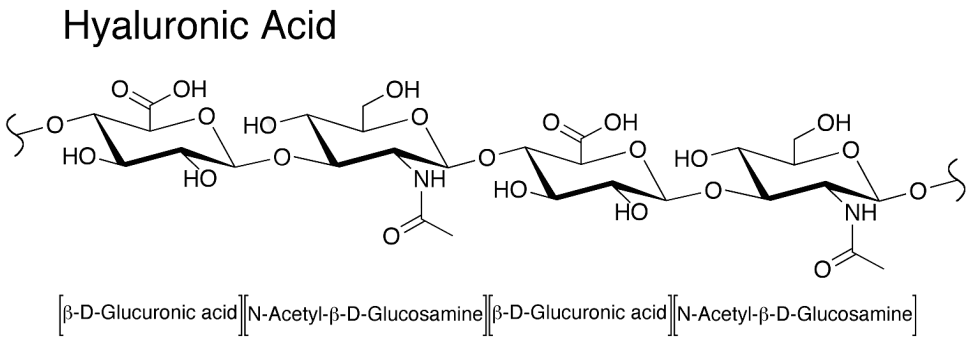

Fig. 1. Structure of hyaluronic acid

HA is a biopolymer which is present in all living organisms and is the largest group of compounds that has the same chemical structure in bacteria and in humans. In animal organisms, hyaluronic acid is synthesized by the cell membrane with hyaluronates synthase, which is involved in connecting alternating glucuronic acid and N-acetylglucosamine molecules. Hyaluronic synthase has a high level of activity, which allows the synthesis of 100 monosaccharide molecules per second under in vitro conditions. There are three different types of hyaluronic synthase: Has 1, Has 2 and Has 3. Has 3 is the most active, able to polymerize large amounts of HA of up to 2×10^5 Da. Hyaluronic acid is present in human skin, cartilage, synovial fluid, the corpus vitreous of the eye, the kidneys, the brain, umbilical cord tissue, urine and serum [1]. Table 1 shows the amount of HA in various parts of the human body.

Table 1

Quantities of hyaluronic acid in human body parts

Locus in the human body	Hyaluronic acid content
an adult weighing 70 kg	15 g HA
dermis	200–500 ug/ml HA
human umbilical cord	4100 ug/ml
synovial fluid of the joint capsule	1400–3600 ug/ml
corpus vitreous of the eye	190- 320 ug/ml
epidermis	100 ug/ml

The amount of hyaluronic acid in the body is dependent upon age – the greatest concentration is in the skin of infants and children, and the smallest, for people over 50 years of age (Fig. 2). The concentration of HA is also dependent on the season – UV

photodegradation is the process leading to photoaging of the skin in the summer, of which the physical symptoms are dry skin and wrinkles. An important property of HA is its high water binding capacity and retention. A single HA molecule is able to bind 200–500 water molecules. Another very important feature of HA is its 'biocompatibility', which means that it does not cause adverse reactions in the body because it naturally occurs in the skin and can be completely absorbed by the body [2]. Figure 2 shows the level of HA in connective tissue.

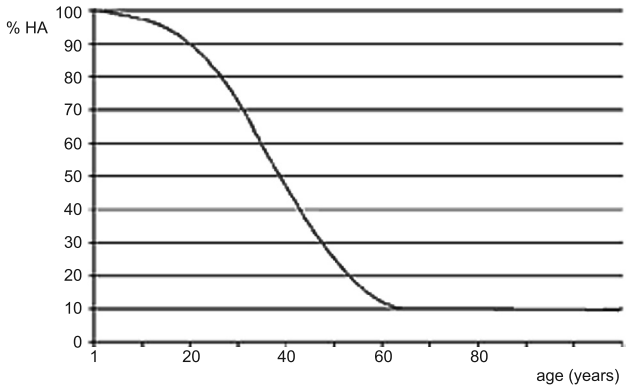

Fig. 2. The level of hyaluronic acid in connective tissue

HA plays an important role in connective tissue, it acts as a matrix. HA helps to keep the skin hydrated and flexibile and protects the retina. HA also affects homeostasis, together with vasopressin, it regulates the reabsorption of water into the spinal cord. An important function of HA is to maintain the connection between the mother and the fetus, the facilitation of the oocyte release during ovulation, the increasing of sperm motility and fertilization efficiency. HA affects a number of processes including the induced expression of cytokines, the stimulation of immune and angiogenic processes. A very important function of HA is its participation in chondrogenesis and providing adequate lubrication of joints which reduces the friction between the moving bones, thereby decreasing the process of osteoarthritis [3].

Articular cartilage is a complex tissue that covers the surfaces in contact with each bone, prevents abrasion and facilitates slippage. Its role is to provide free and accurate movement in the joint [4].

Articular cartilage tissue is alive, resilient, resistant to mechanical stress and has little regenerative capacity. This cartilage is composed of chondrocytes i.e. only cells found in cartilage that produce and maintain the cartilaginous matrix by producing collagen and proteoglycans. In articular cartilage, four basic layers can be distinguished, each with varying amounts of collagen and water (Fig. 3). Zone 1 is called the surface layer and displays the most stiffness. Zone 2 is an intermediate zone, where cells are randomly distributed and have a more spherical shape. Chondrocytes arranged in columns perpendicular to the articular surface are grouped on Zone 3. Zone 4 is the deepest, calcified, and is adjacent to the subchondral bone. Synovial fluid nourishes the articular cartilage. The necessary condition for the proper nutrition of cartilage is the movement and loading of articular surface. Chondrocytes are supplied with oxygen and nutrients from the synovial fluid by diffusion.

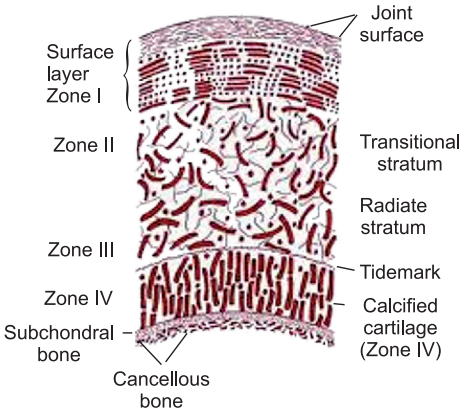

Fig. 3. Articular cartilage matrix

Water makes up about 75% of cartilage – the highest concentration of water is in the deeper layers of the cartilage. The pressure of hydrostatic compression of cartilage causes the extrusion of a small amount of water which forms a layer and reduces friction in the joint.

Other components of the articular cartilage that provides durability and low friction are collagen protein (60% dry weight) and proteoglycan aggregates (30% dry weight). Chondrocytes are sensitive to mechanical stimuli, growth factors, cytokines and receptors. Chondrocytes secrete both the matrix components and the enzymes degrading it. They are responsible for the homeostasis of the cell. Cartilage proteoglycans consist of a protein core to which are attached glycosaminoglycans. This cartilage proteoglycan chondroitin sulfate A, C, and keratan sulfate are important aggrecans capable of binding to HA [5]. Figure 4 shows the appearance of a healthy knee joint in comparison to a degenerate knee joint.

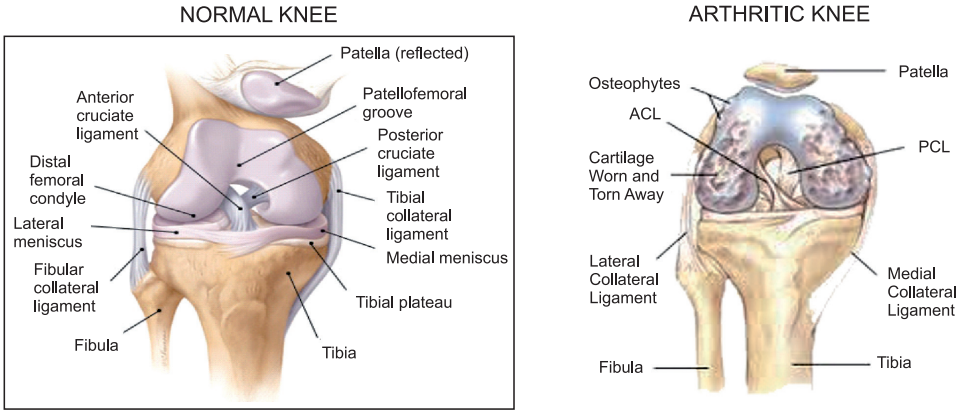

Fig. 4. Healthy knee joint in comparison to degenerate knee joint

Knowledge of the structure and physiology of cartilage allows for understanding the pathomechanisms responsible for the destruction in the course of injury, degenerative

diseases and autoimmune diseases. Degeneration of articular cartilage is a growing problem of civilization. Until recently, the disease was characteristic of old age. Nowadays, more young patients receive medical consultation due to joint pain. The causes of degenerative changes can be: multiple injuries (sports, work); microfractures; chronic stress caused by impaired limb axis; instability or damage to the meniscus; ligamentous instability; rheumatism; obesity [6]. These processes destroy the joints. The disease causes the abnormal changes in synovial fluid, the increased friction of the articular surfaces or the destruction of cartilage. Due to the depth and nature of the damage, articular cartilage is the third most common disease in Central and Eastern Europe (after the ischemic heart disease and vascular diseases of the brain). It usually occurs in the range of 45 to 59 years of age (WHO, 1989), and the other in Western Europe (after the ischemic heart). The prevalence of this condition in the population by age is as follows: under 25 years of age – 4%; under 35 years of age – 5%; over 65 years of age – 70%; in the range 75–79 years – 85%. In Poland, it is estimated that about 8 million people have damage to articular cartilage – 40 % relates to hip and 25% is degeneration of knee joints [8, 9]

Prevention of degradative changes of articular cartilage is possible in early stage. Articular cartilage and synovial fluid cushion the joint. Properties of HA act on smooth movements in all joints, increasing the viscosity of the synovial fluid. Due to the presence of HA, joints are better hydrated, nourished and avoid the release of free radicals.

Research shows that human synoviocytes derived from degenerative arthritis which were incubated with the exogenous HA, synthesize larger amounts of HA and of a higher molecular weight [10].

2. Intra-articular injections of HA

The human body contains approximately 15 grams of pure HA produced by synovial cells. Its defects are increasingly replaced by a synthetic counterpart, introduced by intra--articular injection. Viscosupplementation is a method which consists of intra-articular HA supplementation administered every seven days, and repeated three to five times [11]. This is a common treatment which has been used for over 20 years for osteoarthritis [12–17]. Many studies confirm the effectiveness of viscosupplementation [18–37]. This treatment increases the viscosity and flexibility of synovial fluid [38]. For clinical use, a number of derivatives of HA are available. They are characterized by different molecular weights and viscosities depending upon their source (e.g. rooster combs or hyaluronans secreted by streptococci). Sodium hyaluronan (Hyalgan, Sanofi Synthelabo Inc., New York, NY), and hylan GF-20 (Synvisc, Wyeth-Ayerst Pharmaceuticals, Philadelphia, PA) are available in the United States [29]. Positive effects were observed within 7–14 months of three intra-articular Hylan GF-20 injections using one hundred and fifty-five patients (male and female) with knee osteoarthritis [39]. Hyalgan is a viscous solution of the sodium salt of HA with a molecular weight of between 500.000 and 730.000 Da, it is a highly purified fraction of natural sodium hyaluronate. Synvisc is chemically cross-linked with formaldehyde and vinyl sulfone; its average molecular weight is 6.000.000 Da. Hyalgan has been most commonly administered in a cycle comprising five injections over a 4-week period. More recently, approval has been

given by the Food and Drug Administration (FDA) for a three-injection series. Synvisc is used in a course of one injection weekly for a total of three weeks.

Fig. 5 shows the effect of the Ortovisc preparation for knee pain during 27 weeks of therapy the treatment of osteoarthritis [40].

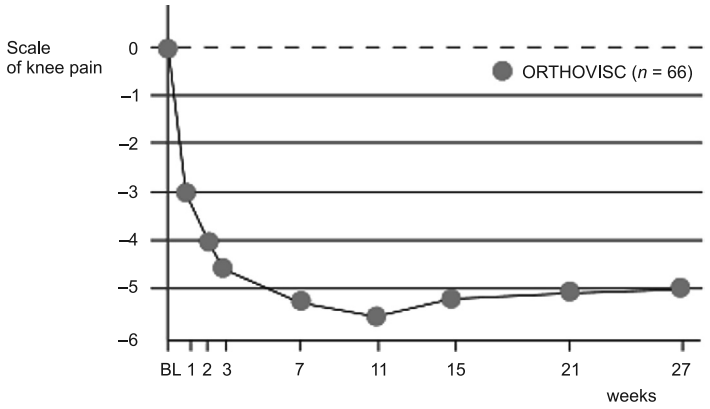

Fig. 5. Orthovisc treatment preparation

The effect of HA on the course of osteoarthritis was identified after clinical trials on patient suffering from this disease. One group of patients was injected with intra-molecular weight hyaluronic acid and the other group receiving a placebo [41, 42]

The study was conducted on 301 patients, who received HA and placebo. Of patients aged over 45 years, 84% were women. The treatment lasted 40 months and involved four cycles of five injections of 2,5 ml 1% solution of HA with a molecular weight of 900 kDa into the knee joint.

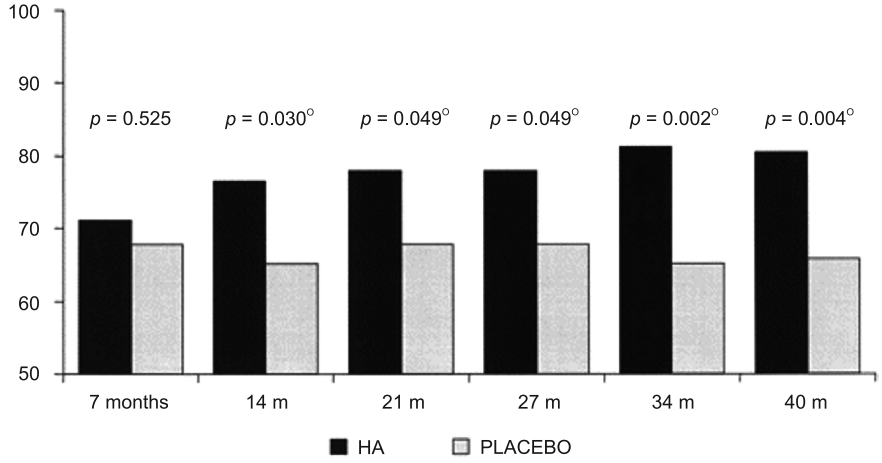

Fig. 6. 40 months of therapy with HA and placebo (Osteoarthritis Research Society International, 2004)

According to the criteria OARSI 2004 – 22% higher response in patients treated with HA (Fig. 6). In general, the clinical results showed that viscosupplementation with hyaluronic acid is most effective in patients aged over 65 years [44–51].

3. Chemical modification of hyaluronic acid

HA is subjected to a process of linear and crosslinking modifications by forming covalent bonds between molecules of HA. Modified HA is less susceptible to chemical and enzymatic degradation, which allows it to remain in the body long enough to produce the desired therapeutic effect [52]. Modification processes, in particular the cross-linking of HA, also enhance the mechanical properties of the material. Chemical modifications typically involve hydroxyl and carboxyl groups of the polymer.

Alkylation of the ammonium salt of hyaluronic acid with an alkyl halide in a solution of DMF leads to the formation of esterified HA biomaterials. Esterification reactions involve carboxylate moieties of the polymer. The degree of esterification affects the size of the hydrophobic patches and forms a stable, rigid chain network polymer more resistant to enzymatic degradation under physiological conditions. Esters of HA are the most utilized derivatized HA products.

These products are applied to the growth of chondrocytes and bone marrow derived mesenchymal cells for the repair of cartilage and bone defects.

Crosslinking HA is necessary to obtain implantable hydrogel with controlled degradability and mechanical properties. Crosslinking hydrogels is the most common modification of HA [52]. Crosslinking (binding a polymer with other polymers) of the hyaluronic acid results in its stability and extends the natural degradation [53]. Degradation of crosslinked HA in the body lasts for several months, whereas the degradation of non-crosslinked HA takes a few hours. Viscosity of the crosslinked HA increases and depends on the degree of cross-linking between the chains of HA. Thanks to this property remain in the body long enough to produce the desired therapeutic effect.

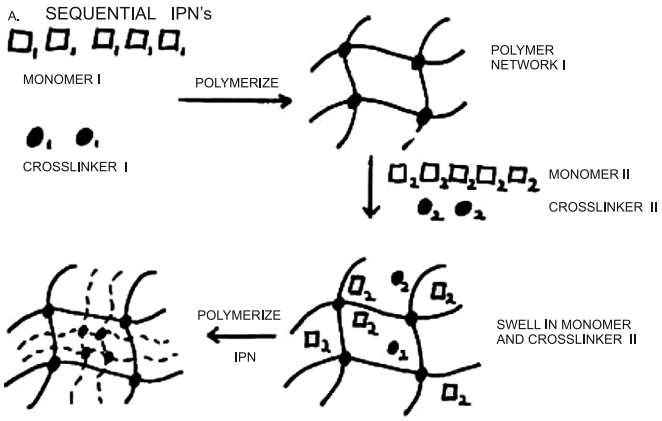

Fig. 7. Basic synthesis methods for IPNs.

An interpenetrating polymer network, IPN, is defined as a blend of two or more polymers in a network form. Figure 7 shows the synthesis method of IPNs.

Hydrogels of collagen/chondroitin sulfate/hyaluronan interpenetrating polymer network were used for cartilage tissue engineering [54].

The task of tissue engineering is the development of substitutes for damaged tissue by creating three-dimensional scaffolds with living cells and bioactive molecules, which allow the proliferation and differentiation of cells. These structures can be created by seeding cells within the scaffold or by the injection of cells into the damaged tissue. Injectable scaffolds have been used to repair articular cartilage. Injectable biocompatible and biodegradable scaffolds derived from chitosan and oxidized hyaluronic acid [55] and injectable hydrogel made from methacrylated glycol chitosan (MeGC) and photocrosslinking HA with a ryboflavin photoinitiator under visible light were found to be very good options for cartilage repair [56].

Lisognoli investigated human mesenchymal stromal (MSCs) cells in a hyaluronian-based polymer scaffold (Hyaff ®-11) by electron microscopy techniques, immunohistochemistry and real time PCR. There was a significant proliferation of cells TGFβTGFβ MSCs and increased expression of collagen type II, IX within 21 days.

Hyaff-11 was also used as scaffolding for cartilage defects [57–61]. Autocrosslinked polysaccharide (ACP) polymers are inter and intra-molecular esters of hyaluronan (HA) where part of the carboxyl group is esterified with hydroxyl groups of the same or different molecules of polysaccharides. The autocross-linked polymer (ACPTM, Fidia) is used as a scaffold for the repair of tissue defects. This biomaterial has been used as a scaffold and showed faster regeneration of tissue defects than Hyaff 11 [62].

Scaffold based on HA is a kind of bioactive tissue engineering with a specific interaction between the scaffold and growing cells by cell receptors (CD44, RHAMM, ICAM-1) for the growth and repair of tissues. Chung IPNs made with sodium hyaluronic acid/sodium alginate (HA/SA) scaffold, where HA and SA were cross-linked with diglycidyl ether of polyethylene glycol (PEGDG) and calcium chloride. The study used rabbit chondrocytes which are seeded in a HA/SA scaffold. Researchers noticed an increase in the quantity of DNA in chondrocytes after 21 days which confirmed their proliferation and increased the quantity of collagen type II. These studies demonstrated that porous HA/SA scaffolds

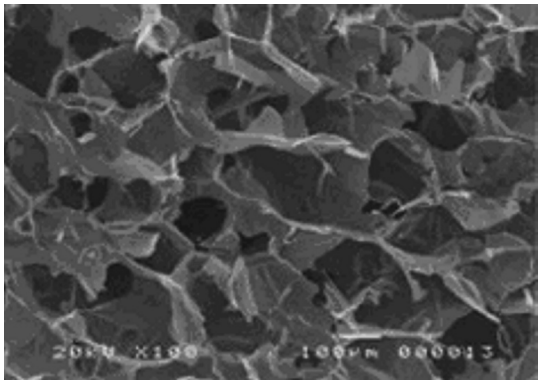

Fig. 8. SEM image of fabricated HA70/SA30.

may be used for three-dimensional culture of chondrocytes. A low pore size HA/SA (70/30) scaffold about 200 μm is preferable for durability and chondrocyte differentiation (Fig. 8) [63].

Hydrogels made from the crosslinked polymers with a high water content can provide local delivery of therapeutic agents, because of this benefits are called “intelligent materials”.

4. Conclusions

Intra-articular injections of HA provides hope for improvements in the treatment of patients suffering from arthritis, where the concentration of hyaluronic acid conditioning the viscoelastic properties of synovial fluid and proper movement in the joint is reduced. Viscosupplementation is a treatment for osteoarthritis involving the intra-articular injection of HA in appropriate quantities and time intervals. The number publications presented in this work confirms of analgesic, anti-inflammatory and articular tissue protect functions of HA. Viscosupplementation is an alternative method for treating arthritis. Injectable, biodegradable scaffolds based on HA in the form of hydrogels are important biomaterials for tissue engineering and drug delivery. Hydrogels derived from HA are ideal scaffolds as they resemble the extracellular matrices of tissues comprised of various glycosaminoglycans (GAGs).

References

[1] Rügheimer L., *Hyaluronian: A matrix component*, Proc. AIP Conf. 1049, 2008, 126-132.

[2] Czajkowska D., Milner-Krawczyk M., Kozanecka M., *Kwas hialuronowy – charakterystyka, otrzymywanie i zastosowanie*, Wydział Chemiczny, Instytut Technologii i Biotechnologii Środków Leczniczych, Politechnika Warszawska. Biotechnol. Ford Sci., 75(2), 2011, 55-70.

[3] Volpi N., Schiller J., Stern R., Soltes L., *Role, metabolism, chemical modifications and application of Hyaluronan*, Volume 16, Number 14, May 2009, 1718-1745(28).

[4] Levangie P.K., Norkin C.C., eds., *Joint structure and function: a comprehensive analysis. 3rd ed. Philadelphia*, FA Davis, 80 (8), 2005.

[5] Ulrich-Vinther M., Maloney M.D., Schwarz E.M., Rosier R., Keefe R.J., *Articular cartilage biology*, J. Am. Acad. Orthop. Surg., 11, 2003, 421-430.

[6] Marczyński W., *Patologia chrząstki stawowej – dynamika zmian, zapobieganie*, Wiadomości Lekarskie, LX, 2007, 1-2.

[7] Kang R., Ghivizzani S.C., Muzzonigro T.S., Herndon J.H., Robbins P.D., Evans C.H., *Orthopaedic applications of gene therapy: from concept to clinic*, Clin. Orthop. Relat. Res., 375, 2000, 324-337.

[8] Brief A.A., Mauer S.G., DiCesare P.E., *Use of glucosamine and chondroitin sulfate in the management of osteoarthritis*, J. Am. Acad. Orthop. Surg., 9, 2001, 71-78.

[9] Górecki A. i wsp., *Epidemiologia, stan profilaktyki, diagnostyki i leczenie chorób układu kostno-stawowego w Polsce*, Dekada kości i stawów 2000–2010, Kraków 2000.

[10] Brandt K.D., Block J.A., Michalski J.P., Moreland L.W., Caldwell J.R., Lavin P.T., *Efficacy and safety of intra-arcikular sodium hyaluronate in knee osteoarthritis*, ORTOVISC Study Group. Clin. Orthop. Relat. Res., 385, 2001, 130-43.

[11] Bert J.M., Waddell D.D., *Viscosupplementation with hylan g-f 20 in patients with osteoarthrosis of the knee*, Ther Adv Musculoskelet Dis., 2(3), Jun 2010, 127-32.
[12] Sanofiaventis Hyalgan [prescribing information], Sanofiaventis US LLC: Bridgewater, NJ, 2007.
[13] Seikagaku Supartz [product information], Seikagaku, Tokio 2007.
[14] Ferring Pharmaceuticals Euflexxa [prescribing information], Ferring Pharmaceuticals, Saint--Prex, Switzerland, 2006.
[15] Genzyme Biosurgery., Synvisc (hylan G-F 20) [product information], Genzyme Biosurgery: Cambridge, MA, 2006.
[16] Anika Therapeutics., Orthovisc (sodium hyaluronate) [product information], Anika Therapeutics, Woburn, MA, 2005.
[17] Scientific Group WHO, *The burden of musculoskeletal conditions at the start of the new millennium*, World Health Organ. Tech. Rep. Ser., 919, 2003, I-IX, 1-218.
[18] Raman R., Dutta A., Day N., Sharma H.K., Shaw C.J., Johnson G.V., *Efficacy of hylan G-F 20 and sodium hyaluronate in the treatment of osteoarthritis of the knee–a prospective randomized clinical trial*, Knee, 15, 2008, 318-324.
[19] Kirchner M., Marshall D., *A double-blind randomized controlled trial comparing alternate forms of high molecular weight hyaluronan for the treatment of osteoarthritis of the knee*, Osteoarthritis 14, Cartilage 2006, 154-162.
[20] Waddell D., Bricker D., *Clinical experience with the effectiveness and tolerability of hylan G-F 20 in 1047 patients with osteoarthritis of the knee*, J Knee Surg., 19, 2006, 19-27.
[21] Clarke S., Lock V., Duddy J., Sharif M., Newman J.H., Kirwan J.R., *Intra-articular hylan G-F 20 (Synvisc) in the management of patel-lofemoral osteoarthritis of the knee (POAK)*, Knee, 12, 2005, 57-62.
[22] Kemper F., Gebhardt D., Meng T., Murray C., *Tolerability and short-term effectiveness of hylan G-F 20 in 4253 patients with osteoarthritis of the knee in clinical practice*, Curr. Med. Res. Opin., 21, 2005, 1261-1269.
[23] Caborn O., Rush J., Lanzer W., Parenti O., Murray C.*A*., *Randomized, single-blind comparison of the efficacy and tolerability of hylan G-F 20 and triamcinolone hexacetonide in patients with osteoarthritis of the knee*, J. Rheumatol. 31, 2004, 333-343.
[24] Kahan A., Lieu P., Salin L., *Prospective randomized study comparing the medicoeconomic benefits of hylan G-F 20 vs. conventional treatment in knee osteoarthritis*, Joint Bone Spine, 70, 2003, 276-281.
[25] Neustadt D., *Long-term efficacy and safety of intra-articular sodium hyaluronate (Hyalgan) in patients with osteoarthritis of the knee*, Clin. Exp. Rheumatol., 21, 2003, 307-311.
[26] Raynaud J., Torrance G., Band P.A., *Prospective, randomized, pragmatic, health outcomes trial evaluating the incorporation of hylan G-F 20 into the treatment paradigm for patients with knee osteoarthritis* (part 1 of 2), Clinical results. Osteoarthritis Cartilage, 10, 2002, 506-517.
[27] Evanich J., Evanich C., Wright M., Rydlewicz J., *Efficacy of intraarticular hyaluronic acid injections in knee osteoarthritis*, Clin. Orthop. Relat. Res., 390, 2001, 173-181.
[28] Huskisson E., Donnelly S., *Hyaluronic acid in the treatment of osteoarthritis of the knee*, Rheumatology, 38, 1999, 602-607.
[29] Wobig M., Bach G., Beks P., Dickhut A., Runzheimer J., Schwieger G., Vetter G., Balazs E., *The role of elastoviscosity in the efficacy of viscosupplementation for osteoarthritis of the knee: A comparison of Hylan G-F 20 and a lower-molecular-weight hyaluronan*, Clinical Therapeutics, Volume 21, Issue 9, September 1999, 1549-1562.
[30] Wobig M., Beks P., Dickhut A., Maier R., Vetter G., *Open-label multicenter trial of the safety and efficacy of viscosupplementation with hylan G-F 20 (Synvisc) in primary osteoarthritis of the knee*, J. Clin. Rheumatol., 5, 1999, S24-S31.

[31] Altman R., Moskowitz R., *Intraarticular sodium hyaluronate (Hyalgan) in the treatment of patients with osteoarthritis of the knee: A randomized clinical trial*, Hyalgan Study Group, J. Rheumatol., 25, 1998, 2203-2212.

[32] Wobig M., Dickhut A., Maier R., Veller G., *Viscosupplementation with hylan G-F 20: a 26-week controlled trial of efficacy and safety in the osteoarthritic knee*, Clin. Ther., 20, 1998, 410-423.

[33] Lussier A., Cividino A., McFarlane C., Olszynski W., Potashner W., De Medicis R., *Viscosupplementation with hylan for the treatment of osteoarthritis: Findings from clinical practice in Canada*, J. Rheumatol., 23, 1996, 1579-1585.

[34] Carrabba M., Paresce E., Angelini M., Re K., Torchiana E., Perbellini A., *The safety and efficiency of different dose schedules of hyaluronic acid in the treatment of painful osteoarthritis of the knee with joint effusion*, Eur. J. Rheumatol. Inflamm., 15, 1995, 25-31.

[35] Scale D., Wobig M., Wolpert W., *Viscosupplementation of osteoarthritic knees with hylan: a treatment schedule study*, Curr. Ther. Res., 55, 1994, 220-232.

[36] Dougados M., Nguyen M., Listrat V., Amor B., *High molecular weight sodium hyaluronate (Hyalectin) in osteoarthritis of the knee: a 1 year placebo-controlled trial*, Osteoarthritis Cartilage 1, 1993, 97-103.

[37] Grecomoro G., Martorana D., Di Marco C., *Intra-articular treatment with sodium hyaluronate in gonarthrosis: a controlled clinical trial versus placebo*, Pharmatherapeutica, 5, 1987, 137-141.

[38] Moskowitz W.R., *Hyaluronic Acid Supplementation*, Current Reumatology 2000, Reports, Volume 2, Issue 6, 466-471.

[39] Conrozier T., Mathieu P., Schott A.M., Laurent I., Hajri T., Crozes P., Grand P., Laurent H., Marchand F., Meignan F., Noel E., Rozand Y., Savoye J.F., Vignon E., *Factors predicting long--term efficacy of Hylan GF-20 viscosupplementation in knee osteoarthritis*, Joint Bone Spine, 70(2), 2003, 128-133.

[40] Brandt K.D., Block J.A., Michalski J.P., Moreland L.W., Caldwell J.R., Lavin P.T., *Efficacy and safety of intra-arcikular sodium hyaluronate in knee osteoarthritis*, ORTOVISC Study Group, Clin. Orthop. Relat. Res., 385, 2001, 130-43.

[41] Navarro-Sarabia F., Coronel P., Collantes E., *A 40-month multicentre, randomised placebo--controlled study to assess the efficacy and carry-over effect of repeated intra-articular injections of hyaluronic acid in knee osteoarthritis*, Annals of the rheumatic diseases, 08/2011, 70(11), 2011, 1957-1962.

[42] Lester D.K., Hang K., *Gait Analysis of Knee Arthritis Treated With Hyaluronic*, Acid the Journal of Arthroplasty, 25(8), 2010.

[43] Keith M.P., *Updates on Intra-Articular Hyaluronic Acid Therapy for Knee Osteoarthritis*, Am J. Orthop., 41(4), 2012, E61-E63.

[44] Bannuru R.R, Natov N.S., Dasi U.R., Schmidt C.H. McAlindon, *Terapeutic trajectory following intra-articular hyaluronic acid injection In knee osteoarthritis – meta-analysis*, Osteoarthritis and Cartilage, 2011, 19611-619.

[45] Wang C., Lin J., Chang C., Lin Y., Hou S., *Therapeutic effects of hyaluronic acid on osteoarthritis of the knee. A meta-analysis of randomized controlled trials*, J Bone Joint Surg. Am 86A, 2004, 538-545.

[46] Marshall O., Johnell O., Wedel H., *Meta-analysis of how well measures of bone mineral density predict occurrence of osteoporotic fractures*, BMJ, 312, 1996, 1254-1259.

[47] Chen Y., Peng O., Sun C., Wang W., Li J., Zhang W., *Clinical study on sodium hyaluronate intra-articular injection in treatment of degenerative osteoarthritis of knee*, Zhongguo Xiu Follow up Chong lian Wai Ke Za Zhi, 16, 2002, 19-20.

[48] Hempfling H., *Intra-articular hyaluronic acid after knee arthroscopy: a two- year study*, Knee Surgery, Sports Traumatology, Arthroscopy, 15, 5, 2007, 537-546.

[49] Zietz P., Selesnick H., *The use of hylan G-F 20 after knee arthroscopy in an active patient population with knee osteoarthritis*, Arthroscopy, 24, 2008, 416-422.
[50] Huskin J., Vandekerckhove B., Delince P., *Multicentre, prospective, open study to evaluate the safety and efficacy of hylan G-F 20 in knee osteoarthritis subjects presenting with pain following arthroscopic meniscectomy*, Knee Surg. Sports Traumatol. Arthrosc., 16, 2005, 747--752, analysis. 3rd ed. Philadelphia: FA Davis 80:8.
[51] Lo G., LaValley M., McAlindon T., Felson D., *Intra-articular hyaluronic acid in treatment of knee osteoarthritis. A meta-analysis*, JAMA, 290, 2004, 3115-3121.
[52] Collins M.N., Birkinshaw C., *Hyaluronic Acid Based Scaffolds for Tissue Engineering-a Review*. Carbohydrate polymers, 92.2, 2013, 1262-79, Web. 23.
[53] Bergman K., Hilborn J., Bowden T., *Hyaluronic Acid Crosslinking Chemistry*, Journal Article 2005, 7-8.
[54] Guo Y., Yuan T., Xiao Z., Tang P., Xiao Y., Fan Y. & Zhang X., *Hydrogels of collagen/chondroitin sulfate/hyaluronan interpenetrating polymer network for cartilage tissue engineering. Journal of materials science,* Materials in medicine, 23(9), 2012, 2267-79.
[55] Tan H., Chu CR, Payne K.A., Marra K.G., *Injectable in situ forming biodegradable chitosan--hyaluronic acid based hydrogels for cartilage tissue engineering*, Biomaterials, 30(13), 2009, 2499-506.
[56] Park H., Choi B., Hu J., Lee M., *Injectable chitosan hyaluronic acid hydrogels for cartilage tissue engineering*, Acta Biomater, 9(1), 2013, 4779-4786.
[57] Lisignoli G., Toneguzzi S., Zini N., Piacentini A., Cristino S., Tschon M et al., *Hyaluronan-based biomaterial (Hyaff-11) as scaffold to support mineralization of bone marrow stromal cells*, La Chirurgia Degli Organi de Movimento, 88(4), 2003, 363-367.
[58] Lisignoli G., Cristino S., Piacentini A., Toneguzzi S., Grassi F., Cavallo C., Zini N., Solimando L., Maraldi M.N., Facchini A., *Cellular and molecular events during chondrogenesis of human mesenchymal stromal cells grown in a three-dimensional hyaluronan based scaffold*, Biomaterials October 2005, Volume 26, Issue 28, 5677-5686.
[59] Lepidi S., Grego S., Vindigni V., Zavan B., Tonello C., Deriu G.P., Abatangelo G., CortivoR., *Hyaluronan Biodegradable Scaffold for Small-caliber Artery Grafting: Preliminary Results in an Animal Model*, 417, 2006, 411-417.
[60] Radice M., Brun P., Cortivo R., Scapinelli R., Battaliard C., Abatangelo G., *Hyaluronan-based biopolymers as delivery vehicles for bone-marrow-derived mesenchymal progenitors*, Journal of biomedical materials research, 50(2), 2000, 101-9 (retrieved from: http://www.ncbi.nlm.nih.gov/pubmed/10679672).
[61] Kim M., Garrity S., Erickson I.E., Huang A.H., Burdick J.A., Mauck R.L., *Optimization of Macromer Density in Human MSC-Laden Hyaluronic Acid (HA) Hydrogels*, 2012, 211-212.
[62] Allison D.D., Grande-Allen K.J., *Review. Hyaluronan: A Powerful Tissue Engineering Tool*, Tissue Engineering, Vol. 12, No. 8, August 2006, 2131-2140.
[63] Chung C.W., Kang J.Y., Yoon I.S., Hwang H.D., Balakrishnan P., Cho H.J., Chung K.D., Kang D.H., Kim D.D., *Interpenetrating polymer network (IPN) scaffolds of sodium hyaluronate and sodium alginate for chondrocyte culture*, Colloids Surf. B Biointerfaces., 1, 88(2), Dec 2011, 711-6.

TECHNICAL TRANSACTIONS | **CZASOPISMO TECHNICZNE**
CHEMISTRY | CHEMIA
1-Ch/2014

BARBARA LARWA*, KRZYSZTOF KUPIEC*

TEMPERATURE PROFILES IN GROUND HEAT EXCHANGERS

PROFILE TEMPERATUR W GRUNTOWYCH WYMIENNIKACH CIEPŁA

A b s t r a c t

A mathematical model of a ground heat exchanger cooperating with a heat pump was presented. The model is based on a one-dimensional heat conduction equation with an internal heat source. On the basis of the solutions to the model equations, both the temperature distribution of different types of ground at different times of year as well as the time courses of temperature at different depths are shown. Calculations based on the presented model can be useful for the simulation and design of this apparatus.

Keywords: *transient heat conduction*, *renewable heat sources*, *ground heat exchangers*

S t r e s z c z e n i e

W artykule przedstawiono model matematyczny gruntowego wymiennika ciepła. Model opiera się na jednowymiarowym równaniu przewodzenia ciepła z wewnętrznym źródłem ciepła. Na podstawie rozwiązań równań modelu uzyskano profile temperatur w gruncie w zależności od czasu i rodzaju gruntu, a także czasowe przebiegi temperatur na różnych głębokościach. Obliczenia oparte na zaprezentowanym modelu mogą być wykorzystane do symulacji i projektowania tych aparatów.

Słowa kluczowe: *nieustalone przewodzenie ciepła*, *odnawialne źródła energii*, *gruntowe wymienniki ciepła*

* M.Sc. Eng. Barbara Larwa, Ph.D. Eng. Krzysztof Kupiec, prof. PK, Faculty of Chemical Engineering and Technology, Cracow University of Technology.

1. Introduction

Geothermal and solar energy systems are renewable heat sources. Geothermal heat pumps with vertical heat exchangers, also called ground-coupled heat pump (GCHP) systems, which use the ground as a heat source, have been gaining increasing popularity, especially for heating or cooling buildings, thanks to their high energy efficiency. Heat pumps allow the use of natural energy resources, which may come from atmospheric air, soil, surface water or groundwater. As the cost of energy continues to rise, the heat pump is becoming a key element in an energy recovery system with great potential for energy saving.

Ground heat exchangers are essential parts of ground-source heat pumps and the accurate prediction of their performance is of fundamental importance. The ground heat exchanger (GHE) is designed for extraction and injection of heat from/into the ground by a heat transfer fluid which is circulating in a closed cycle. The heat transfer fluid is water or an organic liquid with a low freezing point (e.g., an aqueous solution of ethylene glycol).

In a zone of a specific depth (6 m to approx. 50 m), the ground has a constant temperature throughout the year which is approximately equal to the mean annual air temperature. This is due to complex interactions between the heat coming from the surface and that which is rising from the depths of the Earth. At a depth below 6 m, the ground temperature directly corresponds to the climatic conditions. The heat is most intensively received by the geothermal collector during the winter season, and the ground regenerates, especially in warmer periods such as spring and summer. Ground regeneration follows mainly due to solar radiation and atmospheric rainfall, which ensures that the ground again accumulates heat for the next heating season.

The value of the temperature deviations from the annual average depends on the properties of the ground. When the ground is more saturated with water and when it contains more minerals, then the accumulation properties and thermal conductivity have the greater values. The range of power one unit can collect from the ground is between 10–35 W/m^2 ground surface (sandy ground, dry: 10–15 W/m^2; sandy, wet: 15–20 W/m^2; ground loam, dry: 20–25 W/m^2; loamy, wet: 25–30 W/m^2; water-bearing ground: 30–35 W/m^2).

Most embedded heat exchangers for houses are installed either horizontally or vertically in the ground. Horizontal ground heat exchangers can be made in various configurations – in series or coil systems. The exchangers are made mostly of plastic pipes (PVC, polyethylene, polypropylene) arranged at a depth of 1.2–2.0 m. The temperature increase of the heat carrier in the ground is 3 to 4 K. The average temperature of fluid medium depends on the type of the ground along with the depth at pipes are arrangement.

The modeling of ground heat exchanger occupies many researchers. The ground heat exchanger layout follows a spiral pattern characterized by three parameters – length, depth, and spacing. In [1], the influence of each parameter on the amount of heat extracted from the ground and on the ground temperature at the control point is assessed.

In research [2], a numerical model of heat transfer in the ground was developed for determining the temperature distribution in the vicinity of the pipe. The finite difference approximation is used for numerical analysis.

The aim of the study [3], was to validate the effects of parameters such as the depth of the buried earth coupled heat exchanger, the mass flow rate of the water-antifreeze

solution on the performance of a horizontal ground-source heat pump (GSHP) system used for space heating experimentally.

In research [4] on the optimum design of slinky-coil horizontal ground heat exchangers, a commercial finite-element simulator was used to simulate the performance of slinky-coil horizontal ground heat exchangers taking into account the energy balance at the ground surface.

Because of the complexity of the boundary conditions, the heat conduction equation has been solved numerically using an alternating direction implicit finite difference formulation and the effects of manipulating the solution parameters on the results were investigated in the work carried out in [5].

In most studies, a mathematical model and its verification was presented. However, few of them present the effect of soil properties on the performance of the ground as a heat source. The influence of this factor is presented in this paper. The aim of this paper is to present a mathematical model of a horizontal ground heat exchanger, and the results obtained on the basis of the solutions to equations of the model as well as its qualitative verification. In this model, the ground is treated as a semi-infinite body with an internal heat source.

2. Mathematical model

A system which consists of a lower and upper heat exchanger where a working fluid (glycol solution) circulates between them has been considered. The lower heat exchanger is located under the ground, while the upper exchanger is a part of the heat pump. In winter conditions, in the lower exchanger, the liquid absorbs heat from the ground and transfers it to the boiling thermodynamic medium in the heat pump. In summer conditions, the working fluid transfers the heat to the ground, thus cooling off at the same time, and then absorbs the heat from the condensing thermodynamic medium in operative heat pump (in this case as the air conditioner). Therefore, due to the season of the year, one is faced with a cyclical process consisting of alternating heating and cooling of the ground.

For the upper heat exchanger the temperature of the working fluid, which receiving (or collecting) the heat from the operating fluid is unchangeable. Through the surface of the ground, heat is exchanged with the environment. The ground surface has a temperature periodically changing in time (on an annual basis).

Fig. 1 presents the location and orientation of the ground heat exchanger, where x is position coordinate and H is the depth at which the heat exchanger is located. In this model, the flow through the parallel arrangement of heat exchanger pipes was replaced by a flow through a horizontal cuboid channel of very small thickness. The heat is transferred into and from the ground symmetrically by both the lower and the upper surface of the heat exchanger. It is assumed that the temperature of liquid in the exchanger is constant with the position (not in time) and thus, the flow through the channel is equivalent to the flow through a perfect mixing tank.

In the upper heat exchanger, the temperature of the thermodynamic medium receiving (or collecting) heat from the operating fluid is constant. This is due to phase transition of the thermodynamic medium in the heat pump. Temperature T_v, however, varies for

different periods of operation. For condensation (summer months), the temperature of the thermodynamic medium T_v is higher than in winter conditions in which medium evaporation is present.

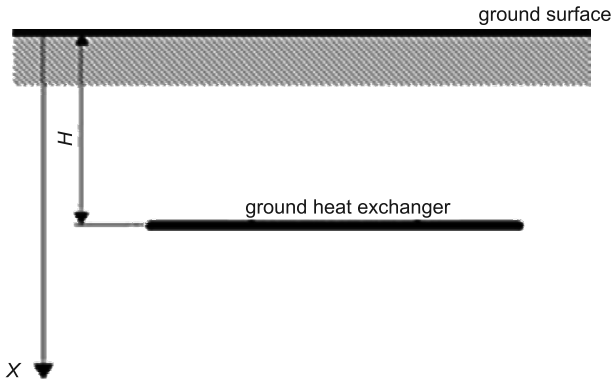

Fig. 1. The location and orientation of GHE

The operating fluid of specific heat c_L flows through the ground at a flow rate $\dot{m}_L$. The liquid temperature varies from T_{in} at the inlet to the heat exchanger to T_{out} at the outlet (Fig. 2). In winter conditions, the liquid is heated $T_{out} > T_{in}$, opposite to summer conditions.

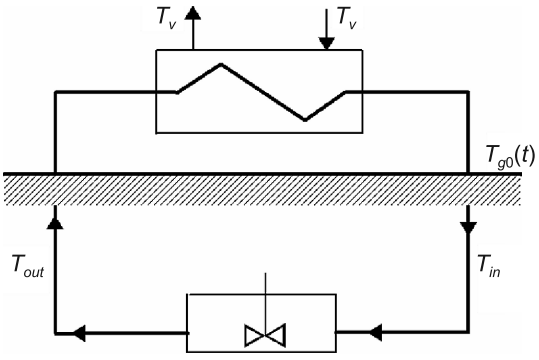

Fig. 2. The circulation of working fluid between the lower and upper heat exchangers

The heating surface area of the upper heat exchanger is A_{up} and the overall heat transfer coefficient in the heat exchanger is U. Instantaneous heat flux transferred in the upper and the lower heat exchanger is equal to:

$$\dot{Q} = \dot{m}_L c_L (T_{out} - T_{in}) \tag{1}$$

The heat flux is positive when the heat is received from the ground. Therefore, for the winter, $\dot{Q}$ is positive, while for the summer - negative. Heat transfer equation for the upper heat exchanger takes the form:

$$\dot{Q} = UA_{up} \frac{T_{out} - T_{in}}{\ln \dfrac{T_v - T_{out}}{T_v - T_{in}}} \tag{2}$$

From the above equation results the relationship between the temperatures T_{in} and T_{out}:

$$T_{in} = T_v - (T_v - T_{out}) \exp\left(- \frac{UA_{up}}{\dot{m}_L c_L} \right) \tag{3}$$

Heat is transferred through the ground surface with the surroundings. The atmospheric air in contact with the ground has a temperature T_0 periodically changing in time (on an annual basis) $t_0 = 24 \cdot 365.24$ h:

$$T_0 = 10.0 + 11.0 \cdot \cos\left(\frac{2\pi}{t_0} t \right) \tag{4}$$

where:

t – time, h.

In this model, the ground is treated as a semi-infinite body. The heat conduction equation for the plate with an internal heat source placed at H distance from the ground surface (Fig. 1) was used. The model includes only vertical heat transfer due to the small thickness of the heat exchanger. For transient conduction in an infinite plate with an internal heat source, the following relationship is valid [6]:

$$\frac{\partial T_g}{\partial t} = \frac{\partial}{\partial x} \left(a_g \frac{\partial T_g}{\partial x} \right) + \frac{q_v}{\rho_g c_g} \tag{5}$$

where:

T_g – ground temperature,
t – time,
a_g – thermal diffusivity of ground, m^2/s,
x – distance from the ground surface,
q_v – performance of the heat source, W/m^3,
ρ_g – density of the ground,
c_g – specific heat of the ground.

The performance of the heat source is the rate of heat generation per unit volume of the plate. This value is related to the transport of heat between the working fluid flowing through the ground heat exchanger and the ground. Heat performance is:

$$q_v = -\frac{\dot{Q}}{V} \tag{6}$$

where:

V – the volume of the horizontal cuboid with a very small thickness.

The following initial condition was assumed:

$$t = 0, \quad T_g = T_b \tag{7}$$

where:

T_b – ground temperature at great depth.

The boundary condition for the ground surface takes the form:

$$x = 0, \quad T_g = T_0 \tag{8}$$

where:

$T_0(t)$ – the air temperature, varying periodically and it is defined by the formula (4).

In numerical calculations, for the distance from the ground surface H_{inf}, it must be assumed that the temperature will remain constant with the position (in theory of the apply to $x \to \infty$). The second boundary condition is therefore:

$$x = H_{\text{inf}}, \quad T = T_b \tag{9}$$

The finite difference method (Crank-Nicolson scheme) was used for solving model equations.

3. Simulation of the process

The figures presented below show the results of calculations made on the basis of the mathematical model described above.

Ground heat exchangers usually work periodically to allow for partial thermal regeneration of the ground. The working conditions of the ground heat exchanger are as follows:

a) when the energy supply to the heat pump: $T_0 < 10$°C and $T_{out} > T_V + 7$ (heating season)
b) when receiving energy from the air conditioner $T_0 > 20$°C (hot summer months).

When neither the first nor the second condition is realized, the ground heat exchanger is turned off.

There are various types of ground. Each of these has different characteristics such as density, thermal conductivity and specific heat – these are summarized in the Tab. 1. As one can see, the individual parameters of the various ground types have very different values. In this study, the layers of sand/gravel and grained ground have been considered.

The remaining numerical data:

– the number of nodes with respect to the coordinate position of $n = 300$,
– the mass flow rate of the operating fluid $\dot{m}_L = 0.2$ kg/s,
– the product of the heat transfer coefficient and the heating surface area of the upper exchanger $(hA_{\text{up}}) = 200$ W/K,
– heating surface area of the lower heat exchanger $A_{\text{down}} = 500$ m^2,
– the distance between the lower heat exchanger and the surface of the ground $H = 2$ m,
– the temperature of the thermodynamical medium in winter and summer conditions $T_v = -5$°C or $T_v = 40$°C,
– $H_{\text{inf}} = 20$ m,
– $T_b = 10$°C.

Table 1

Parameters of various types of ground [7]

Type of Ground	Density [kg/m^3]	Thermal conductivity [W/(mK)]	Thermal diffusivity [10^6 m^2/s]	Specific heat [J/(kgK)]
Grounds, humidity 9%	1440	0.98	0.452	1506
Grounds, humidity 13%	1600	1.50	0.521	1799
Humid ground	1800	1.45	0.602	1338
Sand, dry	1650	0.70	0.506	838
Sand, humidity 15%	1780	0.92	0.375	1384
Dry sand	1998	1.60	0.324	2472
Wet sand	1500	1.88	0.105	1199
Sand/gravel	**1950**	**2.00**	**0.977**	**1050**
Grained ground	**2000**	**0.52**	**0.141**	**1844**

3.1. Temperature profiles in the ground

The calculations were performed for the ground with varying thermal diffusivity. The ground temperature profiles for different values of thermal diffusivity were shown in Figs. 3–5. The lines in the figures relate to each month. Numbers (1–11) were determined number of months, i.e. 1 – January 2 – February, etc. One can see the differences in the profiles for each month in following years. These differences result from arbitrarily assumed initial condition (7) and subsequent years are disappearing as they reach a cyclic steady state. Profiles relate the case where to/from the ground is not taken or delivered heat (the ground heat exchanger is completely turned off). Fig. 3 concerns the case where the variation of thermal diffusivity is described by formula:

$$\begin{aligned} a_g &= 0.977 \cdot 10^{-6}\ \mathrm{m^2/s} \quad \text{for} \quad x \le 2\ \mathrm{m} \\ a_g &= 0.141 \cdot 10^{-6}\ \mathrm{m^2/s} \quad \text{for} \quad x > 2\ \mathrm{m} \end{aligned} \tag{10}$$

The above function determines the ground structure: from the ground surface to the depth of 2 m there is sand/gravel, and less than 2 m – grained ground. In Fig. 3 the clearly visible deformation profiles at x = 2 m can be seen, i.e. at the point where ground changes its properties by leaps and bounds. The temperatures in subsurface layer with high thermal diffusivity are only slightly changed with the position.

A similar situation occurs when there is a change in the type of soil at a depth of 4 m (Fig. 4), i.e. according to the relationship:

$$\begin{aligned} a_g &= 0.977 \cdot 10^{-6}\ \mathrm{m^2/s} \quad \text{for} \quad x \le 4\ \mathrm{m} \\ a_g &= 0.141 \cdot 10^{-6}\ \mathrm{m^2/s} \quad \text{for} \quad x > 4\ \mathrm{m} \end{aligned} \tag{11}$$

Then, the profiles deformations occur at a depth of 4 m. The heat conduction rate is significantly higher in sand/gravel layer than in the layer of grained ground. This causes the ground at a depth of 4 m to be at a temperature close to the temperature at the surface.

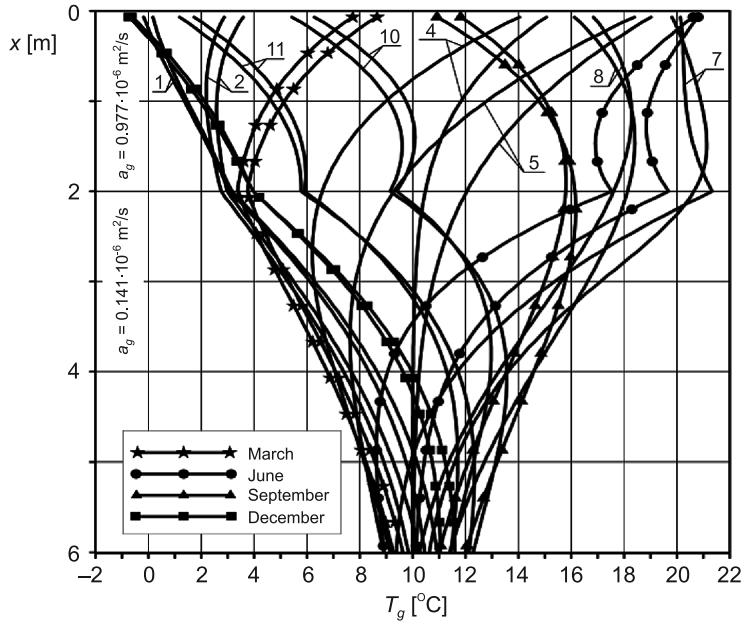

Fig. 3. Temperature profiles of ground with varying thermal diffusivity at a depth of $x = 2$ m. The thermal diffusivity of the upper layer is higher than for the bottom one

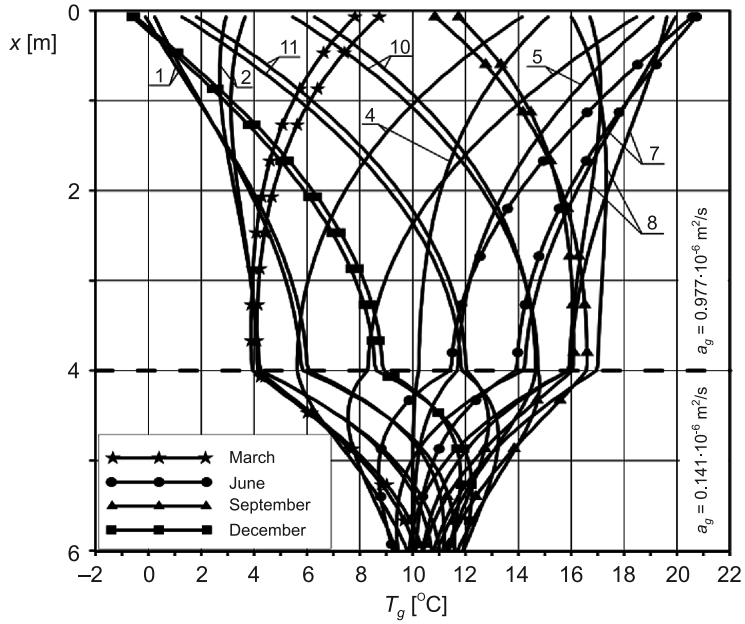

Fig. 4. Temperature profiles of ground with varying thermal diffusivity at a depth of $x = 4$ m. The thermal diffusivity of the upper layer is higher than that of the bottom one

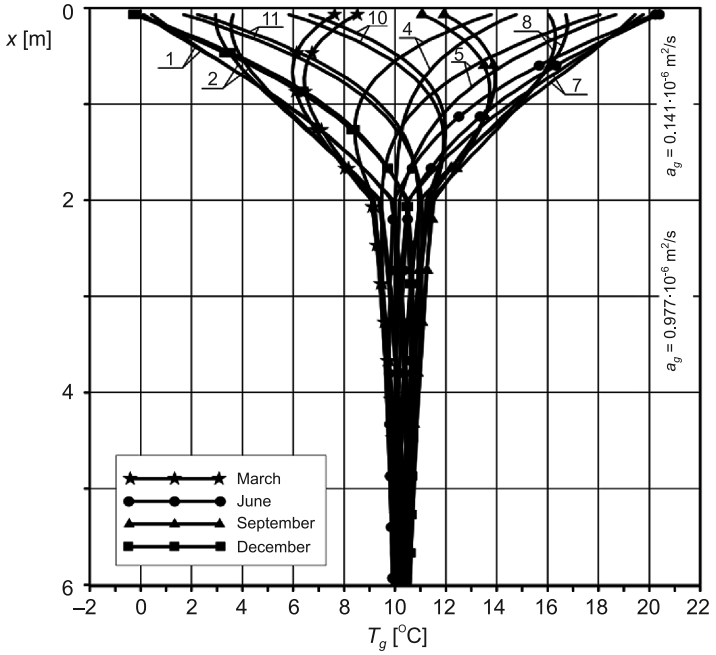

Fig. 5. Temperature profiles of ground with varying thermal diffusivity at a depth of $x = 2$ m. The thermal diffusivity of the upper layer is lower than that of the bottom one

The temperature profiles for a depth in the range 0–2 m, where ground is formed by layer of grained ground, below 2 m – sand/gravel layer, are shown in Fig. 5. Therefore:

$$\begin{aligned} a_g &= 0.141 \cdot 10^{-6} \text{ m}^2/\text{s} \quad \text{for} \quad x \leq 2 \text{ m} \\ a_g &= 0.977 \cdot 10^{-6} \text{ m}^2/\text{s} \quad \text{for} \quad x > 2 \text{ m} \end{aligned} \tag{12}$$

In this case, the layer of the ground with a higher thermal diffusivity is below the lower diffusion layer. This causes little change in temperature at a depth of 2 m (temperature profiles are similar to the vertical lines), and thus, their waveforms are only slightly different for each month (ground temperature in the range of 9–11°C). Large temperature changes occur in the upper part of the ground with a low thermal diffusivity.

Comparing the waveforms in Figs. 3 and 5, one should consider the meaning of the upper layer of soil (depth range 0 to 2 m). In Fig. 3, one can see that for the value of the function described a_g, Eq. (10), the upper layer is not significant for the decomposition of a lower temperature because the temperature of the upper layer is similar to the temperature of the ground surface. Totally different case should be interpreted when variation of thermal diffusivity is described by the function (Eq. (12)). Then, the upper layer of the ground is a buffer, which insulates the bottom layer from the impact the ground surface temperature, as shown in Fig. 5.

3.2. Time courses of ground temperatures at different depths

Based on numerical analysis, the time courses of the ground at different depths were determined (Fig. 6a–e). The dotted lines (•) determine temperature courses when the ground heat exchanger (located at a depth of 2 m) is turned on, while the solid lines refer to when the heat exchanger is completely turned off. The value of the heat transfer coefficient between the air and the ground was assumed as $h = 10$ W/(m^{2}K).

In Fig. 6a, the temperature time courses on the surface of the ground were shown. In addition, in Fig. 6a, ambient air temperature, periodically variable according to the relationship (4) and varying in the range from −1°C to 21°C, was presented. Courses of all three lines differ slightly. Therefore, the temperature of the ground surface is practically the same regardless of whether the exchanger is enabled or not. This should be interpreted as follows: heat transfer into the ground to a depth of 2 m below the surface causes only slight changes in temperature on the surface. However, small differences in temperature between the ground surface and the air are associated with a small heat flux transferred between the ground and the air. It should be noted that the difference in temperature between the ground and the air must not be zero because the heat is collected (or received) from the ground through the surface. In winter conditions, the ground supplies heat to the environment, while in summer ground extracts heat. Hence, the temperature difference is discussed alternately positive or negative.

At a depth of 1m, significant changes occur in the time courses of the ground temperature (Fig. 6b) as compared to the above discussed passes for $x = 0$. When the heat exchanger is turned off, the ground temperature profile remains periodically changing, but has a lower amplitude than on the ground surface. In summer conditions there is an increase of temperature of the ground, which is related to the supply of heat to the ground – inversely in winter, when there is a noticeable temperature drop. Courses of temperatures for the attached and completely turned off heat exchanger are significant.

A similar situation occurs at a depth of 2 m, which is the depth of the heat exchanger location in Fig. 6c. There is a clear difference between the temperatures when the heat exchanger is turned off and on. Noteworthy is the fact that the temperature deformations (when heat exchanger is turned on) are related to the periodic work (on – off) of this device. When the heat exchanger is completely turned off, the periodical variation of the amplitude of the temperature of the ground is lower than the ground surface ($x = 0$) or to $x = 1$ m.

In Fig. 6d, temperature profiles of the ground at a depth of 4 m are presented. Differences in temperature between the on and off heat exchanger are much smaller, temporary changes in temperature waveforms are clearly flattened.

However, at a depth of 10 m (Fig. 6e), temperature variations do not occur in practice, the work of the heat exchanger has therefore a negligible effect on the temperature of the ground, which is about 10°C.

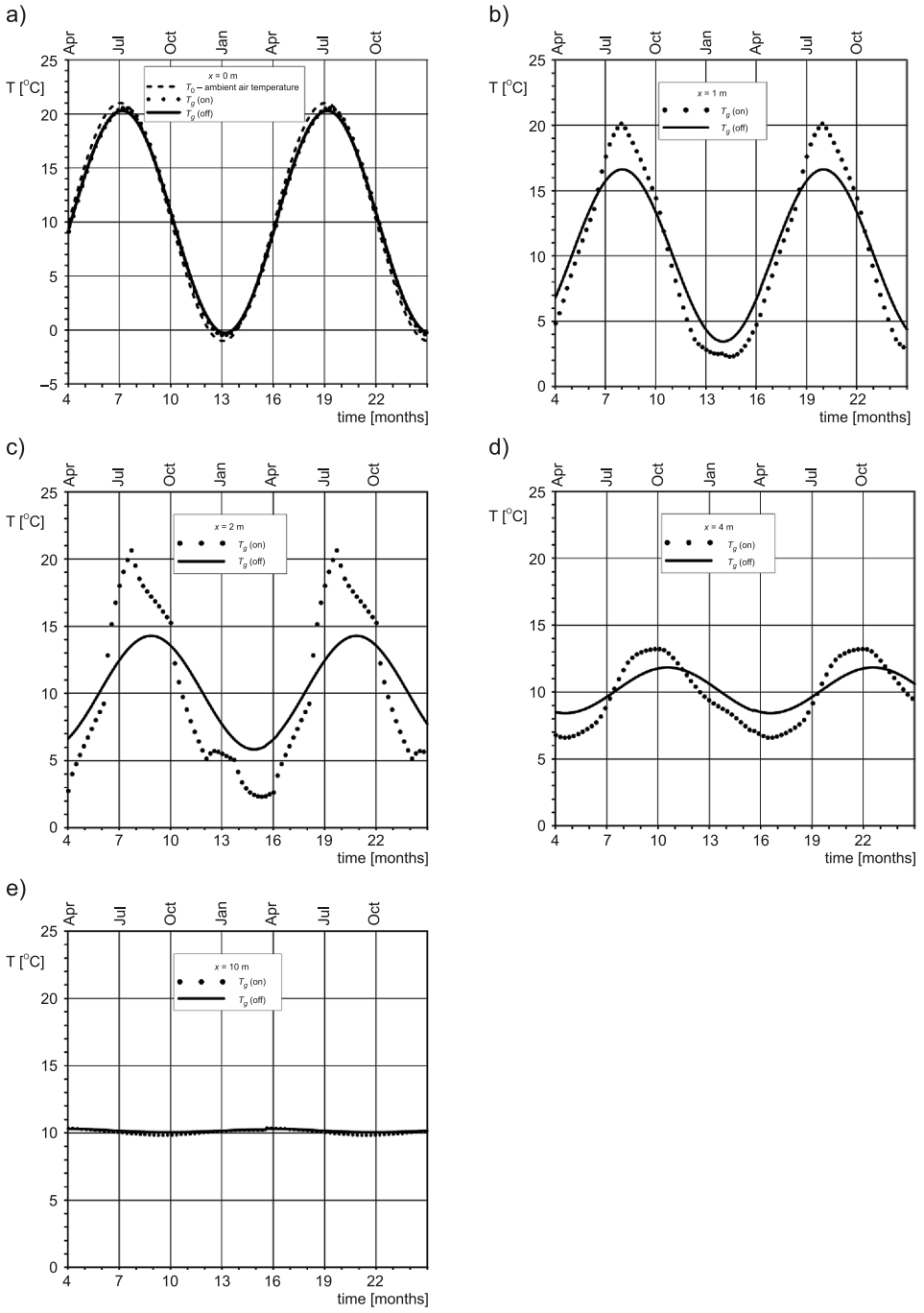

Fig. 6. Time course temperature profiles of ground at depth: a) 0 m, b) 1 m, c) 2 m, d) 4 m, e) 10 m

4. Conclusions

1. The presented model of the ground heat exchanger is based on a one-dimensional heat conduction equation with an internal heat source.
2. The model describes the temperature distributions in the ground correctly depending on the location, time and properties of the ground.
3. The ground temperature is affected by many factors, the presented model takes all of them into account.
4. Calculations based on the presented model can be useful in predicting the impact of different process parameters on the heat pump's ability to heat.
5. The model can be used to simulate the thermal regeneration of the ground after the end of the heating season.

References

[1] Fontaine P., Marcotte D., Pasquier P., Thibodeau D., *Geothermics*, Vol. 40, Issue 3, September 2011, p. 211-220.
[2] Esen H., Inalli M., Esen M., *Building and Environment*, Vol. 42, Issue 3, 2007, p. 1126-1134.
[3] Esen H., Inalli M., *Applied Thermal Engineering*, Volume 24, Issues 14–15, October 2004, p. 2219-2232.
[4] Fujii H., Nishi K., Komaniwa Y., Chou N., *Geothermics*, Volume 41, January 2012, p. 55-62.
[5] Florides G.A., Christodoulides P., Pouloupatis P., *Applied energy*, vol. 92, 2012, p. 523-533.
[6] Carslaw H.S., Jaeger J.C., *Conduction of Heat in Solids*, second ed., Clarendon Press, Oxford, 1959.
[7] Calculation program *AWADUKT Thermo*.

TECHNICAL TRANSACTIONS | CZASOPISMO TECHNICZNE
CHEMISTRY | CHEMIA
1-Ch/2014

MARTA MARSZAŁEK*, ZYGMUNT KOWALSKI*, AGNIESZKA MAKARA*

PHYSICOCHEMICAL AND MICROBIOLOGICAL CHARACTERISTICS OF PIG SLURRY

FIZYKOCHEMICZNA I MIKROBIOLOGICZNA CHARAKTERYSTYKA GNOJOWICY ŚWIŃSKIEJ

Abstract

Pig slurry is classified as a natural fertilizer of animal origin, being a mixture of faeces, urine, remains of fodder and water used for the elimination of faeces. It is generated in non-bedding pig farming conditions, where animals are kept on slatted floors (grate or slotted floor). This paper presents the general characteristics of pig slurry, its physicochemical properties and its microbiological composition. Also, factors affecting slurry properties are discussed.

Keywords: *pig slurry*, *physicochemical properties*, *microbiological composition*, *fertilizing components*

Streszczenie

Gnojowica świńska klasyfikowana jest jako nawóz naturalny pochodzenia zwierzęcego będący mieszaniną kału, moczu, resztek paszy oraz wody stosowanej do usuwania odchodów. Powstaje ona w warunkach bezściółkowego chowu trzody chlewnej, w którym zwierzęta utrzymywane są na podłogach ażurowych (szczelinowych lub rusztowych). W niniejszym artykule przedstawiono ogólną charakterystykę gnojowicy świńskiej, jej właściwości fizykochemiczne oraz skład mikrobiologiczny. Omówiono także czynniki wpływające na właściwości gnojowicy.

Słowa kluczowe: *gnojowica świńska*, *właściwości fizykochemiczne*, *skład mikrobiologiczny*, *składniki nawozowe*

* M.Sc. Eng. Marta Marszałek, Prof. Ph.D. Eng. Zygmunt Kowalski, Ph.D. Eng. Agnieszka Makara, Institute of Inorganic Chemistry and Technology, Faculty of Chemical Engineering and Technology, Cracow University of Technology.

1. Introduction

Slurry is liquid agricultural waste generated in the non-bedding method of pig farming, it is a mixture of animal excrements and technological water used for sanitary purposes in livestock housing. The non-bedding system of pig farming, the development of which commenced in Poland in the early 1970s, results in large volumes of slurry which must be appropriately managed [1–3]. According to the Act on Fertilizers and Fertilization [4], slurry is a natural fertilizer. Therefore, its use for agricultural purposes is most appropriate from the point of view of environment protection and it is also the most economically justifiable option [1–6]. It must, however, be stressed that irrational or excess fertilization with slurry can contribute to the contamination of the natural environment, particularly in areas with a high concentration of pig farms and a deficit of agricultural fields where slurry can be applied. Slurry can be a source of odour nuisance and can contaminate the air with ammonia and greenhouse gases (methane, carbon dioxide, nitrogen oxide (I) and hydrogen sulphide). Slurry can also cause the leaching of fertilizing components into groundwater, the eutrophication of surface waters, as well as soil degradation due to supersaturation with phosphates or acidification with ammonia. Furthermore, in the case of either a lack of or improper hygienization methods, slurry can cause a potential sanitary-epidemiological threat due to the spread of pathogenic bacteria in the environment [7–10].

2. Non-bedding system of pig farming

During recent decades, interest in non-bedding pig farming has been growing among farmers. This is where animals are kept on slatted floors (slotted and grate floors) or partially--slotted floors (partially-grated floors) and where part of the floor is full, and some is in slat form. The choice of this raising system is usually related to a lack of sufficient volume of bedding materials (straw), the opportunity of reducing human labour and the easier elimination of excrements and keeping livestock housing clean. Furthermore, the system allows for effective disinfection of the pigsty, owing to which, it assures high hygienic standard and thus reduces the opportunity for the spread of disease. Slatted floors must be made of appropriate materials (plastic, concrete, metal, glass-fibre) and must be characterised with optimally selected beam widths and slots in order to limit damage to animal feet and to ensure easy permeation of faeces to channels made under the floor where faeces can be stored and via which they flow, or from which they are pumped into tanks outside the pigsty. Due to higher investment costs (as compared to bedding systems), non-bedding systems are more frequently applied in large industrial farms than in individual farms. In Poland, most large farms, built both in the 1970s and in the last decade, apply non-bedding systems. Despite many advantages, non-bedding technologies are often criticised. The criticism is principally related to the problem of the correct storage, management and utilization of the slurry [1, 11–13].

3. General characteristics of pig slurry

Pig slurry is a mixture of: faeces and urine in the natural ratio, which approximately amounts to 40% faeces and 60% urine; water used for keeping the pigsty clean (animal washing, station cleaning, channel flushing); remains of fodder. Faeces contain undigested, digested and unabsorbed parts of fodder, raw fibre, cellulose, woody parts, parts of plants in various degree of decomposition, mineral materials, water, excretions from the digestive system, as well as bacteria and products of their metabolism. Urine is a water solution of various organic and inorganic substances, including nitrogen compounds from the metabolism of protein and non-protein substances containing nitrogen, as well as vitamins, hormones and enzymes. The proportion of water in slurry should not exceed 20% in relation to the volume of excrements as production of very diluted slurry (e.g. due to uncontrolled or excess water consumption at the farm) generates costs related to the storage, transportation and management of the slurry in a manner safe for the environment [1–3, 7]. It is generally adopted that slurry containing up to 6–8% dry matter is classified as diluted, while over 6–8% as dense. The slurry produced in a typical Polish breeding farm differs from slurry generated in farms in other countries. Usually, slurry from Polish farms is characterised by its lower dry matter content. By type, slurry can be divided into complete and incomplete. Complete slurry does not contain addition of liquid manure (which is fermented urine from bedding stations of animals with small addition of water and manure water, namely leachate from farmyard manure) and other wastewater. Incomplete slurry can contain liquid manure and wastewater or one of these admixtures [1–3, 11, 14].

The volume of slurry generated in a farm depends on the size of livestock, the purpose of animal raising, and the intensity of feeding, which affects the volume of excrement and the volume of water consumed. It is assumed that the volume of faeces and urine per one livestock unit (1 LU – reference unit for aggregation of livestock in a farm, corresponding to an animal with bodyweight of 500 kg or several animals with total body weight of 500 kg) amounts to 45 kg per day, on average. Normative consumption of technological water in livestock building must not exceed 10 dm^3 per day. Therefore, daily production of slurry per 1 LU amounts to approximately 55 kg (mass density of slurry = 1 kg/dm^3) [1, 2, 15].

Slurry is a polydispersive system, the solid phase of which with various degree of stratification occurs in the form of suspension (macroflocs and colloidal), or in the dispersed form as molecular solutions. Due to such a composition and the fermentation process occurring in the slurry, and as their result the phenomena of flotation and sedimentation, pig slurry containing up to 8% dry matter is stratified into three fractions: surface (scum); medium (liquid, most diluted layer, contains the least solid particles); bottom (the most visible layer, with a high share of mineral parts). Particular layers differ with the content of dry matter and fertilizing components, hence before transporting the slurry to the fields, it must be carefully mixed so as to achieve a homogeneous fertilizer and to introduce the same amount of nutrients to the soil for plants [1–3, 6, 11, 15]. The size of solid fraction particles in the slurry varies widely from several angstroms to 100 millimetres. About 45% of dry matter includes particles with dimensions from 0.2 to 0.5 mm, which largely comprise parts of faeces and the remains of undigested fodder. Over 50% of solid particles are smaller than 50 μm, whereas a significant portion is attributable to colloidal

fraction. The finest colloidal particles in the solid fraction of the slurry constitute from 9 to 30%. Colloids form the smallest parts of faeces, dead and live microorganisms, mucous substances, humic acids and other materials [11].

4. Physicochemical properties of pig slurry

The following have a material impact on the physical properties of pig slurry: quantity and quality of organic and inorganic substances in faeces; water content; storage conditions, such as temperature and access to air; biological-chemical and fermentation processes taking place in the slurry [11, 14]. Properties of diluted slurry are similar to properties of liquids, while of dense slurry, the properties are similar to a plastic substance. The liquid limit of slurry is rather low and remains within the range of 5–10 Pa. Slurry can be treated as a Newtonian fluid if it contains up to 5% dry matter [3, 14]. The viscosity of slurry increases with the increase of dry matter content. The density of slurry ranges from 0.9 to 1.1 g/cm^3, whereas for calculations, it is assumed that slurry density is such as water density, namely 1 g/cm^3. The lower the specific heat of slurry, the higher the dry matter content in the slurry. The freezing point of slurry is around –2°C, and it decreases with an increasing content of urine and a decreasing amount of water. The freezing and defrosting of dense slurry occurs faster than in the case of diluted slurry as dense slurry has a lower specific heat. The electric conductivity of slurry is rather high and increases with an increasing dry matter content [3, 14].

In the aspect of chemical composition, slurry is not a uniform material. The chemical composition of slurry varies. This depends on many factors, such as the type and the age of animals (Table 1), their feeding system and maintenance, the quality of fodder, as well as the dilution of the slurry and its storage method. The greatest impact on the concentration of particular elements and chemical compounds in the slurry is from its dilution with water. The more diluted the slurry, the less the quantity of chemical compounds it contains. Another important factor is the method (temperature, tank parameters, frequency of homogenisation) and duration of slurry storage. During storage, losses occur principally in the aspect of organic matter and nitrogen. The volume of such losses for dry matter remains within the range of 4–16%, while for nitrogen, at a level of around 8% [1, 11, 14, 15].

Pig slurry is characterised by a high degree of hydration, on average containing 6–8% dry matter, whereas about 70–80% of dry matter comprises organic materials. Indirect ratios that can point to the amount of organic matter in the slurry include BOD_5 (five days' biochemical oxygen demand), COD (chemical oxygen demand) and TOC (total organic carbon). The biochemical oxygen demand of the slurry is difficult to precisely determine as slurry is a substance subject to continuous dynamic biological and chemical changes. Due to the domination of chemical transformations in slurry, a more reliable assessment of its organic matter content can be obtained through COD determination. The parameter defines the content of organic compounds, both undergoing and not undergoing biological decomposition. However, the best indirect ratio of organic compounds in the slurry is deemed as total organic carbon content [3, 5, 11, 14, 16]. Studies by many authors [3, 5, 11, 16–18] revealed that pig slurry is characterised by a very high biochemical oxygen demand and

a rather high chemical oxygen demand (Table 2). The reaction of typical pig slurry is usually slightly alkaline (Table 2) [5, 11, 17–21].

Table 1

Impact of type and age of animals on physicochemical composition of pig slurry (average content in % of fresh matter) acc. to [11, 14]

Parameter	Piglets	Weaners	Sows	Finishers
Dry matter	1.27	3.95	4.95	8.62
Organic dry matter	0.85	2.98	3.76	6.37
Mineral dry matter	0.42	0.97	1.19	2.25
Total carbon	0.47	1.72	2.00	3.35
Total nitrogen	0.20	0.40	0.43	0.57
Ammonium nitrogen	0.16	0.25	0.24	0.27
Phosphorus	0.02	0.07	0.10	0.12
Potassium	0.12	0.16	0.17	0.36
Calcium	0.03	0.11	0.20	0.20
Magnesium	0.02	0.04	0.04	0.05
Sodium	0.03	0.03	0.04	0.06

Table 2

Comparison of physicochemical parameters of pig slurry from various countries

Parameter	Poland [5]	Poland [16]	Denmark [17]	Spain [18]	Spain [19]	Canada [20]	Russia [21]
pH	7.29	8.11	7.09	7.43	7.80	7.48	7.05
Dry matter [%]	2.30	3.80	–	–	1.29	4.05	1.25
COD [mgO_2/dm^3]	62800	47820	70000	31600	16613	–	14000
BOD_5 [mgO_2/dm^3]	17500	20250	–	14200	5000	–	–
$N\text{-}NH_4^+$ [mg/dm^3]	5700	1204	4800	2010	1767	4625	470
$P\text{-}PO_4^{3-}$ [mg/dm^3]	724	–	400	–	–	–	190
P_{total} [mg/dm^3]	–	255	1600	760	–	1335	220
N_{total} [mg/dm^3]	–	1363	5600	–	–	–	760

Slurry is an important source of fertilizing macrocomponents (Table 3), which can be used for agricultural production as pig excrements contain from 70 to 80% of nitrogen and phosphorus, and from 70 to 95% potassium and calcium, contained in fodder for animals. Phosphorus is almost entirely excreted in faeces, while most potassium, in urine. Nitrogen in slurry occurs in organic combinations (proteins, amino-acids, urea, uric acid, hippuric acid) and mineral combinations (ammonia, nitrates). About 50–60% nitrogen in pig slurry occurs in the form of easily soluble ammonia nitrogen used by plants, but during slurry storage, as a result of nitrification process, NH_4^+ volume can increase to even 70% of the total nitrogen. Most frequently, slurry nitrogen covers 50–75% of the demand of plants for this component

while the rest is supplemented with mineral fertilizers. Phosphorus, similarly to nitrogen, occurs in the slurry in inorganic compounds (over 40%) and organic compounds (proteins, nucleotides, phospholipids, esters), whereas over 35% of phosphorus is in the form of easily soluble compounds, while 48% is in the form of hydrolysing compounds. Over 90% of the total potassium contained in slurry can be diluted in water, hence this component is largely absorbed by plants. The content of magnesium, calcium and sodium in slurry usually meets the demand of plants for such elements [3, 11, 14].

Table 3

Fertilizing component content in pig slurry depending on dry matter content acc. to [15]

Dry matter content [%]	Content in [%] of fresh matter				
	Nitrogen	Phosphorus	Potassium	Calcium	Magnesium
Below 2	0.19	0.04	0.11	0.06	0.01
2.1–4.0	0.29	0.07	0.14	0.06	0.02
4.1–6.0	0.29	0.08	0.10	0.09	0.02
6.1–8.0	0.29	0.07	0.14	0.08	0.02
8.1–10.0	0.41	0.15	0.19	0.13	0.04
10.1–12.0	0.53	0.15	0.25	0.13	0.02
Over 12	0.56	0.23	0.28	0.24	0.04

Pig slurry is also rich in microelements: iron; boron; zinc; manganese; copper; molybdenum; cobalt; selenium; while the volume of heavy metals (lead, cadmium, mercury, arsenic) does not create a risk to the natural environment (Table 4). Table 4 indicates that the microelement occurring in slurry in the largest quantities is iron, while selenium is present in the smallest quantities [1, 2, 11, 22]. Slurry is a natural fertilizer containing all nutrients necessary for the correct growth and development of plants. It is a quick-acting fertilizer, comparable to mineral fertilizers in this aspect. It must, however, be remembered that the maximum dose of natural fertilizer applied during the year cannot exceed 170 kg of nitrogen per 1 hectare of farming land, which corresponds to 45 m^3 of slurry per hectare. Slurry used as fertilizer contains on average 8% dry matter and applied for example at a dose of 10 m^3/ha provides the soil with 64 kg of nitrogen, 40 kg of phosphorus and 30 kg of potassium [11, 23, 24].

Slurry is also a source of emission to the air of ammonia, greenhouse gases (methane, carbon dioxide, nitrogen oxide (I), hydrogen sulphide) and odorants. Due to the anaerobic decomposition of organic matter in the slurry occurring during its storage, gas products are emitted to the air, such as ammonia, methane, carbon dioxide, hydrogen sulphide and nitrous oxide. Also, about 400 volatile organic and inorganic compounds are released of high odour nuisance, these occur due to chemical reactions and the activity of micro-organisms. Substances responsible for odour formation can be classified into four main groups: volatile sulphur-containing compounds; indoles and phenols; volatile fatty acids; ammonia and volatile amines. Among the most important odorants causing the unpleasant odour of slurry, there are ammonia, hydrogen sulphide, diacetyl, p-cresol, indoles, phenols, mercaptans, amino mercaptans, skatoles, amines and methyl sulphides [1, 2, 7, 11, 24–28].

Table 4

Average content of microelements and heavy metals in pig slurry acc. to [1, 2]

Element	Content [mg/kg dry matter]
iron	1315.00
zinc	328.60
manganese	175.00
copper	104.00
boron	36.00
molybdenum	1.35
cobalt	0.90
selenium	0.21
lead	5.80
cadmium	0.62
arsenic	< 0.20
mercury	< 0.03

5. Microbiological composition and biological properties of pig slurry

The microbiological composition of pig slurry is varied and its clear determination is thus difficult. Slurry is characterised by a high level of bacterial population, it can contain saprophytic microorganisms, pathogenic bacteria, viruses and fungi, as well as eggs and oocysts of gastro-intestinal parasites [11, 29, 30]. In slurry, there can be micro-organisms excreted by animals together with faeces, urine, milk, blood, purulent discharges, nasal and throat discharges, as well as discharges from vaginal tracts and amniotic fluid.

Most bacteria forming part of slurry microflora include anaerobic bacteria and facultative anaerobic bacteria. The level of aerobic bacteria in slurry is rather low. The prevailing population is formed by bacteria from the Enterobacteriaceae family (Gram-negative intestinal bacteria in the shape of rod, facultative anaerobes) and the Streptococcus family (streptococci – type of spherical Gram-positive, aerobic or facultative anaerobic bacteria) [25, 30]. From slurry, one can also isolate bacteria of the Peptostreptococcus genus (Gram--positive anaerobic bacteria), the Lactobacillus genus (type of rod-shaped Gram-positive, anaerobic bacteria), the Clostridium genus (Gram-positive, obligate anaerobic bacteria of rod shape), the Enterococcus genus (enterococci – Gram-positive, facultative anaerobic cocci), the Escherichia genus (Gram-negative bacteria of rod shape, facultative anaerobes), and the Bacteroides genus (Gram-negative bacillus bacteria, facultative anaerobes) [25, 30–32]. In slurry, there can also be bacteria of the following genera: Salmonella (type of rod-shaped

Gram-negative, facultative anaerobic bacteria); Brucella (Gram-negative bacilli, causing contagious disease – brucellosis); Mycobacterium (Gram-positive aerobic bacteria of bacillus shape); Rickettsia (Gram-negative bacteria that can present as cocci, rods or thread--like) [11, 16, 29, 30, 33].

The use of slurry as fertilizer can cause the spread of parasite diseases due to its risk of contaminating with invasive forms of parasites, such as: Eimeria; Trichuris; Moniezia; Fasciola; Ascaris [11, 33]. An important issue is also the presence of antibiotics and other medical preparations in the slurry, which broad therapeutic and prophylactic use in animal breeding causes contamination of waters and soil with pharmaceuticals, as well as the formation of dangerous, antibiotic resistant strains of micro-organisms that are transferred to the environment [7, 33]. Fertilization with slurry that has not been subjected to appropriate hygienization processes and contains bacteria resistant to antibiotics can be a source of transfer of genes of antibiotic resistance to other micro-organisms present in soil [30, 33].

Despite the fact that pathogenic forms constitute a small percentage of the entire microflora present in slurry, due to their high resistance to environmental factors and their possibility of contaminating water, their contribution to the spread of many diseases can be significant. This is encouraged by the physicochemical properties of slurry, which is not subject to the process of self-heating, and in the absence of conditioning processes, can cause the microbiological contamination of soil, waters, and plants. It must be stressed that the appropriate storage of slurry before its use for agricultural purposes is very important due to a lack of opportunity for its self-heating and the risk of proliferation of some microbes in the early phase of storage [30, 33]. The activity period of bacteria, viruses, fungi, and parasites in the stored slurry highly varies and depends on the type of slurry, the species of micro-organism, and ambient temperature. Eggs of parasites can be invasive during periods lasting from several days up to a year, while viral pathogenicity can range from 70 to 300 days [29, 33]. According to the data [1], at a temperature of 8°C, eggs of Ascaris suum (large roundworm of pigs) have a lifespan of 85 days, while adult proglottids of Taenia solium (also called the pork tapeworm) have a lifespan of 76 days. Available literature also indicates that most pathogens of the Salmonella genus order undergo reduction during slurry storage (Table 5). The gradual elimination of bacteria is due to the temperature conditions, the presence of autochthonous micro-organisms and the content of nutrients. Longer survival of Salmonella bacilli in pig slurry was evident at a temperature of 4°C as compared to a temperature of 20°C, and in slurry containing above 5% of dry matter. The shorter survival of bacteria analysed at higher temperatures is explained by the fact that natural microflora develops stronger, this has an antagonistic effect on the pathogenic micro-organisms of the Salmonella genus [16, 29, 30].

Micro-organisms introduced to the soil together with slurry are subject to the impact of various factors, the most important are: soil reaction, organic matter content, temperature and moisture relations in soil. The thermal requirements of faecal micro-organisms do not allow for permanent occupation of the soil environment, although within a short period from when slurry is applied to agricultural fields, the bacteria can proliferate in soil. Finally, however, they undergo a partial or complete elimination from the soil environment. The pace of faecal microbe death in the soil environment varies. According to literature, bacteria survival time can range from several days to even up to several years. Longer survival is

usually found in winter, although alternating periods of freezing and thawing contribute to decreases in the micro-organism population size. In soils rich with organic matter with rich indigenous soil microflora, micro-organisms introduced with slurry can undergo rapid elimination due to high competition for nutrients, and the presence of matter, faecal bacteria populations can also undergo a rapid reduction due to competition for nutrients with autochthonous micro-organisms [29, 30, 33].

Table 5

Survival of selected Salmonella bacilli in the stored pig slurry (pH = 7.5 – 8.0) under natural conditions acc. to [29]

Salmonella bacilli	Survival (days)
Salmonella dublin	39
Salmonella typhimurium	39
Salmonella partayphi B	39
Salmonella anatum	47
Salmonella manchester	47

A very serious threat to the environment causes irrational, too intensive fertilization with slurry. The application of excessive doses of slurry, particularly in cases where it has not been subjected to any hygienization processes, can lead to a distorted capacity for soil self-purification and the spread of parasitic diseases. Literature indicates that Ascaris eggs can preserve their invasive nature in soil for up to around two years, while their presence on plants was observed for several months. Infections of humans and animals can be due to the consuming of plants from fields generously fertilized with animal waste, as viruses and bacteria can penetrate into the root systems and stems of the plants, which points to a possibility of internal and external contamination of plants with pathogenic micro--organisms [29, 30, 33]. Due to the possible risk to the health of humans and animals, it is very important to appropriately prepare slurry for its use in agriculture. Processes of initial hygienization of slurry, which lead to a reduced number of microbes can include, for example, aeration, anaerobic digestion, or the biological treatment of slurry with the activated sludge method [11, 30, 33].

6. Conclusions

Pig slurry is a liquid waste product generated in non-bedding pig farming systems. It constitutes a mixture of faeces, urine, the remains of food and water used for sanitary and cleaning purposes. The chemical composition of pig slurry varies and depends on many factors. A major impact on the concentration of particular elements and chemical compounds in slurry is from its dilution with water. The more diluted the slurry, the less chemical compounds it contains. Typical pig slurry is characterised by a slightly alkaline reaction, a high degree of hydration, and a high chemical and biochemical oxygen demand. Slurry is a material rich with fertilizing macrocomponents (nitrogen, phosphorus,

potassium, calcium), and microelements, necessary for correct plant growth, hence its most appropriate and most rational management should be related to its use for agro-technical purposes as natural fertilizer. Among the factors limiting the agricultural usage of slurry is its sanitary-epidemiological aspect. Due to its rich microbiological content (bacteria, viruses, eggs and oocysts of parasites), slurry can be a source of pathogenic micro-organism spread in the environment. However, based on the results of the studies presented in many literature items, one can state that the appropriate application of slurry, in line with the requirements of agricultural engineering, and the observation of principles relating to hygiene, does not pose a microbiological risk of contamination to waters and soils with pathogens.

References

[1] Maćkowiak Cz., *Zasady stosowania gnojowicy*, Zalecenia nawozowe, Cz. IV, IUNG, Puławy 1994.

[2] Maćkowiak Cz., *Gnojowica – jej właściwości i zasady stosowania z uwzględnieniem ochrony środowiska*, Materiały szkoleniowe 75/99, IUNG, Puławy 1999.

[3] Kutera J., Hus S., *Rolnicze oczyszczanie i wykorzystanie ścieków i gnojowicy*, Wydawnictwo Akademii Rolniczej we Wrocławiu, Wrocław 1998.

[4] Ustawa z dnia 10 lipca 2007 r. o nawozach i nawożeniu, Dz.U. 2007 nr 147 poz. 1033.

[5] Konieczny K., Kwiecińska A., *Oczyszczanie gnojowicy z zastosowaniem technik membranowych*, Polska Inżynieria Środowiska Pięć Lat po Wstąpieniu do Unii Europejskiej (pod redakcją Ozonek J., Pawłowska M.), Monografie Komitetu Inżynierii Środowiska Polskiej Akademii Nauk, 58, 2009, 147-151.

[6] Krzywy E., *O gnojowicy raz jeszcze*, Aura 4, 2004, 16-17.

[7] Pawełczyk A., Muraviev D., *Zintegrowana technologia oczyszczania ciekłych odpadów z hodowli trzody chlewnej*, Przemysł Chemiczny 82/8-9, 2003, 2-4.

[8] Gonzalez-Fernandez C., Nieto-Diez P.P., Leon-Cofreces C., Garcia-Encina P.A., *Solids and nutrients removals from the liquid fraction of swine slurry through screening and flocculation treatment and influence of these processes on anaerobic biodegradability*, Bioresource Technology 99, 2008, 6233-6239.

[9] Walker P., Kelley T., *Solids, organic load and nutrient concentration reductions in swine waste slurry using a polyacrylamide (PAM)-aided solids flocculation treatment*, Bioresource Technology 90, 2003, 151-158.

[10] Chelme-Ayala P., Gamal El-Din M., Smith R., Code K.R., Leonard J., *Advanced treatment of liquid swine manure using physico-chemical treatment*, Journal of Hazardous Materials 186, 2011, 1632-1638.

[11] Kutera J., *Gospodarka gnojowicą*, Wydawnictwo Akademii Rolniczej we Wrocławiu, Wrocław 1994.

[12] Winnicki S., Pleskot R., Zając G., *Ekspertyza: Technika i technologia produkcji trzody chlewnej*, Instytut Budownictwa, Mechanizacji i Elektryfikacji Rolnictwa w Poznaniu, Poznań 2009, publikacja dostępna w serwisie: www.agengpol.pl – 18.01.2013.

[13] Dokument Referencyjny o Najlepszych Dostępnych Technikach dla Intensywnego Chowu Drobiu i Świń, Ministerstwo Środowiska, Warszawa 2005.

[14] Hus S., *Chemia wody, ścieków i gnojowicy*, Wydawnictwo Akademii Rolniczej we Wrocławiu, Wrocław 1995.

[15] Gorlach E., Mazur T., *Chemia rolna*, Wydawnictwo Naukowe PWN, Warszawa 2001.

[16] Szejniuk B., Budzińska K., Wroński G., Kostrzewa M.M., Jurek A., *Przeżywalność pałeczek Salmonella Enteritidis w gnojowicy świńskiej*, Rocznik Ochrony Środowiska, Tom 13, 2011, 2049-2060.
[17] Karakashev D., Schmidt J.E., Angelidaki I., *Innovative process scheme for removal of organic matter, phosphorus and nitrogen from pig manure*, Water Research 42, 2008, 4083-4090.
[18] Moral R., Perez-Murcia M.D., Perez-Espinosa A., Moreno-Caselles J., Paredes C., *Estimation of nutrient values of pig slurries in Southeast Spain using easily determined properties*, Waste Management 25, 2005, 719-725.
[19] Rufete B., Perez-Murcia M.D., Perez-Espinosa A., Moral R., Moreno-Caselles J., Paredes C., *Total and faecal coliform bacteria persistence in a pig slurry amended soil*, Livestock Science 102, 2006, 211-215.
[20] Mondor M., Masse L., Ippersiel D., Lamarche F., Masse D.I., *Use of electrodialysis and reverse osmosis for the recovery and concentration of ammonia from swine manure*, Bioresource Technology 99, 2008, 7363-7368.
[21] Kalyuzhnyi S., Sklyar V., Epov A., Arkhipchenko I., Barbolina I., Orlova O., Kovalev A., Nozhevnikova A., Klapwijk A., *Sustainable treatment and reuse of diluted pig manure streams in Russia. From laboratory trials to full-scale implementation*, Applied Biochemistry and Biotechnology Vol. 109, 2003, 77-94.
[22] Sanchez M., Gonzales J.L., *The fertilizer value of pig slurry. I. Values depending on the type of operation*, Bioresource Technology 96, 2005, 1117-1123.
[23] Dyrektywa Rady 91/676/EEC z dnia 12 grudnia 1991 r. dotycząca ochrony wód przed zanieczyszczeniami powodowanymi przez azotany pochodzenia rolniczego (tzw. Dyrektywa Azotanowa).
[24] Zbytek Z., Talarczyk W., *Gnojowica a ochrona środowiska naturalnego*, Technika Rolnicza Ogrodnicza Leśna 4, 2008, 12-14.
[25] Zhu J., *A review of microbiology in swine manure odor control*, Agriculture, Ecosystems and Environment 78, 2000, 93-106.
[26] Le P.D., Aarnink A.J.A., Jongbloed A.W., van der Peet Schwering C.M.C., Ogink N.W.M., Verstegen M.W.A., *Effects of crystalline amino acid supplementation to the diet on odor from pig manure*, Journal of Animal Science 85, 2007, 791-801.
[27] Ye F.X., Zhu R.F., Li Y., *Deodorization of swine manure slurry using horseradish peroxidase and peroxides*, Journal of Hazardous Materials 167, 2009, 148-153.
[28] Predicala B., Nemati M., Stade S., Lagu C., *Control of H_2S emission from swine manure using Na-nitrite and Na-molybdate*, Journal of Hazardous Materials 154, 2008, 300-309.
[29] Strauch D., *Survival of pathogenic micro-organisms and parasites in excreta, manure and sewage sludge*, Rev. sci. tech. Off. int. Epiz., 10 (3), 1991, 813-846.
[30] Olszewska H., Skowron K., Skowron K.J., Gryń G., Świąder A., Rostankowska Z., Dębicka E., *Przeżywalność wybranych bakterii wskaźnikowych w składowanej gnojowicy świńskiej*, Ekologia i Technika Vol. XIX, Nr 2, 2011, 62-68.
[31] Cotta M.A., Whitehead T.R., Zeltwanger R.L., *Isolation, characterization and comparison of bacteria from swine faeces and manure storage pits*, Environmental Microbiology 5 (9), 2003, 737-745.
[32] Whitehead T.R., Cotta M.A., *Characterisation and comparison of microbial populations in swine faeces and manure storage pits by 16s rDNA gene sequence analyses*, Anaerobe 7, 2001, 181-187.
[33] Olszewska H., *Aspekty higieniczne rolniczego wykorzystania gnojowicy*, Rozprawy nr 116, Wydawnictwo Uczelniane Akademii Techniczno-Rolniczej, Bydgoszcz 2005.

TECHNICAL TRANSACTIONS | CZASOPISMO TECHNICZNE
CHEMISTRY | CHEMIA
1-Ch/2014

PEKKA PARVINEN*, KRYSTYNA WIECZOREK-CIUROWA**

SIMPLIFIED METHODS FOR THE DETERMINATION OF HYDROGEN SULPHIDE ACID IN SEDIMENT CONTAMINATED BY MINING ACTIVITIES

UPROSZCZONE METODY OZNACZANIA KWASU LOTNYCH SIARCZKÓW W OSADACH SKAŻONYCH PRZEZ DZIAŁALNOŚĆ GÓRNICZĄ

Abstract

The concentration level of hydrogen sulphide acid in the sediment contaminated by mining activities can be applied as criteria ability of sediments to bind the heavy metals and mobility of such metals. The determination of hydrogen sulphide acid (HSA) by molecular absorption spectrometry and combustion-IR analysis in sediment samples is described. The liberation of H_2S is performed through the addition of the concentrated sulphuric or hydrochloric acid. The liberated hydrogen sulphide is measured directly using molecular absorption spectrometry (MAS) and by absorbing the HSA in a silver nitrate solution and measuring the precipitated sulphur by combustion (the IR method). The lowest determinable concentrations were at the level of 2–10 μg g^{-1}.

Keywords: *state of sediment*, *hydrogen sulphide acid determination*, *molecular absorption spectrometry*, *silver sulphide precipitation*

Streszczenie

Lotny kwas siarki może być stosowany jako ilościowe kryterium jakości osadów wskazując ich zdolność wiązania metali ciężkich. Opisano możliwość oznaczania tego kwasu (AVS) w osadach metodą absorpcyjnej spektrometrii molekularnej i analizy spalania-IR. Wydzielanie siarkowodoru przeprowadza się przez dodanie stężonego kwasu siarkowego lub kwasu solnego. Uwalniany H2S jest mierzony bezpośrednio metodą molekularnej spektrometrii absorpcyjnej (MAS) jak również absorbując go w roztworze azotanu srebra i mierząc strąconą siarkę przez spalanie techniką IR. Najniższe możliwe do oznaczenia stężenia były w zakresie 2–10 μ g^{-1}.

Słowa kluczowe: *stan osadu, oznaczanie kwasu siarkowodorowego*, *absorpcyjna spektrometria molekularna*, *wytrącanie siarczku srebra*

* Ph.D. Pekka Parvinen, Labtium Oy, Outokumpu, Finland.
* Prof. Ph.D. D.Sc. Krystyna Wieczorek-Ciurowa, Faculty of Chemical Engineering and Technology, Cracow University of Technology.

1. Introduction

The sulphur cycle in aquatic environments is generally the main factor controlling the mobility of metallic elements between the sediment and the water phase. In the sediments are the dissolved metallic elements as metal sulphides [1–5]. The amount of the acid volatile sulphur, H_2S, from the precipitated sulphides can be used as the determination method of easily available sulphide in sediment giving simultaneously indicating the mobility of the heavy metals [6–8]. Acid volatile sulphur is defined as the fraction of sulphide which is extractable by cold hydrochloric acid. The determinations of HSA are performed by liberating the H_2S gas through acidification of the sample using hydrochloric acid (4–8 M). Generally, the formed hydrogen sulphide is absorbed in different solutions and determined by gravimetric, photometric, titrimetric, chromatographic and conductometric methods [1, 3, 9–12].

Current methods for the determination of HSA are often cumbersome, time consuming and generally require liquid samples and that is why different kinds of pre-treatment techniques are required.

The aim of presented study was to evaluate and develop quick and simple procedures to determine HSA in sediment samples for environmental control. These procedures are based on the liberation of HSA from sediment as H_2S and its direct determination using gas phase molecular absorption, combustion IR – analysis, etc. [13–15].

2. Experimental Method

2.1. Apparatus

The molecular absorption of H_2S was measured using a Perkin Elmer 4100 atomic absorption spectrometer with a 15 cm long absorption cell adjusted over the burner head. The system is described in Fig. 1 [15, 16]. For the measurements performed at the absorption maximum of H_2S at 196.0 nm, the selenium hollow-cathode lamp (Perkin Elmer) was used as the irradiation source [16].

The other determination of HSA was performed through combustion infrared analysers LECO and ELTRA after the absorption of the liberated H_2S and its precipitation by silver nitrate.

2.2. Materials

All the reagents were Merck pro-analytical grade. A standard sulphide solution (10000 mg l^{-1}) was prepared by dissolving $Na_2S{\cdot}9H_2O$ in distilled water containing 1% of NaOH (the solution was checked and standardised by iodometric titration). The working standard sulphide solutions and reference solutions were prepared by diluting this solution. The reference solid material was prepared by adding 5.0, 10.0 and 20.0 mg of sulphide in the form of potassium sulphide to 100 g of quartz (< 2 mm). The homogenisation was performed using the swing mill for milling the components for one minute in order to obtain a homogenous mixture. The standard and reference sulphide solutions and

materials were prepared daily. The concentrated sulphuric or hydrochloric acid was used as the reaction solution.

2.3. Procedure

The experimental set-up for the determination of H_2S by MAS is presented in Fig. 1. The sample was weighted in the reaction tube and subsequently, the acidic reaction solution was injected into the tube in order to liberate the H_2S gas. After the reaction solution was added to the sample, the formed H_2S was introduced into an absorption cell by carrier gas and the peak height of the generated absorption signal was measured. The volume of liquid standards and samples was 200 µl and the weights of solid standards and samples were between 0.01 and 1.0 g. For the liberation of H_2S gas, 1 ml of the sulphuric acid reaction solution was used in the determinations for 0.01–1.0 g of sample. The flow rate of the carrier gas used was 6 l min^{-1}.

When the analysis was performed by absorption and precipitation of liberated H_2S gas in the absorption tube by an $AgNO_3$ solution (0.1 M), the sample amounts were 10–20 ml or 5–50 g. As the reaction solution 10–30 ml of hydrochloric acid (6 M) was used. The formed H_2S was transported to absorption tube by carrier gas. The precipitated silver sulphide was filtered and the dried filter was placed in the sample cup of the sulphur analyzer and routine analysis was performed. The procedure used in the liberation of H_2S gas and its absorption is presented in Fig. 1.

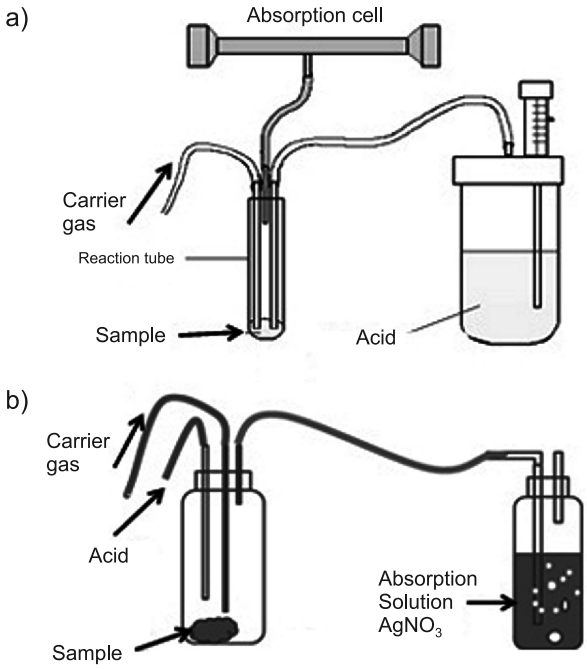

Fig. 1. The measurement systems: a) the system where the H_2S is measured by molecular absorption and b) the system where the liberated H_2S is absorbed and precipitated

3. Results and Discussion

3.1. The measurement of artificial samples

The basic reaction which describes the liberation of the H_2S in the reaction tube is:

$$S^{2-}_{(aq)} + 2H^{+}_{(aq)} \rightarrow H_2S(g)$$

This reaction is very fast and the liberation of H_2S is immediate. In the liberation of H_2S, a sulphuric acid solution was used in addition to a hydrochloric acid solution that has been traditionally used in the determination of HSA. The dry samples had to be moistened before adding the acid solution, because when the acid is injected onto the dry sample, in some cases, only the surface reacts forming a cover under which the remaining part of the sample only slowly gets into contact with the acid causing slower evaporation of H_2S. Under correct conditions, the reaction is immediate following the addition of the reaction solution.

In the case of the MAS method, the dead volume of the reaction system together with the connection to the absorption cell has been minimised at 18 ml in order to keep the concentration of the formed H_2S in the absorption measurement cell as high as possible. The shape of the absorption peak was dependent upon the flow rate of the carrier gas as well as on the type of the absorption cell used. With the high flow rate and open absorption cell, it was possible to obtain very sharp absorption peaks. In the case of using the hydrochloric acid instead of sulphuric acid as the reaction solution, a slower liberation of H_2S was observed. The absorptions were about half of size of those obtained with the use of sulphuric acid (peak height was taken into account in determination). When the determinations were performed by measuring the area of the absorption signal, the results were quite similar for both of the acids.

Sulphuric acid was selected as the reaction solution in the MAS measurement for practical reasons, because by that procedure, a repeatable and stable absorption signal was obtained which allowed for the shortest measurement times. In the case of the MAS procedure, the flow rate of the carrier gas which brings the liberated H_2S to the absorption cell, was selected to be 6 l min^{-1}. At this rate, the H_2S, after one second in the absorption cell, gives an adequate signal for its the determination.

The reaction and mixing time after the addition of the reaction solution was chosen to be as short as possible, about one second, after which the gas flow was introduced into the reaction tube. In these measurements, the peak height for quantification was because the liberation of H_2S is quick and repeatable. The lowest determinable concentration of acid volatile sulphide by the MAS procedure was at a level of 2 µg g^{-1} and the corresponding sensitivity (A 1%) was 0.5 µg g^{-1}. The method is quick and the time required for one determination, after the sample has been measured to the reaction tube, is 20 seconds. Within one hour, 20–30 samples can be completely and easily measured.

When the method that is based on the absorption of the liberated H_2S in the absorption solution the reaction speed and gas flow rate are not critical same it is possible to use bigger sample amounts those demand only increase of the added acid volume. Hydrochloric acid (6 M) was used as the reaction/liberation solution and the liberated H_2S was absorbed in the silver nitrate solution where silver sulphide was formed and precipitated.

The precipitated silver sulphide was filtered, drying and sulphur analysis was performed by the combustion infrared method. The detection limit of the method lies at a level of 10 µg of S.

The developed method was first tested by different kinds of soil and mineral samples by adding the known amounts of hydrogen sulphide acid as sodium sulphide to the reaction tube with one to ten gram of sample (Table 1). The results of measurements were in a good agreement with the theoretical values. As the mineralised form of the sulphides they have not anymore capacity to bind heavy metals from water, therefore they were tested as freshly milled sulphide ores (Cu-Ni and pyrite). As expected, the amount of H_2S separated from the ore gave less than 0.1% of the total amount of sulphides.

Table 1

The results of determination of HSA from artificial samples by MAS and combustion – IR absorption method after precipitation

Sample	Sulphide added µg	MAS µg	precip- abs.-Eltra µg
1	20	20.5	20.7
2	50	48.0	50.8
3	100	95.3	101.7
4	200	184.0	199.4
5	500	483.3	514.6

Table 2

HSA concentrations measured in sediment samples contaminated by mining activities. The measurements were performed by molecular absorption and by absorption-precipitation – combustion IR (Eltra) methods

Sample	MAS µg/mg	Precip.- abs.-Eltra µg/mg
S 1	3.3	4.7
S 2	6.5	5.2
S 3	11.9	15.8
S 4	14.8	16.7
S 5	21.4	23.8
S 6	24.8	24.1
S 7	25.8	26.8
S 8	34.5	37.4
S 9	35.3	41.6
S 10	35.4	33.1

3.2. The measurement of real samples

The tested samples were origin from the sediment heavily polluted by handling of ores where the mineral concentrations was between 0.1–5 % and the level of the contaminants such as Cu and Zn between 100 and 500 mg kg^{-1}. As the reference the total sulphur was measured by combustion infrared method and the part of non-volatile sulphur by measurement after the treatment of the sample with HCl. From those results, the amount of vaporised sulphide sulphur was estimated. The good agreement was found between the results obtained by molecular absorption and the precipitation-combustion IR method with those obtained by the reference combustion IR method that was used in order to get the level of acid volatile sulphide in the samples. Tables 1 and 2 present the results obtained in the determination of the different samples where it can be seen that the accuracy of the results obtained are sufficient. In the case of the real samples, their low homogeneity and different sizes of solid particles caused deviation in the analytical results.

4. Conclusions

The quickly determination of acid volatile sulphides represents a good consider changing 'good' to more 'practical' method for evaluating the state of the sediment including its ability to bind the heavy metals and evaluate their mobility. For the determination of HSA in different kinds of sediment samples, the studied methods where the liberated H_2S is measured either directly by molecular absorption or it is absorbed in solution by precipitation and determined by combustion IR method are providing good analytical tools and practices. No special sample preparation is needed and the time consumption of the analysis is much lower than in traditional methods. The pieces of analytical equipment needed are an atomic absorption spectrometer or a combustion IR analyser – both of these are basic pieces of equipment in every mine laboratory. It was shown that the sensitivities and precision of the methods are satisfactory. The experimental results suggest that for the determination of HSA, these simple and accurate methods would provide a good analytical tool for practical reasons.

References

[1] Anwar J., Waheed-Uz-Zaman, Hameed A., Yasmeen F., J. Chem. Soc. Pak., 20/4, 1998, 235-239.
[2] Müller B., Stierli R., Anal. Chim. Acta, 40, 1999, 257-264.
[3] Cutter G.A., Oats T.J., Anal. Chem., 59, 1987, 717-721.
[4] Lindsay W.L., *Chemical Equilibria in Soil*, John Wiley, New York 1979.
[5] Crouzet C., Kedziorek M.A.M., Altmann R.S., Bourg A.C.M., Environ. Tech., 21, 2000, 285.
[6] Di Toro D.M., Mahony J.D., Hansen D.J., Scott K.J., Hicks M.B., Mayr S.M., Remond M.S., Environ. Toxicol. Chem., 9, 1990, 1487-1502.
[7] Leonard E.N., Mattson V.R., Benoit D.A., Hoke R.A., Ankley G.T., Hydrobiologia, 271, 1993, 87-95.
[8] Fiedler H.D., Rubio R., Rauret G., Casals I., Talanta, 48, 1999, 403-407.

[9] Crompton T.R., *Determination of Anions, A Guide for the Analytical Chemist*, Springer–Verlag, Berlin–Heidelberg 1996, 324-336.
[10] Pawlak Z., Pawlak A.S., Talanta, 48, 1999, 347-353.
[11] Tack F.M., Lapauw F., Verloo M.G., Talanta, 44, 1997, 2185-2192.
[12] Brown K.A., McGreer E.R., Taekema B., Cullen J.T., Aquat. Geochem., 17, 2011, 821-839.
[13] Syty A., Anal. Chem., 51, 1979, 911-914.
[14] Parvinen P., Lajunen L.H.J., At Spectrosc., 15, 1994, 83-86.
[15] Parvinen P., Wieczorek-Ciurowa K., Chem. Anal., 4, 1996, 477-481.
[16] Parvinen P., Wieczorek-Ciurowa K., Chem. Anal., 50, 2005, 761-768.

TECHNICAL TRANSACTIONS | **CZASOPISMO TECHNICZNE**
CHEMISTRY | CHEMIA
1-Ch/2014

TEODORA SIKORA*, KRYSTYNA WIECZOREK-CIUROWA*

PROSPECTS OF USING MECHANOCHEMICAL SYNTHESES IN THE FABRICATION OF COMPOSITE POWDERS FOR TRIBOTECHNOLOGY

PERSPEKTYWY UŻYCIA SYNTEZ MECHANOCHEMICZNYCH DO WYTWARZANIA PROSZKÓW KOMPOZYTOWYCH DLA TRIBOTECHNOLOGII

A b s t r a c t

The aim of tribotechnological research is the reduction of tribo-couple wear through the optimization of the functional properties of the materials. Polymer matrix composites enriched by powdered materials (e.g. metal-ceramic composite powders) have a wide range of applications in the field of tribotechnology. The possibilities of producing such fillers via green, environmentally-friendly syntheses using the high-energy ball milling process are presented.

Keywords: *mechanochemistry*, *frictional materials*, *tribology*, *composite powders*

S t r e s z c z e n i e

Optymalizacja właściwości użytkowych w oparciu o ograniczenie zużycia powierzchni par trących jest przedmiotem badań tribotechnologii. Szerokie zastosowanie w tej dziedzinie znajdują materiały kompozytowe z osnową polimerową, uszlachetniane materiałem proszkowym, m.in. proszkami kompozytowymi metaliczno-ceramicznymi. Przestawiono możliwości wytwarzania takich napełniaczy na drodze ekologicznych syntez z użyciem wysokoenergetycznego procesu mielenia.

Słowa kluczowe: *mechanochemia*, *materiały cierne*, *tribologia*, *proszki kompozytowe*

* Ph.D. Student Eng. Teodora Sikora, Prof. Ph.D. D.Sc. Krystyna Wieczorek-Ciurowa, Faculty of Chemical Engineering and Technology, Cracow University of Technology.

1. Introduction

In ancient times, mankind tried to improve the strength and mechanical properties of functional materials. Around 800 BC, bricks made in the Near East were reinforced with straw and then sun-dried – as a consequence, they were stronger and were more compression resistant than fired bricks. This was the first step towards composite materials engineering. Composites are defined as materials composed of at least two different components, i.e. the matrix and the filler. The specific properties of the composite are greater than the sum of its parts. The new materials show specific, advanced mechanical and chemical features due to synergy of the components' properties.

The intensive development of materials engineering at the beginning of the 20th century caused a growing interest in new methods of composite materials production. Simultaneously, pro-ecological, environmentally friendly methods of materials production became increasingly desired. One of these methods, mechanochemical synthesis, has been in use since the 1960s. Based on the changing of mechanical energy to chemical energy, it allows for the obtaining of functional materials such as alloys, intermetallics, composite powders, catalytic precursors and ceramics with a wide range of properties (e.g. perovskite ceramics) [1]. The application of mechanochemically synthesized ceramic-ceramic and ceramic-metallic powders as fillers of polymer matrix composites (PMCs) could improve the properties of functional materials and lower the costs of their production.

Nowadays, the automotive and machinery industries are important consumers of composite materials. Polymer composites with particulate reinforcement are known to have high values of wear resistance and hardness. These properties can be tailored to the specific field of application. For this reason, complex functional materials are the most commonly used components for tribo-elements [2, 3].

The main object of tribology is the investigation of phenomena observed in the contact of solids. These macro and micro-interactions between two mating surfaces have a crucial influence on the tribological characteristics of the material. Furthermore, tribology deals with practical issues relating to wear factors of tribo-couple surfaces. The creation of reasonable and useful tribological systems based on the requirements defined by tribology is an objective of tribotechnological investigation. In other words, tribotechnology is involved in developing practical applications of tribology. Mainly, it is focused on the optimization (increasing or decreasing) of the friction coefficient in the friction node and on wear decreasing technologies.

Mechanochemical synthesis is a relatively new technology of powders production. The powdered materials can be used as fillers of polymeric matrix to form the elements of frictional couples. This explains why mechanochemical synthesis can be a new approach for tribotechnology.

2. Composite materials for tribotechnology

The term 'composites' defines a wide group of materials differing in their physicochemical properties, composition or structure. Composites are classified into numerous groups by their

origin, type of reinforcement, application or type of matrix. Different materials are applied as the matrix: metals (MCMs – Metal Matrix Composites); ceramics (CMCs – Ceramic Matrix Composites); polymers (PMCs – Polymer Matrix Composites) [4].

The PMCs are the specific group of materials for tribological applications. Such materials are widely used in the automotive industry as components of braking systems, bearings, clutches, etc. The polymeric matrix decreases the mass of tribo-elements and increases their corrosion resistance, vibration damping capacity and ease of shaping. However, the disadvantages of polymer matrices are their increased thermal expansion, swelling in contact with lubricants and lower thermal conductivity. Therefore, modification of polymer properties to counteract these disadvantages by using various fillers is required.

The wear resistance is the primary factor which determines the usefulness of composites in tribology. It is documented that wear performance can be markedly improved by using a composite filler or various combinations of fillers. This modification of adding fillers may considerably extend the service life of composites. This parameter depends on the filler type, volume fraction and its distribution within the matrix.

The type of filler has a critical effect on the properties of composites and its application. Using powdered reinforcement is the most commonly applied means of increasing its mechanical strength [5]. However, the improvement of mechanical properties not only depends on the filler type, but also on the size and shape of reinforced particles. Numerous papers report on the straight influence of the above-mentioned parameters on electrical and thermal conductivity, thermal resistance [6], mechanical strength, flammability and optical properties of composites [7]. Composites filled with smaller particles present higher levels hardness and stiffness [8], thus meeting the basic requirements of materials for the automotive industry [9].

3. Manufacturing of the composite fillers

Tribological systems (tribo-couples) filled with particles consist of strengthening components (mica, silica, basalt tuff) and modifiers of properties (inorganic compounds, composite powders). The proper selection of modifiers depends on the intended use of the material. Modifiers such as Al_2O_3, SiO_2, SiC, ZnO, ZrO_2 and Fe_3O_4 increase and stabilize the friction coefficient. Particles of MoS_2, ZnS, CuS and graphite are used as lubricants to reduce friction and wear [10]. Tailoring the type and filling ratio of friction modifiers allows for the obtaining of a material that displays excellent wear and friction characteristics.

Powdered fillers can be produced by a variety of traditional techniques, such as sol-gel, impregnation, reduction [11], plasma process [12] or, alternatively, by means of mechanochemical synthesis. The essence of mechanochemical synthesis is the manufacturing of new materials via solid-state reactions induced by high-energy milling. The mechanical energy is introduced and accumulated in the milled material in the form of stress and lattice defects. These phenomena promote the creation of new systems and compounds. Mechanochemical synthesis is a one-step process, thus, the manufacturing of composites is easier and faster. Additionally, the method generates virtually no waste and does not require the application of solvents. Mechanical synthesis is an universal and

useful method because it offers flexibility in the selection of substrates, the reactions are carried out in the solid-state. Therefore, the application of mechanical synthesis for the production of metallic-ceramic and ceramic-ceramic powders is gaining ground as an interesting alternative to traditional routes for the manufacturing of composite fillers.

4. Composite powders – selection of the best polymer matrix fillers

The applicability of composite powders as fillers of the polymer matrix mainly depends on the particle shape, size, size distribution and chemical homogeneity.

The mean size of the filler particles is a crucial parameter of the composite material properties**.** The term *nanocomposites* is applied to polymers filled with nanoparticles (an average particle size of 10–100 nm). In microcomposites, particles with a diameter higher than 100 nm are used.

The shape of the filler particles is a supplementary parameter of reinforcement characterization. The classical theory of manufacturing ceramic powders indicates that a spherical shape is most convenient for sintering. However, for some applications, spherical powders show unsatisfactory properties. For example, platelet-shaped particles of ferrites (e.g. $BaFe_{12}O_{19}$) show better magnetic properties [13]. A wide-range of applications is also observed for composites filled with SiC whiskers. These acicular particles significantly improve fracture toughness of the material.

Particle size distribution is the key parameter in functional materials. Most of the ceramic materials require a narrow size distribution, especially when the manufactured material is intended for consolidation by sintering.

Producing monodisperse powders is as unfavorable as manufacturing material with a wide particle size distribution. These types of powders tend to form dense geometric packing areas joined with groups of loosely coupled grains. The described phenomena are unfavorable during sintering processes and cause the formation of wide pores in the sintered material. Moreover, monodisperse powder is prone to create mechanically stable agglomerates. The slightest differentiation of grain size can be obtained by 'wet' methods of particle manufacturing (e.g. sol-gel or precipitation methods). Methods based on the grinding of materials allow for the production of powdered material with diverse grain sizes. These powders tend to mechanical densification (hot pressing) and sintering.

Filler distribution in the matrix – in most cases, the homogeneous distribution of filler particles in the matrix is of paramount importance with respect to the intended tribological applications. The technology of composite manufacturing (including the method of matrix-reinforcement homogenization) depends on the type of manufactured composite and component properties (e.g. type of polymer matrix).

Functionally graded materials (FGMs) are a group of very special engineering composites. These materials have a graded composition and show the variation of properties as a function of the place where these parameters are measured. In other words, FGMs are the composites wherein the filler-matrix volume ratio or type of the reinforcement change along the defined direction. Nowadays, functionally graded structures are increasingly applied in numerous engineering systems including sensors, electronics, magnetic components, machine

parts and many others [8, 14]. FGMs are applied everywhere where smoothly changing properties are desired and cannot be realised in uniform materials. For example, the material structure may possess a smooth transition from hard phases (with good sliding properties on the one side), to a structure with high toughness and thermal conductivity on the other (inner) side. With their gradual variation in composition, FGMs may exhibit good resistance to wear and thermal stress and hence, are readily applied for sliding bearings and rollers [8].

5. Effects of the fillers on the mechanical properties of PMCs

Erosion of the contact sides is a serious problem in engineering systems. This phenomenon involves the progressive loss of material and generates high costs with regard to industrial processes. It is well-known that the erosion rate of the polymer composites is higher than that of the neat polymers [15]. Erosion refers to the gradual wear of tribo-couple surfaces through the repeated impact of small solid particles which are the wear products of tribo-couple cooperation. Especially the coarse particles being accelerated to the very high velocities in a gas or liquid carrier, entrapped between the contacting surfaces may lead to serious degradation of both sliding-pair components. Except for erosion, additional unwanted processes such as thermal, chemical and physical reactions take place in the friction zone [16, 17].

Depending on the particle impingement angle, two different erosive wear mechanisms are proposed - ductile erosion and brittle erosion. In ductile erosion, the maximum material removal occurs at impingement angles (α) lying between 15 and 30°. Brittle erosion is observed at $\alpha \approx 90°$. In PMCs, the maximum wear rate is observed for α ranging from 45 to 60°, therefore, the erosion mechanism is defined as *semi-ductile* [18, 19].

When discussing the erosion rate of PMCs, it is necessary to consider a few important factors including:

– the type of polymer matrix (thermosetting or thermoplastic),
– the type of filler material (fibers or particles) and its characteristics (brittleness, hardness, length and aspect ratio, orientation in the matrix, etc.),
– the volume fraction of fillers.

It has been proven that particulate fillers can be successfully used as erosive wear modifiers [20, 21]. Composites filled with very hard particles (e.g. Al_2O_3) show better erosion resistance than materials filled with softer particles (e.g. the mixture of SiC and fly ash). The reduction in material loss can be explained by two reasons. Firstly, the bulk hardness of composite increases when hard particles are applied. Secondly, a high amount of the erodent energy can be absorbed by other particulate fillers, thus decreasing the energy absorbed by the matrix and, optionally, fibers [16]. The synergistic effect of those phenomena markedly decreases the rate of erosion and consequently, increases the service life of the interacting elements.

The study is partially supported by the Polish Ministry of Science and Higher Education, projects C-1/KWC/DS/2013-14 and C-1/DS-M/2013-14.

References

[1] Wieczorek-Ciurowa K., *Mechanochemical Synthesis of Metallic-Ceramic Composite Powders*, R. Banerjee, I. Manna (Eds.), *Ceramic Nanocomposite*, Woodhead Publ. Ltd, Abington Hall, Great Abington Cambridge, UK, 2010.

[2] Friedrich K., Chang L., Haupert F., *Current and Future Applications of Polymer Composites in the Field of Tribology* [in] Nicolais L., Meo M., Milella E. (Eds.), *Composite Materials: A Vision for the Future*, Springer-Verlag London Ltd, London, UK, 2011.

[3] Zhang Z., Friedrich K., *Tribological characteristics of Micro- and Nanoparticle Filled Polymer Composites* [in] Friedrich K., Fakirov S., Zhang Z. (Eds.), *Polymer Composites. From Nano- to Macro-Scale*, Springer Science+Business Media, Inc., 2005.

[4] Basu B., Kalin M., *Tribology of Ceramics and Composites. A Materials Science Perspective*, Ch. 2, John Wiley & Sons, Inc., 2011, 7-17.

[5] Friedrich K., Chang L., Haupert F., *Current and Future Applications of Polymer Composites in the Field of Tribology* [in] Nicolais L., Meo M., Milella E. (Eds.), *Composite Materials. A Vision for the Future*, Springer-Verlag London Ltd., 2011, 127-167.

[6] Nikkeshi S., Kudo M., Masuko T., *Dynamic Viscoelastic Properties and Thermal Properties of Ni Powder-Epoxy Resin Composites*, Journal of Applied Polymer Science, vol. 69, 1998, 2593-2598.

[7] Hanemann T., Vinga-Szabo D., *Polymer-Nanoparticle Composites: From Synthesis to Modern Applications*, Materials, vol. 3, 2010, 3468-3517.

[8] Friedrich K., Zhang Z., Schlarb A. K., *Effects of Various Fillers on the Sliding Wear of Polymer Composites*, Composites Science and Technology, vol. 65, 2005, 2329-2343.

[9] Garces J.M., Moll D.J., Bicerano J., Fibiger R., McLeod D.G., *Polymeric Nanocomposites for Automotive Applications*, Advanced Materials, vol. 12, 2000, 1835-1839.

[10] Bahadur S., Schwartz C., *Mechanical and Tribological Behaviour of Polymers Filled with Inorganic Particulate Fillers* [in] Sinha S.K., Briscoe B.J. (Eds.), *Polymer Tribology*, Imperial College Press, London 2009, 416-448.

[11] Hussain F., Hojjati M.I., Okamoto M., Gorga R.E., *Polymer-matrix Nanocomposites, Processing, Manufacturing, and Application: An Overview*, Journal of Composite Materials, vol. 40, 2006, 1511-1575.

[12] Vollath D., *Plasma Synthesis of Nanopowders*, Journal of Nanoparticle Research, vol. 10, 2008, 39-57.

[13] Haberko K., *Proszki Ceramiczne – Budowa i Wymagania*, Inżynieria Materiałowa, vol. 2 (85), 1995, 35-41.

[14] Lee N.J., Jang J., Park M., Choe C.R., *Characterization of Functionally Gradient Epoxy/Carbon Fibre Composite Prepared under Centrifugal Force*, Journal of Materials Science, vol. 32, 1997, 2013-2020.

[15] Arjula S., Harsha A.P., *Study of Erosion Efficiency of Polymers and Polymer Composites*, Polymer Testing, vol. 25, 2006, 188-196.

[16] Płaza S., Margielewski L., Celichowski G., *Wstęp do tribologii i tribochemia*, Wydawnictwo Uniwersytetu Łódzkiego, Łódź 2005.

[17] Patnaik A., Satapathy A., Chand N., Barkoula N.M., Biswas S., *Solid Particle Erosion Wear Characteristics of Fiber and Particulate Filled Polymer Composites: A review*, Wear, vol. 268, 2010, 249-263.

[18] Barkoula N.M., Karger-Kocsis J., *Review. Processes and Influencing Parameters of the Solid Particle Erosion of Polymers and their Composites*, Journal of Material Science, vol. 37, 2002, 3807-3820.

[19] Chowdhury A.A., Nuruzzaman D.M., Rahaman M.L., *Erosive Wear Behaviour of Composite and Polymer Materials – A review*, Recent Patents on Mechanical Engineering, vol. 2, 2009, 144-153.

[20] Patnaik A., Satapathy A., Mahapatra S.S., Dash R.R., *Implementation of Taguchi Design for Erosion of Fiber Reinforced Polyester Composite Systems with SiC Filler*, Journal of Reinforced Plastics and Composites, vol. 27, 10, 2008, 1093-1111.

[21] Patnaik A., Satapathy A., Mahapatra S.S., Dash R.R., *Tribo-performance of Polyester Hybrid Composites: Damage Assessment and Parameter Optimization Using Taguchi Design*, Materials and Design, vol. 30, 2009, 57-67.

TECHNICAL TRANSACTIONS | CZASOPISMO TECHNICZNE
CHEMISTRY | CHEMIA
1-Ch/2014

KRZYSZTOF STANUCH*

INFLUENCE OF VANADIUM DOPPING ON DIELECTRIC PROPERTIES OF BARIUM TITANATE CERAMICS

WPŁYW DOMIESZKOWANIA VANADEM NA WŁAŚCIWOŚCI DIELEKTRYCZNE CERAMIK TYTANIANU BARU

A b s t r a c t

The purpose of this article is to present the impact of vanadium substitution on the dielectric properties of barium titanate. Doping barium titanate ($BaTiO_3$) by different ions such as vanadium V^{5+} provides the possibility of changing its dielectric properties. SEM images indicate the differences between pure $BaTiO_3$ (BT) and $Ba(Ti_{0.98}V_{0.02})O_3$ (BTV2).
Using dielectric measurements, the Curie temperatures (T_c) were calculated – they were found to be equal to 403 K and 396 K, respectively. Moreover, for BTV2 the Curie - Weiss temperature and the Curie constant (C) were determined (T_0 = 368 K and C = 1.46 ×10^5 K, respectively).

Keywords: *Ferroelectric ceramics*, *perovskite*, *barium titanate*, *phase transition*

S t r e s z c z e n i e

Domieszkowanie tytanianu baru $BaTiO_3$ (BT) jonami innych pierwiastków, jak wanad V^{5+}, umożliwia zmiany jego właściwości dielektrycznych. Obserwacje z wykorzystaniem SEM wskazują na różnice w strukturze mikrokrystalicznej między $BaTiO_3$ (BT) a $Ba(Ti_{0.98}V_{0.02})O_3$ (BTV2). Z pomiarów dielektrycznych wyznaczono temperaturę Curie (T_c). Dla BT wynosi ona 403 K, a dla BTV2 396 K. Dla BTV2 określono również temperaturę Curie-Weissa oraz stałą Curie (T_0 = 368 i C = 1.46 × 10^5 K).

Słowa kluczowe: *ceramika ferroelektryczna*, *perowskit*, *tytanian baru*, *przemiana fazowa*

* M.Sc. Eng. Krzysztof Stanuch, Institute of Physics, Pedagogical University, Cracow.

1. Introduction

Some of the most important ferroelectric materials are solid solutions based on barium titanate $BaTiO_3$. They are characterized by a relatively high dielectric constant value that can reach the order of 10^4. The Curie temperature of $BaTiO_3$ is around 403 K [1, 2]. Barium titanate belongs to the group of compounds of an oxygen octahedral perovskite crystal structure, the unit cell of *a* perovskite cubic is shown in Fig. 1. The name is derived from the mineral called perovskite with the chemical formula $CaTiO_3$. Compounds which adopt a structure similar to $CaTiO_3$ belong to a group of perovskites and are described by the general formula ABO_3, where A and B are cations of different sizes, and O is an oxygen anion [1, 3]. Due to its excellent dielectric, piezoelectric and ferroelectric properties, barium titanate began to be used in the end of the 1950s [4, 5]. Nowadays, $BaTiO_3$-based compounds are used for different electroceramical applications such as: multi-layer ceramic capacitors MLCC; ferroelectric random access memory FRAM; piezoelectric sensors; pyroelectric sensors; optoelectronic devices; actuators [1, 5–7]. Long-term studies of $BaTiO_3$ have shown that it is possible to change the dielectric and ferroelectric properties by appropriate substitution or the addition of ions of other elements in addition to or instead of Ba^{2+} in sublattice A and/or Ti^{4+} in *sublattice* B [8–17]. These substitutions can be isovalent when atoms are doped with the same valence or heterovalent, when they have a different valence [5]. Solid solutions based on barium titanate can be obtained through various methods, e.g. using the thermal synthesis of oxides, sol-gel, microwave and mechanochemical methods [18, 19]. Doping by vanadium can change the value of the Curie temperature and dielectric losses in barium titanate [5, 20].

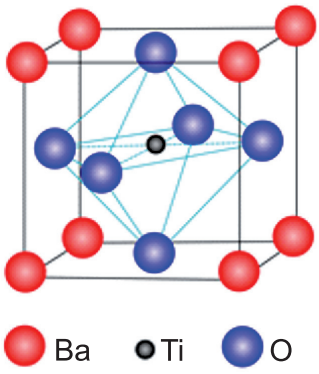

Fig. 1. Unit cell of $BaTiO_3$

2. Experimental

The samples BTV2 and BT were prepared using barium oxalate BaC_2O_4, titanate dioxide TiO_2, and vanadium pentoxide V_2O_5 with a purity of 99.99%. The modification was based on the substitution of V^{5+} (an amount of 2%) in sublattice B (Ti^{4+}). The process of the preparation of BTV2 and of BT in terms of technology, was identical. Pressing was performed at a 0.2 GPa. Samples were synthesized at a temperature of 1373 K for 2 hours. Subsequently, the samples were milled and pressed under a 0.3 GPa and sintered at 1543 K for 2 hours. The last stage of the samples' preparation before dielectric measurements were taken was the application of silver electrodes. Dimensions of the samples were as follows – a diameter of 7 mm and a thickness of 1.5–2.0 mm. A study of the structure and chemical composition of polycrystalline samples BTV2 and BT was made by scanning electron

microscopy (SEM) using a JSM-6610 apparatus coupled with an X-ray energy-dispersive spectrometer (EDS). Dielectric measurements were performed using broadband dielectric spectroscopy. Instrumentation consisted of a dielectric analyzer with high resolution Alpha – AN together with cryogenic temperature control system Quatro Cryosystem and WinDETA Novocontrol software. The samples were measured at the temperature range 148 K to 500 K in steps of 5 K, and from 1 Hz to 10 MHz, respectively. The amplitude of the test voltage was 1 V. Nitrogen gas was used as a cooling and heating medium.

3. Results and discussion

SEM photomicrographs of the microstructure and EDS spectra for BT and BTV2 are presented in Fig. 2–4. Fig. 2a shows the structure of barium titanate with highly visible grains and their boundaries. The proportions in the elements analysis presented in Fig. 2b correspond to the chemical composition of $BaTiO_3$.

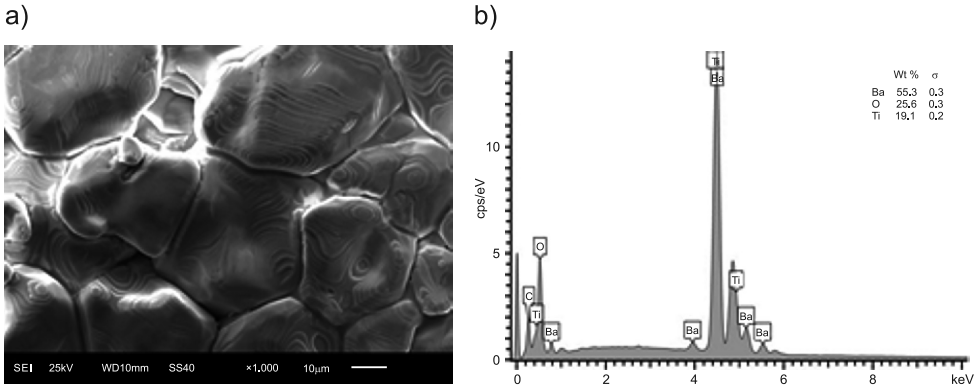

Fig. 2. SEM photomicrograph of the microstructure (a) and the spectrum of the elemental composition of BT ceramics (b)

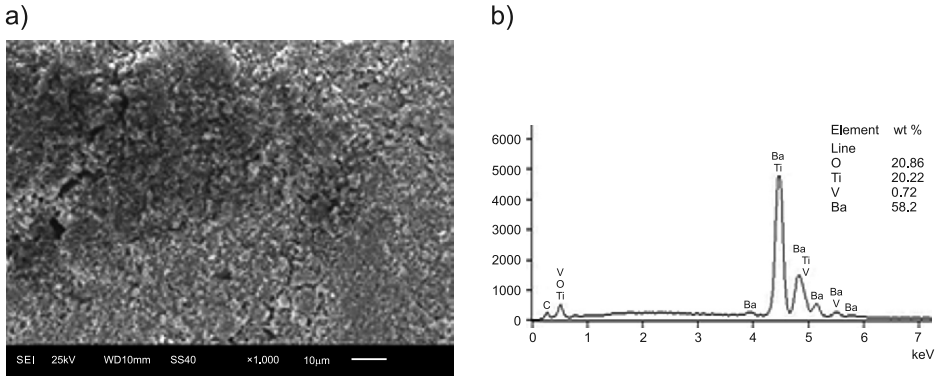

Fig. 3. SEM image of the microstructure (a) and EDS spectrum of the chemical composition of BTV2 ceramics (b)

The SEM photomicrograph of the barium titanate doped by vanadium in Fig. 3a shows a significant difference in the microstructure in comparison to $BaTiO_3$ (Fig. 2a).

An analysis of the chemical composition of BTV2 ceramics is shown in Fig. 3b. The addition of vanadium ions has a destructive influence causing the formation of much smaller crystallite grains. The larger magnification of the SEM image in Fig. 4 reveals the structure of smooth crystallites.

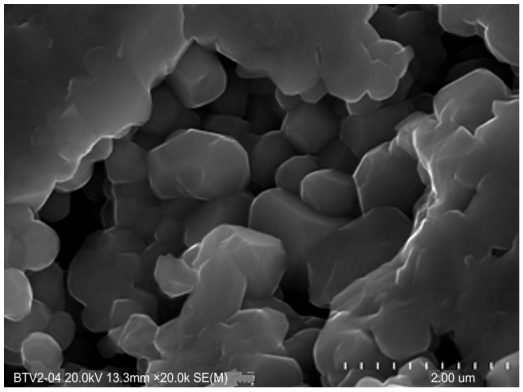

Fig. 4. SEM image of the microstructure of $Ba(Ti_{0.98}V_{0.02})O_3$ ceramics

The results of the dielectric measurements of the polycrystalline samples of BT and BTV2 are presented in Fig. 5a and b. They show the dependence of the real part of the dielectric permittivity $\varepsilon'(T)$ in the temperature range 148 K to 500 K.

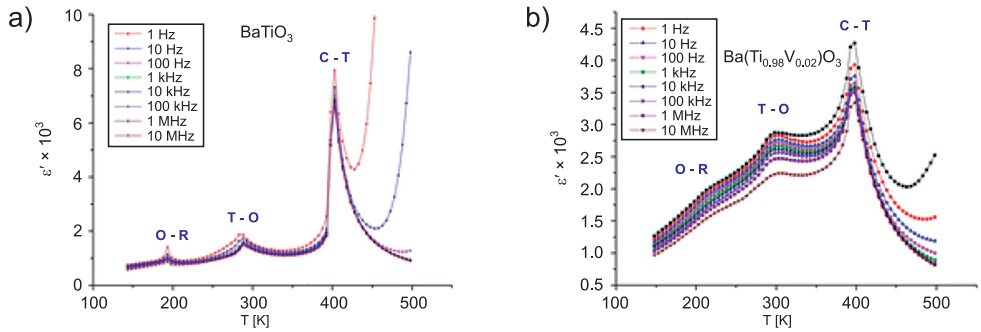

Fig. 5. The temperature dependence of the dielectric permittivity (ε') for: a) BT, b) BTV2

For BT (Fig. 5a), one can see three structural changes: from the cubic to tetragonal (C–T); tetragonal to orthorhombic (T–O); orthorhombic to rhombohedral (O–R) [5, 21]. In the case of BTV2 (Fig. 5b), there are three diffused phase transitions.

Temperature of the paraelectric – ferroelectric phase transition is about 403 K for BT. This value is consistent with the literature data [22]. In the case of the BTV2 sample, T_m = 396 K. It can be seen that 2% vanadium doping, decreased maximum value of the dielectric permittivity, from about 8×10^3 for BT to about 4×10^3 for BTV2.

The reciprocal of the real part of the electric permittivity BTV2 for 1kHz frequency is presented in Fig. 6. For the paraelectric phase ε^{-1} (T) function obeys the rule of Curie--Weiss [5]. The Curie-Weiss temperature T_0 was determined as being 368 K.

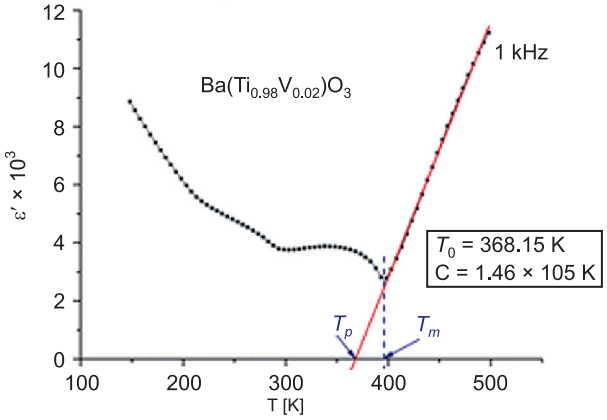

Fig. 6. The temperature dependence of the reciprocal dielectric permittivity (ε^{-1} (T)) for 1 kHz

Using the Curie-Weiss law in the following form:

$$\frac{1}{\varepsilon} = \frac{1}{c}(T - T_0) \tag{1}$$

determined the Curie constant, which is C = 1.46 × 10^5 K at 1 kHz.

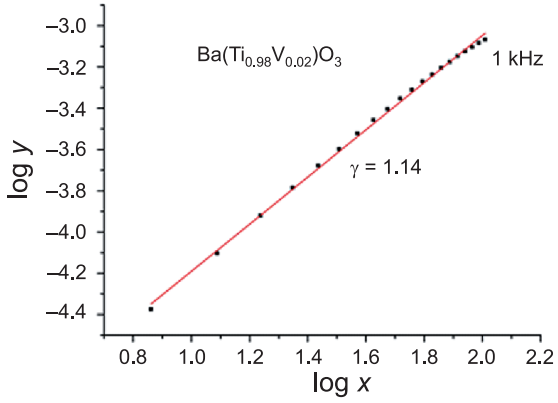

Fig. 7. Dependence log(y) from log(x) by 1 kHz for polycrystalline sample BTV2

Fig. 7 shows the geometrical interpretation of the Curie-Weiss law as the relationship $\log(y) = f(\log(x))$.

$$\frac{1}{\varepsilon} = \frac{1}{\varepsilon_m} + A(T - T_m)^{\gamma} \tag{2}$$

where:

ε_m – the maximum value of the electric permittivity,
T_m – the temperature corresponding to the maximum value ε_m, A,
γ – a constant for the selected frequency

$$x = T - T_m \tag{3}$$

$$y = \varepsilon^{-1} - \varepsilon_m^{-1}$$

For the diffused phase transition value $\gamma \approx 2$, when $\gamma \approx 1$, the transition is a sharp [23–25]. Using linear regression determined that $\gamma = 1.14$ for BTV2. This value indicates a weak *diffusion* of the phase transition.

4. Conclusions

Modifications of $BaTiO_3$ by vanadium ions introduced in sublattice B allows for the changing of its dielectric properties. This is very important in the design of materials used in electroceramics.

In this case, the addition of vanadium ions to the BT causes significant changes in the dielectric permittivity. It was also found that vanadium doping has a destructive influence on the microstructure of ceramics. In the result aggregation of the crystallites in the sintering process for the BTV2 sample creates a structure with a much smaller grains than in the case of BT sample (Fig. 2–4). Using the dielectric spectroscopy method, the Curie temperature T_c for BT was identified as 403 K. However, for BTV2, besides T_c = 396 K, the Curie-Weiss temperature T_0 = 368 K and the Curie constant $C = 1.46 \times 10^5$ K were determined by graphical methods. Using the Curie-Weiss law (2) for the diffuse phase transition a parameter of $\gamma = 1.14$ was obtained. This value indicates that the phase transition is minimally diffused.

The author would like to thank Prof. Czesław Kajtoch and Dr. Wojciech Bąk for their helpful discussions.

References

[1] Hench L.L., West L.K., *Principles of electronic ceramic*, John Wiley & Sons, 1990, 244-247.
[2] Bruno Salvatore A, Swanson Donald K., *High performance Multilayer Capacitor Dielectricsfrom Chemically Prepared Powders*, Journal American Ceramics Society, Vol. 76, 1993, 1233-1241.
[3] Wodecka-Duś B., Czekaj D., *Fabbrication and dielectricproperties of donor doped BaTiO3 ceramics*, Archives of Metallurgy and Materials, Vol. 54, 2009, 923-933.
[4] Lisowski M., *Pomiary rezystywności i przenikalności elektrycznej dielektryków stałych*, Oficyna Wydawnicza Politechniki Wrocławskiej, Wrocław 2004, 9-12.
[5] Cai W., Fu C., Lin Z., Deng X., *Vanadium doping effects on microstructure and dielectric properties of barium titanate ceramics*, Ceramics International, Vol. 37, 2011, 3643-3650.

[6] Stanuch K., *Ferroelectrics capacitors as carriers of information. Problems of Modern Techniques in Engineering and Education – 2008*, Cracow: Institute of Technology, Pedagogical University, 247-252.
[7] Surowiak Z., *Elektroceramika ferroelektryczna*, Wydawnictwo Uniwersytetu Śląskiego, Katowice 2004.
[8] Kajtoch C., *Dilatometrische und dielektrischeAnomalienbei den Phasenumwandlun-gen in* $Ba(Ti_{1-x}Sn_x)O_3$, Ann. Physik, Vol. 2, 1993, 335-338.
[9] Bąk W., Kajtoch C., Starzyk F., *Dielectric properties of* $BaTi_{1-x}Sn_xO_3$ *solid solution*, Materials Science and Engineering B100, Vol. 9, 2003, 9-12.
[10] Kajtoch C., *Dielectric properties of* $Ba(Ti_{1-x}Sn_x)O_3$ *ceramics in the paraelectric phase*, Ceramics International, Vol. 37, 2011, 387-391.
[11] Kajtoch C., Bak W., Garbarz-Glos B., *Study of the phase transition in polycrystalline* $(Ba_{0.90}Pb_{0.10})$ $(Ti_{0.90}Sn_{0.10})O_3$, Condensed Master Physics 2014, DOI: 10.5488/CMP.16.31702.
[12] Kajtoch C., *Time dependences of dielectric constant in* $BaTi_{0.95}Sn_{0.05}O_3$, Ferroelectrics, Vol. 133, 1992, 193-198.
[13] Kajtoch C., *Dipolar polarization in* $Ba(Ti_{1-x}Sn_x)O_3$, Ferroelectrics, Vol. 172, 1995, 465-468.
[14] Kajtoch C., *Glass-like transformation in* $Ba(Ti_{0.70}Sn_{0.30})O_3$, Ferroelectrics, Vol. 192, 1997, 335-337.
[15] Kajtoch C., Bąk W., Garbarz-Glos B., Stanuch K., Tejchman W., Mroczka K., Czeppe T., *Influence of Sr and Zr substitution on dielectric properties of* $(Ba_{1-x}Sr_x)(Ti_{1-x}Zr_x)O_3$, Ferroelectrics, 2013 (in press).
[16] Garbarz-Glos B., Bąk W., Molak A., Kalvane A., *Microstructure, calorimetric and dielectric investigation of hafnium doped barium titanate ceramics*, Phase Transitions, 86, 2013, 917-925.
[17] Kajtoch C., *Dilatometrische und dielektrische Anomalienbei den Phasenumwandlun-gen in* $Ba(Ti_{1-x}Sn_x)O_3$, Ann. Physik, Vol. 2, 1993, 335-338.
[18] Dulian P., Bąk W., Wieczorek-Ciurowa K., Kajtoch C., *Controlled mechanochemical synthesis and properties of a selected perovskite-type electroceramics*, Materials Science Poland, Vol. 31(3), 2013, 462-470.
[19] Dulian P., Wieczorek-Ciurowa K., Bąk W., Kajtoch C., *Możliwości wytwarzania zaawansowanej elektroceramiki na bazie tytanianu baru metodą mechanochemiczną*, Czasopismo Techniczne Technical Transactions, Wyd. Politechniki Krakowskiej, Vol. 9-M/2012, Zeszyt 26, 57-65.
[20] Fu C., Liang J., Cai W., Chen G., Deng X., *Effect of vanadium doping on the electric properties of barium titanatehafnate ceramics*, Journal of Materials Science: Materials in Electronics, 24, 2013, 2438-2444.
[21] Kajtoch C., Gabryś M., Tejchman W., Handke B., *Structural and dielectric properties of polycrystalline* $(Ba_{0.9}Sr_{0.1})TiO_3$, Archives of Materials Science and Engineering, Vol. 33, 2009, 89-92.
[22] Ken-ichi Sakayori, Yasunori Matsui, Hiroyuki Abe, Eiji Nakamura, Mikihiko Kenmoku, Tomoyuki Hara, Daisuke Ishikawa, Akihiro Kokubu, Ken-ichiHirota, Takuro Ikeda, *Curie Temperature of* $BaTiO_3$, Jpn. J. Appl. Phys., 34, 1995, 5443-5445.
[23] Dudek J., Bochenek D., *Wpływ technologii wytwarzania na stopień rozmycia ferroelektrycznych przemian fazowych w ceramice typu PZT*, MateriałyCeramiczne/Ceramic Materials, Vol. 63, 2010, 393-399.
[24] Bak W., Gabrys M., Kajtoch C., Stanuch K., Starzyk F., *Dielectric spectroscopy study of* $Ba_{0.98}Na_{0.02}Ti_{0.98}Nb_{0.02}O_3$ *ceramics*, Archives of Materials Science and Engineering, Vol. 39, 2009, 107-110.

[25] Kajtoch C., Bąk W., Gabryś M., Mroczka K., Handke B., Starzyk F., *Diffused phase transition of polycrystaliline* ($Ba_{0.80}Sr_{0.20})TiO_3$, Archives of Materials Science and Engineering, Vol. 39, 2009, 88-91.

TECHNICAL TRANSACTIONS | CZASOPISMO TECHNICZNE
CHEMISTRY | CHEMIA
1-Ch/2014

BOLESŁAW S. TABIŚ*, WOJCIECH S. STRYJEWSKI*

ZALETY STOSOWANIA BIOREAKTORÓW FLUIDYZACYJNYCH W PROCESIE NITRYFIKACJI MIKROBIOLOGICZNEJ

ADVANTAGES OF THE APPLICATION OF FLUIDIZED BED BIOREACTORS TO A MICROBIOLOGICAL NITRIFICATION PROCESS

A b s t r a c t

The paper presents application possibilities of two and three-phase fluidized bed bioreactors for carrying out a microbiological nitrification process. The advantages and disadvantages of individual bioreactors are described. A quantitative analysis of the fundamental operating variables related to the balance of oxygen and the preservation of the fluidized bed was performed.

Keywords: *nitrification*, *bioreactor*, *fluidization*

S t r e s z c z e n i e

W artykule omówiono możliwości wykorzystania dwu- i trójfazowych bioreaktorów fluidyzacyjnych do realizacji nitryfikacji mikrobiologicznej. Przedstawione zostały zalety i wady poszczególnych rozwiązań procesowych. Dokonano ilościowej oceny podstawowych wielkości związanych z bilansem tlenu i utrzymaniem złoża w stanie fluidalnym.

Słowa kluczowe: *nitryfikacja*, *bioreaktor*, *fluidyzacja*

* Prof. Ph.D. Eng. Bolesław S. Tabiś, M.Sc. Eng. Wojciech S. Stryjewski, Institute of Chemical and Process Engineering, Faculty of Chemical Engineering and Technology, Cracow University of Technology.

Nomenclature

c – concentration [kg/m^3]
d_p – particle diameter [m]
F_V – volumetric flow rate [m^3/h]
H – fluidized bed height [m]
K – interfacial equilibrium constant [–]
Re_g – gas Reynolds number [–]
Re_{mf} – minimum fluidization Reynolds number [–]
u – velocity [m/s]
w_{TA} – yield coefficient [kg T/kg A]
α – conversion factor of carbon substrate [–]
η – dynamic viscosity coefficient [kg/(m×s)]
ξ – recirculation ratio [–]
ρ – density [kg/m^3]
τ_0 – liquid residence time in apparatus [h]

Subscripts

A – refers to carbon substrate A
m – refers to mixing node
mf – refers to minimum conditions of fluidization
r – refers to recirculation stream
T – refers to oxygen

Superscripts

c – refers to liquid phase

1. Introduction

Due to urbanization and developments in agriculture, ammonia nitrogen has become one of the key components of wastewater. The increased concentration of ammonia nitrogen has a negative influence on the quality of surface water. Ammonia in its un-ionized form is highly toxic to fish even at low concentrations of approximately 0.2 mg/l [1]. Futhermore, microbiological processes related to the oxygenation of ammonium ions can lead to a significant decrease of oxygen dissolved in water – this causes disturbances in the water biotic community [2].

Ammonia nitrogen which occurs in waters is formed as a result of the ammonification of substances contained both in municipal wastewater and agricultural leachate. An increase of nitrogen concentration in waters is also caused by the widespread use of fertilizers. Components of fertilizers dissolved in rain waters may then permeate into groundwater.

A separate problem connected with the content of ammonia nitrogen in water occurs in aquaculture. Owners of these cultures, which are dynamically evolving in different parts of the world, aim at reducing the usage of fresh water [3]. Therefore, it is necessary to use recirculating systems. Effluent water from aquaculture contains ammonia nitrogen

from metabolism and food waste. As mentioned above, ammonia nitrogen at relatively low concentrations is toxic to fish. Thus, it is crucial to remove ammonia nitrogen from the recirculated stream.

2. The nitrification process

The requirements for the quality of water destined for human consumption both in Poland [4] and in other countries [5, 6], impose constraints on concentrations of ammonia nitrogen, nitrite nitrogen and nitrate nitrogen. Similarly, an array of constraints on nitrogen compounds in effluents from wastewater treatment plants has been introduced. In these cases, excessive concentrations of nitrogen compounds could be dangerous for people or may be in violation of the law. While exceeding lethal nitrogen concentrations in aquaculture could lead to the dying out of a culture, this is not the limit of the problem as it also leads to financial losses.

Dangers resulting from increases in the ammonia or nitrite nitrogen concentration in water results in the removal of nitrogen compounds from water being a significant practical problem. The use of a microbiological nitrification process or sequence of nitrification-denitrification processes is a typical solution to this problem [2].

The nitrification process basically consists of two phases:

– oxidation of ammonium to nitrite

$$NH_3 + 1.5O_2 \rightarrow NO_2^- + H_2O + H^+ \tag{1}$$

– oxidation of nitrite to nitrate

$$NO_2^- + 0.5O_2H_2 \rightarrow NO_3^- \tag{2}$$

The phases of the nitrification process listed above take place with the participation of different genera of chemoautotrophic bacteria [7]. Chemoautotrophic bacteria are characterized by an ability to use inorganic compounds as a source of electrons.

The first phase of nitrification, during which ammonium is oxidized to nitrite, involves ammonia oxidizing bacteria (nitrite bacteria) of the genera *Nitrosomonas*, *Nitrosococcus*, *Nitrosospira*, *Nitrosolobus* and *Nitrosovibrio*. Oxidation of nitrite to nitrate takes place with the participation of bacteria of the genera *Nitrobacter*, *Nitrococcus*, *Nitrospira* and *Nitrospina.* Both phases of the nitrification process take place in aerobic conditions and the molecular oxygen is an acceptor of electrons.

An analysis of the growth kinetics of nitrification bacteria demonstrates that they are characterized by a relatively small specific growth rate in comparison to heterotrophic bacteria. The biomass doubling of nitrification bacteria requires many hours. The small specific growth rate is of a big significance, because it determines requirements for design of bioreactors for carrying out the nitrification process. It is necessary for designed or applied apparatus to ensure a long enough mean residence time for micro-organisms.

Regarding the aerobic nature of the nitrification process, the content of oxygen in the process environment is of key importance. The theoretical demand for oxygen in the process amounts to 4.57 g O_2/g $N\text{-}NH_4^+$ [2]. A decreased content of oxygen can

lead not only to the limiting of the nitrification process, but also to the dying out of micro--organisms or stopping the process after the first phase which causes an accumulation of nitrite nitrogen.

The pH of the environment also has a vast influence on the process rate. Literature has it that the most beneficial value of pH is 7.8. The activity of nitrifying bacteria is highest in these conditions, but it decreases rapidly when pH falls below 7.0 [1].

Equation (1), which describes a simplified mechanism of the first stage of the nitrification process, shows that in this stage, hydronium ions are released into the process environment. Therefore, the progress of nitrification leads to the acidification of the environment. Maintaining a proper pH value of the reaction mixture is another important practical problem related to the realization of the nitrification process [8].

The activity of nitrifying bacteria is also influenced by other factors such as temperature or the presence of other chemical compounds which inhibit the nitrification process, e.g. chlorate (V) or sodium azide. The most effective growth of micro-organisms takes place at a temperature of ca. 25°C, but below 5°C and above 42°C, the growth rate of bacteria significantly decreases.

In summary, it is possible to list several problems connected with improved efficiency of carrying out the nitrification process through ensuring of the following:

- an appropriately long residence time of micro-organisms in the apparatus,
- the required quantity of oxygen necessary for carrying out the process,
- values of pH and temperature optimal for the process,
- the elimination of substances which have an inhibitory influence on the process.

In order to fulfill the process requirements, a key problem seems to be the selection of proper apparatus. The selection of an appropriate construction which will ensure the possibility of effectively carrying out the process, whilst at the same time avoiding costly maintenance and running, is a typical and, simultaneously, a nontrivial problem for the process engineer.

3. Nitrification in stirred tank reactors

In large wastewater treatment plants, a sequence of microbiological processes nitrification and denitrification is realized.

Historically, one of the first solutions constructed for the removal of nitrogen compounds was a system of two stirred tank bioreactors. One of these tanks is fed with oxygen in order to ensure proper oxygenation, while the other tank is not oxidized in order to ensure anaerobic conditions. In the technology of sewage treatment, two technological schemes are proposed based on stirred tank bioreactors. These schemes are presented in Fig. 1 [7].

The diagram presented in Fig. 1a provides a more intuitive explanation due to the order of the microbiological processes in which the sewage is treated. In this solution, nitrification precedes denitrification, while in Fig. 1b the order of processes is reversed. In both solutions, a partial recirculation of biomass is applied.

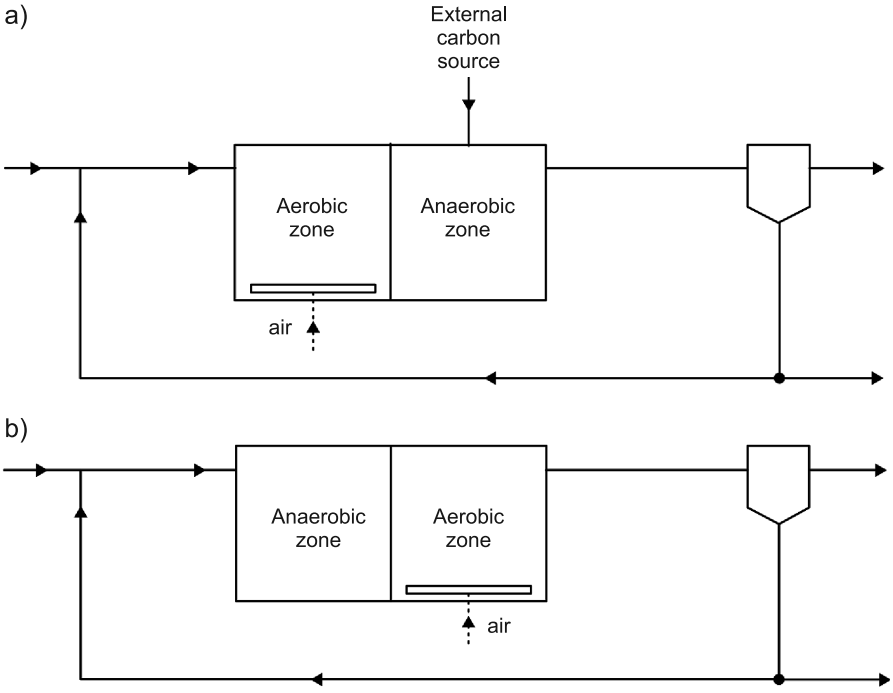

Fig. 1. Schematic diagrams of the nitrification-denitrification process in stirred tank bioreactors with recirculation

An aerobic zone in these systems, from the point of view of bioreaction engineering, is a bubble stirred tank bioreactor and an anaerobic zone is a perfect mixed tank bioreactor. In these types of bioreactors, micro-organisms can occur as both a suspended and an attached biomass. The mean residence time of suspended growth micro-organisms is equal to the residence time of sewage. An extension of the mean residence time of the biomass can be obtained by decreasing the liquid flow rate or by increasing the volume of the bioreactor. However, a decrease of flow rate is connected with a reduction in system productivity. The extension of the mean residence time together with maintenance of system productivity can only be obtained in practice by increasing the volume of the bioreactor. In reality, bioreactors of this type are substantially huge pieces of apparatus. In actuality, the indisputable advantages of this apparatus include its simple construction and low maintenance costs. From a practical point of view, a disadvantage of bubble stirred tank reactors is the lack of a possibility for an independent change of mean residence time of the biomass and liquid phase.

In aquaculture, where recirculation of large amounts of water is applied, a slightly different construction of the bioreactor can be used. This bioreactor enables the immobilization of micro-organisms on the large surface of the solid carrier.

Fixed packing is placed in a reactor. This packing is covered with a biofilm when the apparatus is in operation. There is a considerable interfacial surface between the liquid phase

and the biofilm phase, this results in an increase of mass transfer efficiency between these phases. The presence of a suspended growth biomass and that immobilized on the carrier leads to an increase in the general velocity of the nitrification process. A schematic diagram of such a solution is presented in Fig. 2.

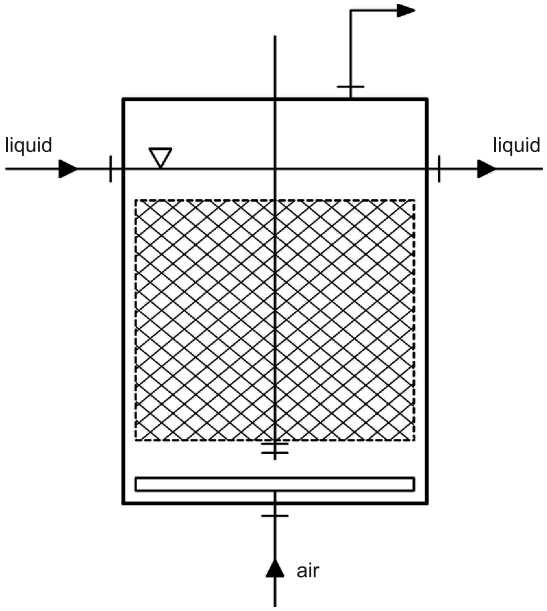

Fig. 2. Schematic diagram of the packed bed bioreactor

The immobilization of micro-organisms on the packing gives the possibility to separate the mean residence time of the liquid and the biomass. Therefore, the elimination of one of the key disadvantages of the bubble stirred tank bioreactor is possible.

Microbiological processes are usually relatively slow, this is why long mean residence times of reaction environment in the apparatus are necessary to carry them out. Appropriate values of the required residence time for the liquid phase can be obtained by reducing the flow rate, which, as mentioned above, results in a decrease in productivity. Additionally, hydrodynamic conditions inside the apparatus are also changed during this process. The shear stress acting on immobilized micro-organisms is lower in comparison to the case with higher flow rate. Low shear stress in the packed bed bioreactors can lead to the uncontrolled growth of the biomass and clogging of the bed.

The application of a packed bed provides the possibility of making the mean residence times of the liquid phase and the biomass independent, furthermore, it leads to an enlargement of the interface between the phases, but it can result in clogging of the bed. Additionally, the proposed solution with solid packing offers limited possibilities of control over the biofilm thickness in the apparatus. These features are considered to be the disadvantages of fixed bed bioreactors.

4. Fluidized bed bioreactors

The effect of bed clogging can be eliminated using fluidized bed bioreactors. In a fluidized bed, the shear stress is significantly higher than in a fixed bed reactor. Additionally, friction between the particles of the bed occurs. On one hand, these phenomena prevent the bed from clogging, but on other hand, they can cause the excessive shearing of biomass which leads to losses of micro-organisms and the slowing down of the microbiological process [9].

The application of biomass immobilization on small carrier particles in a fluidized bed also has important advantages, among which, the following should be pointed out [10]:

– obtaining a high total biomass concentration, which allows for the increasing of the overall process rate,
– the separation of the residence time of the liquid and biomass phases
– a large interphase contact surface between the liquid phase and the biofilm, which ensures a more efficient mass transfer,
– the possibility of constant bed exchange without stopping the process,
– a smaller size of apparatus in comparison to other solutions at the same productivity [11].

Mixing of the fluidized bed leads also to such a placement of bioparticles that lighter particles, on which the biofilm is thicker, appear in the upper part of the bed. This stratification gives the possibility of removing lighter bioparticles and controlling the thickness of the biofilm.

The application of fluidized bed bioreactors is also justified economically. The fluidized bed apparatus is characterized by the low unit costs of the mass transfer surface and the comparison of maintenance costs of different types of bioreactor shows that this type of apparatus is one of the cheapest [12].

Table 1

Examples of the application of fluidized bed bioreactors in aerobic degradation processes

No.	Substance	Micro-organisms	Carrier	References
1	phenol	Pseudomonas putida	activated carbon	Fan Liang-Shih et al. [14], Tang et al. [10]
2	dichloromethane	Pseudomonas, Methylobacterium, Hypomicrobium	charcoal	Gaelli [15]
3	phenoles, napthalenesulphonate	mixed culture	sand	Tijhuis et al. [16]
4	glucose	mixed culture	sand	Ryhiner et al. [17]
5	coal tar	mixed culture	sand	Hueppe et al. [18]
6	napthalenesulphonate	Pseudomonas	sand	Wagner and Hempel [19]
7	trichloroethene	mixed culture	activated carbon	Fennell et al. [20]
8	ammonia nitrogen	mixed culture	sand	Van Bentum et al. [21] Heijnen et al. [22]

The listed advantages of fluidized bed bioreactors make them more efficient than other solutions used in wastewater treatment technology [10, 13] and this has contributed to their considerable popularization. Examples of applications of fluidized bed bioreactors in aerobic degradation processes are presented in Table 1.

5. Nitrification in two and three-phase fluidized bed bioreactors

Fluidized bed bioreactors are often used to remove ammonia nitrogen. Apparatus of this type can be used in a relatively wide range of influent flow rates – this corresponds to the existence of a fluidized bed [11]. Due to the separation of the mean residence times of liquid and biomass, fluidized bed reactors can work at influent flow rates F_{Vf}, for which in bubble stirred tank bioreactors, the washout of biomass would occur.

By means of fluidized bed bioreactors, it is possible to remove as much as 90% of the ammonia nitrogen contained in the liquid phase in one reactor pass [12].

Nitrification as an aerobic process requires ensuring a relevant oxygen concentration in the bioreaction environment. A lack of sufficient oxygen in the environment can slow the process down and may also lead to the unfavorable phenomenon of the anoxia of micro--organisms.

In order to ensure a proper oxygenation, two solutions are applied in fluidized bed apparatus:

– two-phase liquid-solid fluidized bed bioreactor with an external aerator,
– three-phase gas-liquid-solid fluidized bed bioreactor.

A schematic diagram of a circulating fluidized bed bioreactor with external aeration is presented in Fig. 3. The role of an external mass exchanger is the oxygenation of a liquid stream directed to the bioreactor. External aerating apparatus ensures flexibility of the system with regard to the intensity of aeration, which depends on both substrate concentration and its flow rate.

One of the key process parameters crucial to the sufficient oxygenation of the liquid phase in a two-phase fluidized bed bioreactor is a recirculation ratio defined as:

$$\xi = \frac{F_{Vr}^{c}}{F_{V}^{c}} \tag{3}$$

A method of determination of a minimal value of this parameter based on oxygen requirement is presented below.

A mass balance of fresh and recirculated streams in mixing node gives

$$c_{Am}^{c} = (1-\xi)\, c_{Af}^{c} + \xi c_{A}^{c} \tag{4}$$

A relation between the quantity of consumed oxygen and substrate A, which undergoes oxygenation, is given by the following equation:

$$c_{T0}^{c} - c_{T}^{c} = w_{TA}(c_{Am}^{c} - c_{A}^{c}) \tag{5}$$

in which coefficient w_{TA} describes a quantity of oxygen used per mass unit of substrate A.

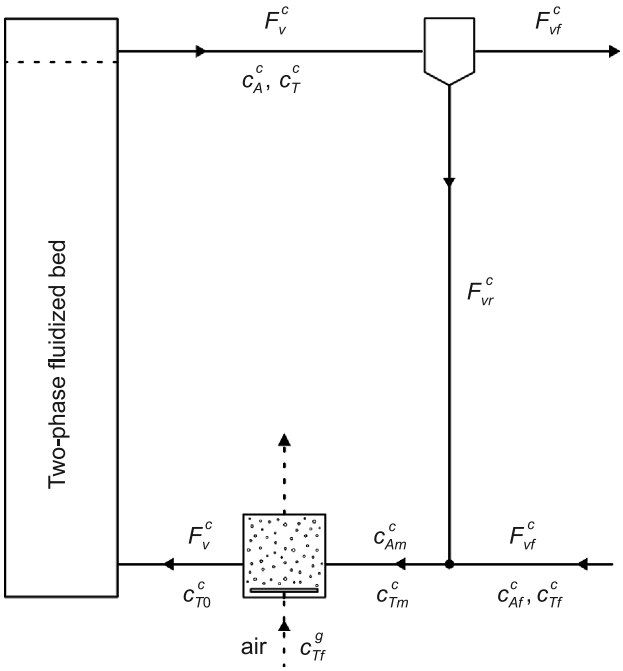

Fig. 3. Schematic diagram of a circulating fluidized bed bioreactor with an aerator in a recirculating loop

A minimal value of recirculation ratio $\xi_{\min}$ can be determined assuming that oxygen is totally consumed while passing through the reactor and that the aerator ensures complete oxygenation of the inlet stream, i.e. up to the point of saturation. These assumptions can be described with equation (6).

$$c_T^c = 0 \quad \text{and} \quad c_{T0}^c = c_T^* = \frac{c_{Tf}^g}{K} \tag{6}$$

Putting equation (6) into equations (4) and (5) we get:

$$\xi_{\min} = 1 - \frac{c_T^*}{w_{TA} c_{Af}^c \alpha} \tag{7}$$

where α is a conversion factor of substrate A defined as:

$$\alpha = \frac{c_{Af}^c - c_A^c}{c_{Af}^c} \tag{8}$$

Fig. 4a shows how value $\xi_{\min}$ forms for a few set values of the yield coefficient w_{TA}.

The application of fluidized bed bioreactors requires ensuring appropriate conditions for expanded fluidization. From the hydrodynamics of the fluidized bed, it follows that it can exist only in a strictly determined range of liquid velocity (between minimal

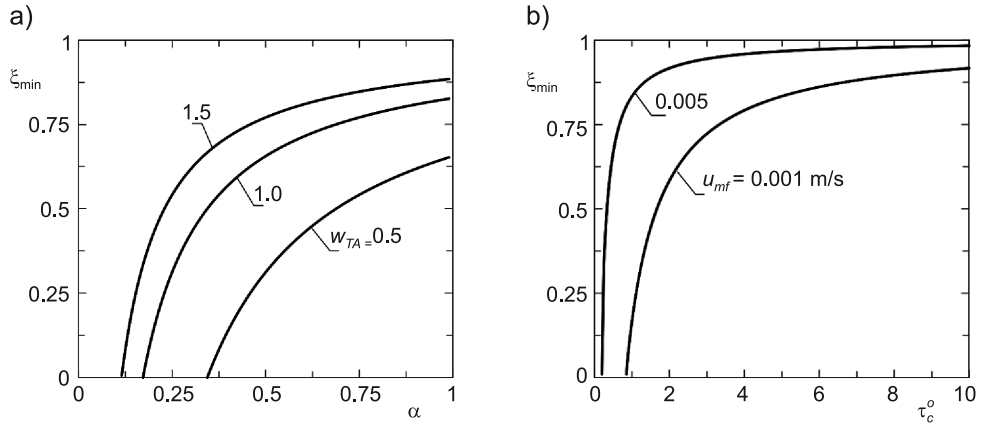

Fig. 4. Relationship of a minimal value of recycle ratio to: a) conversion factor for different values of the w_{TA} coefficient, b) the mean residence time of liquid for different values of u_{mf} ($c^c_{Af} = 0.05$ kg/m^3; $c^*_T = 0.0086$ kg/m^3)

fluidization velocity and the terminal velocity of the particles). Maintaining a proper liquid velocity at small inlet stream flow rates may demand high recirculation ratios. Therefore, the minimal recirculation ratio may also be related to the hydrodynamics of the fluidized bed. The relationship between the value of the recirculation ratio, the minimal fluidization velocity u_{mf}, the height of the bed in apparatus H and the mean residence time of liquid τ_0^c is described by equation (9):

$$\xi_{\min} = 1 - \frac{H}{u_{mf}\tau_0^c} \tag{9}$$

A relationship between $\xi_{\min}$, which was calculated as shown, and the mean residence time of liquid in the system τ_0^c for two chosen values of u_{mf} is presented in Fig. 4b.

While designing the bioreactor shown in Fig. 3, a bigger value out of these $\xi_{\min}$ calculated according to formulas (7) and (9) is mandatory.

As an alternative solution to two-phase bioreactors, three-phase fluidization is applied. Apart from liquid, gas is also supplied to the bioreactor. A schematic diagram of such a system is presented in Fig. 5.

The presence of gas and its flow velocity have a large influence on the minimal fluidized bed velocity of particles. In Fig. 6, results obtained by Macchi and co-authors [23] are presented. The points on the figure represent experimental data. The curves are plots of approximation correlations obtained as a part of this work. The results achieved by Macchi are described by the following equations:

a) for air-glycerol-glass system: $\mathrm{Re}_{mf} = 31.31\,\mathrm{Re}_g^{-0.3033}$, at a value of regression coefficient $R^2 = 0.999$,

b) for air-silicone oil-alumina system: $\mathrm{Re}_{mf} = 29.82\,\mathrm{Re}_g^{-0.2461}$, at a value of regression coefficient $R^2 = 0.994$.

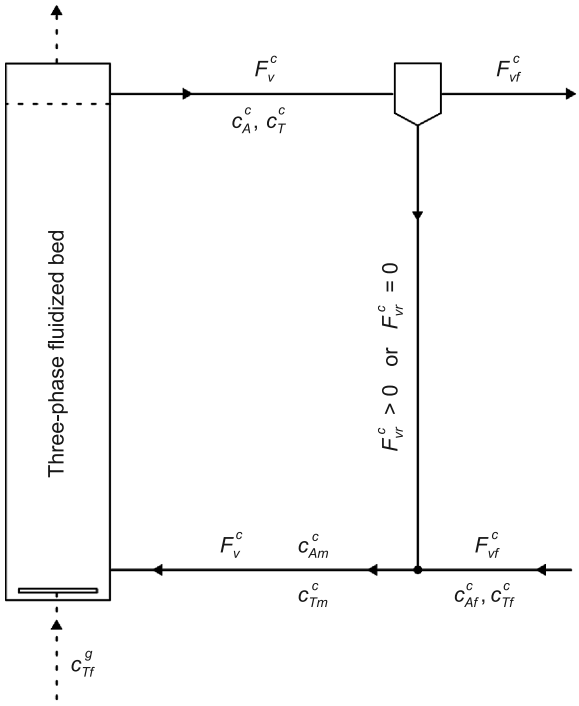

Fig. 5. Schematic diagram of a three-phase gas-liquid-solid fluidized bed bioreactor with partial thickening and recirculation of the biomass

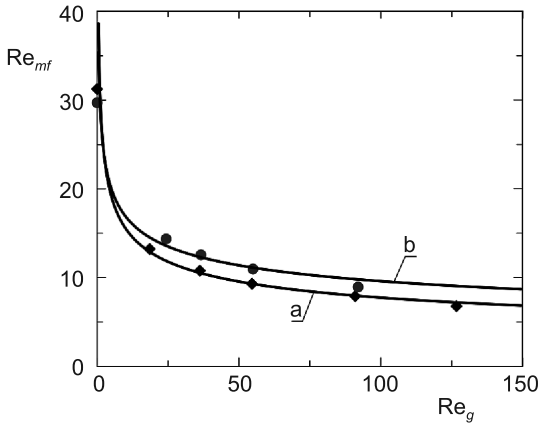

Fig. 6. Relationship of minimum fluidization Reynolds number to gas Reynolds number: a) for air-glycerol-glass system, b) for air-silicone oil-alumina system

Definitions of Reynolds numbers are presented by equations (10).

$$\mathrm{Re}_{mf} = \frac{u_{mf} d_p \rho_c}{\eta_c} \qquad \mathrm{Re}_g = \frac{u_g d_p \rho_c}{\eta_c} \tag{10}$$

According to equation (9), a lower value of minimum fluidization velocity u_{mf} corresponds to a lower minimal recirculation ratio. Thus, from the hydrodynamics point of view, at appropriately high values of gas velocities, liquid recirculation will not be necessary to maintain the fluidized bed.

Air bubbles, which appear in three-phase bioreactors, exert shear stress which leads to the intensification of biomass detachment from low-density particles [24]. Furthermore, air bubble coalescence inside a bioreactor may occur, which results in bubbles raising too quickly and worsening of conditions of mass transfer between liquid and gas.

According to Tang and Fan [10, 14], airlift three-phase bioreactors are also treated as fluidized bed apparatus. A schematic diagram of a piece of apparatus of this type is presented in Fig. 7. Circulation in airlift fluidized bed apparatus is as a result of the density difference of fluids in a riser and downcomer. Therefore, the application of additional pumps in order to force circulation is not necessary – this is a significant advantage of this solution.

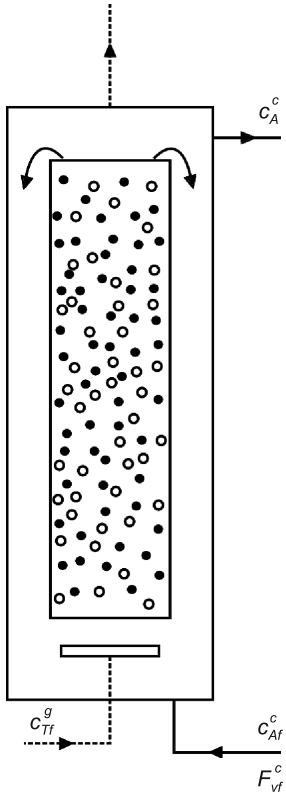

Fig. 7. Schematic diagram of three-phase airlift apparatus

The presence of gas bubbles and liquid circulation ensures effective mixing of the reaction environment. Airlift bioreactors are also used for carrying out the microbiological nitrification process [25, 26]. The conversion factor of ammonia nitrogen during nitrification in a bioreactor of this type may amount to as much as 0.99 [27]. However, it is worth mentioning that because of the operation principle of airlift bioreactors based on density difference of fluids in different zones, this apparatus has to be relatively high.

The design of fluidized bed reactors is relatively complex [12]. One of the key problems is the selection of a proper diameter, material and mass fraction of particles of a fluidized bed [28].

In the fluidized apparatus described above, gas and liquid flow in the same direction, i.e. the bioreactor is fed with these materials from the bottom. Introducing liquid feeding from the top of the apparatus leads to the formation of an inversed fluidized bed. The application of an inversed fluidized bed gives the possibility of limiting shear stress in the bed, a greater control of the biofilm thickness and prevents particles from being carried up [29]. With regard to the hydrodynamics of the inversed fluidized bed, it is necessary to use particles of slightly lower density than that of liquid phase. Polymers are usually used as carriers of micro-organisms in this type of bed.

6. Fluidized beds with chemically active particles

Equation (1) shows that in the first stage of the nitrification process, protons are released to the reaction environment. The hydronium ions which are formed cause a decrease in the pH of the environment. As it was mentioned above (point 2) a level of pH below neutral leads to a rapid reducing of the growth rate of the nitrifying bacteria, which results in a lower overall efficiency of the process. Maintaining the proper pH in a reaction environment is possible due to the dosage of appropriate chemical compounds, e.g. carbonates or hydroxides. Using a specific compound, which would make the environment neutral, as carrier in the fluidized bed could be a cheaper and more rational solution. In literature [8], chalk is suggested as a carrier. From the chemical point of view, chalk is mainly calcium carbonate. Chalk may be successfully used as a carrier biofilm and it simultaneously allows for the neutralization of hydronium ions formed during the nitrification process. A drawback to this solution is the necessity of filling in chalk losses during operation of the apparatus. Additionally, from the design point of view, it is necessary to take into consideration the kinetics of chalk decomposition. However, it does not constitute a disadvantage of the process because the application of chalk as a biofilm carrier is in this case, economically justified.

7. Conclusions

The processes of ammonia nitrogen removal from municipal and industrial wastewater have a serious influence on the improvement of parameters of effluents from wastewater treatment plants. Furthermore, they are also useful in the treatment of water for human consumption. In some branches of agriculture, such as aquaculture, they are necessary for the rational management of surface waters.

The biological removal of nitrogen compounds may be carried out in different types of bioreactors. In practice, both large continuous stirred tank bioreactors and the more efficient fluidized bed apparatuses are used.

From a process engineering point of view, it is more advantageous to apply fluidized bed bioreactors due to the higher overall biomass concentration, lack of bed clogging, separation of residence times of liquid and biomass, intensification of mass transfer between liquid and biofilm and the possibility of controlling the thickness and age of the biofilm.

The literature shows the application of both two-phase (liquid-solid) and three-phase (gas-liquid-solid) bioreactors applied for the nitrification process. These solutions and the significance of the recirculation ratio in fluidized bed bioreactors are presented in this work, as well as a method of determination of minimal recirculation ratio is proposed.

It is worth noting that fluidized bed bioreactors are smaller in relation to other solutions with the same productivity, which is an additional advantage. The application of fluidized bed apparatuses, apart from process advantages, is also economically justified because they have relatively low maintenance costs.

The fluidized bed allows for the filling in of particles during the operation of the bioreactor which makes the controlling of the biofilm age easier and provides the possibility of using chemically active particles. In the case of the microbiological nitrification process, it is necessary to ensure the proper pH of the environment, which may be practically obtained by using chalk particles as the biofilm carrier. Then the particles neutralize the formed hydronium ions and allow to ensure the constant value of pH of the environment.

In summary, carrying out the microbiological nitrification process in fluidized bed bioreactors is justified both from practical point of view and economically, but the selection of specific apparatus demands a deeper quantitative analysis related to the studied design case.

References

[1] Hapagonian D.S., Riley J.G., *A closer look at the bacteriology of nitrification*, Aquacult. Eng., 18, 1998, 223-244.

[2] Sadecka Z., *Podstawy biologicznego oczyszczania ścieków*, Wydawnictwo Seidel-Przywecki Sp. z o.o., Warszawa 2010.

[3] Gutierrez-Wing M.T., Malone R.F., *Biological filters in aquaculture: Trends and research directions for freshwater and Marine applications*, Aquacult. Eng., 34, 2006, 163-171.

[4] *Rozporządzenie Ministra Zdrowia w sprawie jakości wody przeznaczonej do spożycia przez ludzi z dnia 29 marca 2007 r.*

[5] *Nitrification*, United States Environmental Protection Agency, Washington 2002.

[6] Gujer W., *Nitrification and me – A subjective review*, Water Res., 44, 2010, 1-19.

[7] Klimiuk E., Łebkowska M., *Biotechnologia w ochronie środowiska*, Wydawnictwo Naukowe PWN, Warszawa 2003.

[8] Green M., Ruskol Y., Lahav O., Tarre S., *Chalk as the carrier for nitrifying biofilm in a fluidized bed reactor*, Water Res., 35, 2000, 284-290.

[9] Elenter D., Milferstedt K., Zhang W., Hausner M., Morgenroth E., *Influence of detachment on substrate removal and microbial ecology in heterotrophic/autotropic biofim*, Water Res., 41, 2007, 4657-4671.

[10] Tang W.-T., Fan Liang-Shih, *Steady State Phenol Degradation in a Draft-Tube, Gas-Liquid-Solid Fluidized-Bed Bioreactor*, AICHE J., 33, 1987, 239-249.
[11] Nicolella C., van Loosdrecht M.C.M., Heijnen J.J., *Wastewater treatment with particulate biofilm reactors,* J. Biotechnol., 80, 2000, 1-33.
[12] Summerfelt S.T., *Design and management of conventional fluidized-sand biofilters*, Aquacult. Eng., 34, 2006, 275-302.
[13] Schuegerl K., *Three-phase-biofluidization-Application of three-phase fluidization in the biotechnology – A review*, Chem. Eng. Sci., 52, 1997, 3661-3668.
[14] Fan Liang-Shih, Fujie K., Long Teng-Rui, Tang W.T., *Characteristics of draft tube gas-liquid--solid fluidized bed bioreactor with immobilized living cells for phenol degradation*, Biotechnol. Bioeng., 30, 1987, 498-504.
[15] Gaelli R., *Biodegradation of dichloromethane in waste water using a fluidized bed bioreactor*, Appl. Microbiol. Biotechnol., 27, 1987, 206-213.
[16] Tijhuis L., Loosdrecht van M.C.M., Heijnen J.J., *Formation and growth of heterotrophic aerobic biofilms on small suspended particles in airlift reactors*, Biotechnol. Bioeng., 44, 1994, 595-608.
[17] Ryhiner G., Petrozzi S., Dunn I.J., *Operation of a three- phase biofilm fluidized sand bed reactor for aerobic wastewater treatment*, Biotechnol. Bioeng., 32, 1988, 677-688.
[18] Hueppe P., Hoeke H., Hempel D.C., *Biological treatment of effluents from coal tar refinery using immobilized biomass*, Chem. Eng. Technol., 13,1990, 73-79.
[19] Wagner K., Hempel D.C., *Biodegradation by immobilized bacteria in an airlift-loop reactor – Influence of biofilm diffusion limitation*, Biotechnol. Bioeng., 31, 1988, 559-566.
[20] Fennell D.E., Nelson Y.M., Underhill S.E., White T.E., Jewell W.J., *TCE degradation in a methanotropic attached-film bioreactor*, Biotechnol. Bioeng., 42, 1993, 859-872.
[21] Bentum van W.A.J., Loosdrecht M.D.M., Heijnen J.J., *Control of heterotropic layer formation on nitrifying biofilms in a biofilm airlift suspension reactor*, Biotechnol. Bioeng., 53, 1997, 397--405.
[22] Heijnen J.J., van Loosdrecht M.C., Mulder R., Mulder A., Welteverde R., *Scaleup of aerobic airlift suspension biofilm reactor*, International Symposium Environmental Biotechnology, 22–25 April, Osteend, Belgium, 211-217.
[23] Macchi A., Bi H., Grace J.R., McKnight C.A., Hackman L., *Dimensional hydrodynamic similitude in three-phase fluidized beds*, Chem. Eng. Sci., 56, 2001, 6039-6045.
[24] Dunn I.J., Tanaka H., Uzman S., Denec M., *Biofilm fluidized-bed reactors and their application to waste water nitrification*, Annals of the New York Academy of Science, 413, 1983, 168-183.
[25] Merchuk J.C., *Airlift Bioreactors: review of recent advances*, Can. J. Chem. Eng., 81, 2003, 324-337.
[26] Garrido J.M., van Benthum W.A.J., van Loosdrecht M.C.M., Heijnen J.J., *Influence of dissolved oxygen concentration on nitrite accumulation in a biofilm airlift suspension reactor*, Biotechnol. Bioeng., 53, 1997, 168-178.
[27] Jin R.-C., Zheng P., Mahmood Q., Zhang L., *Performance of a nitrifying airlift reactor using granular sludge*, Sep. Purif. Technol., 63, 2008, 670-675.
[28] Tabiś B., Gomułka M., *Wpływ ciała stałego na właściwości stacjonarne trójfazowego bioreaktora fluidyzacyjnego*, Inż. Ap. Chem., 44, 2005, 5, 3-6.
[29] Bandaru K.S.V.S.R., Murthy D.V.S., Krishnaiah K., *Some hydrodynamic aspects of 3-phase inverse fluidized bed*, China Part., 5, 2007, 351-356.

TECHNICAL TRANSACTIONS | CZASOPISMO TECHNICZNE
CHEMISTRY | CHEMIA
1-Ch/2014

ANNA WASSILKOWSKA*, ANNA CZAPLICKA-KOTAS*, MICHAŁ ZIELINA*,
ANDRZEJ BIELSKI*

AN ANALYSIS OF THE ELEMENTAL COMPOSITION OF MICRO-SAMPLES USING EDS TECHNIQUE

ANALIZA SKŁADU PIERWIASTKOWEGO W MIKROOBSZARZE PRZY UŻYCIU TECHNIKI EDS

Abstract

A classic example of the application of electron-dispersive spectroscopy (EDS) is the observation of the microstructure of solid samples using scanning electron microscope (SEM). This provides the possibility of taking measurements of chemical composition in very small areas. Measurements can be performed on any bulk sample through adjusting the X-ray excitation parameters to the elements of its expected composition. Examples of the applications of the EDS technique in the context of environmental engineering have been presented.

Keywords: *scanning electron microscope*, *X-ray emission*, *energy dispersive spectrometer*, *characteristic spectrum*, *detection limits*

Streszczenie

Obserwacje mikrostruktury litych próbek przy użyciu skaningowego mikroskopu elektronowego (SEM) z możliwością wykonania lokalnego pomiaru składu chemicznego w bardzo małym obszarze, to klasyczny przykład zastosowania spektroskopii dyspersji energii (EDS). Pomiar wykonywany jest na dowolnej próbce stałej, stosując parametry wzbudzenia promieniowania rentgenowskiego adekwatne do pierwiastków, spodziewanych w składzie próbki. Omówiono przykłady zastosowania techniki EDS w zagadnieniach związanych z inżynierią środowiska.

Słowa kluczowe: *elektronowy mikroskop skaningowy*, *emisja promieni X*, *spektrometr dyspersji energii*, *widmo charakterystyczne*, *granica wykrywalności*

* Ph.D. Eng. Anna Wassilkowska, Ph.D. Eng. Anna Czaplicka-Kotas, Ph.D. Eng. Michał Zielina, Ph.D. Eng. Andrzej Bielski, Faculty of Evironmental Engineering, Cracow University of Technology

1. Introduction

Energy dispersive spectroscopy (EDS) is a micro-analytical technique conventionally used in scanning electron microscopy (SEM) for the local determination of chemical elements in solid samples [1–3]. The sample is made from a solid material, stable in a vacuum of up to 1.5×10^{-3} Pa. The sample is then bombarded with electrons with energy levels of up to 30 keV. Another requirement for SEM is that the sample under investigation should fit dimensionally to the specimen chamber of the microscope. Samples are placed in a special holder with the surface to be subjected to analysis facing upwards [3].

Using the EDS method, the chemical composition of small objects is measured by placing the material in the vacuum chamber where it is illuminated with a focused electron beam from above. Electrons bombarding the specimen surface are scattered into the material and may ionize the specimen atoms by knocking out secondary electrons from the stationary shells. The resulting gaps in the electron shell are filled by an avalanche of electrons from the outer shells of the atom. The ionized atoms emit X-ray quanta of discrete energy, which are characteristic of the chemical elements of the material under investigation. The photons from the X-ray emission are collected by an EDS detector placed near the sample and transmitted through an electronic system to the multi-channel analyzer, in which the pulses are separated according to their amplitude. The number of quanta (the intensity) of characteristic X-rays emitted in a given time interval by the atoms of the investigated element is proportional to the concentration of that element in the sample. The complete energy-dispersive spectra are transferred to the dedicated computer equipped with a special software system for the collection, observation, calculation and storage of the spectral data.

The EDS microanalysis is regarded as a non-destructive technique because the specimen prior to analysis does not differ from the specimen after the analysis [4]. The aim of this paper is to demonstrate the effectiveness of the EDS method in material investigations performed by means of conventional SEM.

2. A brief description of the EDS technique

A single EDS measurement means the acquisition of an energy-dispersive spectrum in which (at discrete energies) the characteristic peaks of the chemical constituents are present. To determine the element concentration from the peaks obtained, it is necessary to process the spectrum (Fig. 1) [5]. The main outcome from the measurement is the value of the relative intensity of the spectral lines (*K-ratio*) measured after the optimization of the shape of the peaks (Fig. 1, pp. 3–6). The concentration of the *i*-th element in the specimen is calculated from the equation [1]:

$$\frac{C_i}{C_{(i)}} = \mathrm{ZAF} \cdot \frac{I_i}{I_{(i)}} = \mathrm{ZAF} \cdot K\text{-}ratio \tag{1}$$

where:

$C_i/C_{(i)}$ – relative concentration of the element in specimen and in standard;
$I_i/I_{(i)}$ – relative intensity of spectral lines (equal to *K-ratio*);
ZAF – correction factor for quantitative determination of the *i*-th element.

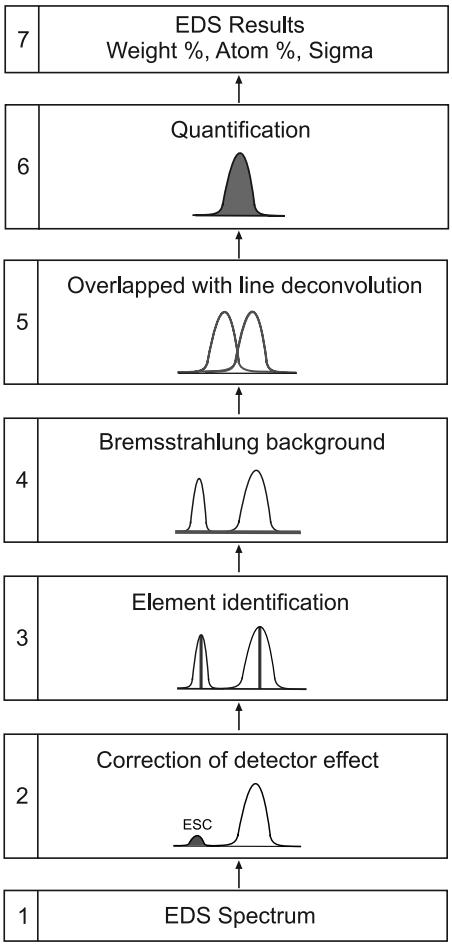

Fig. 1. Flowchart of the modeling of the emission spectrum [5]

The description of the quantitative EDS microanalysis technique is given in detail in several monographs [1, 5, 6]. Kalner and Zilberman [6] give a variety of parameter tables for the correction of ZAF and the *K-ratio*, useful for the manual calculation of element concentrations in the studies of metals and alloys. This procedure should be understandable in the absence of a fully automated system or if there is lack in confidence in the interpretation of the microanalysis results obtained from computer calculations. Currently, the entire analysis of the EDS spectrum, consisting of the qualitative identification of peaks and the calculation of the concentration of the constituent elements, is performed automatically within a minute. The proper implementation of the measurement of the spectrum requires advance planning of the experiment and a skilled operator of the microscope. In the work of Szummer [5], the corresponding algorithms (Fig. 1) implemented in the software instrumentation of modern EDS spectrometers are obtained in detail.

2.1. Electron-beam instrumentation

The most important part of SEM is the vacuum column that contains an electron gun with the applied accelerating voltage and an electron optical system, focusing the electron beam on the specimen surface.

Figure 2 illustrates the scattering paths of electrons in the material (of density ρ and atomic number *Z*) for different electron beam accelerating voltages (in kV). The drawing is the result of the Monte Carlo simulation of the electron scattering phenomena in a homogeneous material [1]. Since the signal of the image in SEM is gathered point by point during the scanning of the beam over the surface of the specimen, the diameter of the electron beam determines the resolution of the scanning images. And so, at a voltage of 30 kV and a beam emission from a tungsten cathode, the minimum beam diameter is about 10 nm (0.01 μm) [7]. A narrow diameter of the beam is possible (for example, on a single nanoparticle), but this is contrary to the requirement of the maximum beam current for optimal sensitivity of EDS microanalysis. The beam current increases with the beam diameter. For the qualitative analysis of elemental composition, the optimum beam diameter is from 0.1 to 1 μm, and for quantitative analysis, diameters of up to 5 μm are recommended [7]. These values are correlated with the spatial resolution of the characteristic X-ray emission from the specimen.

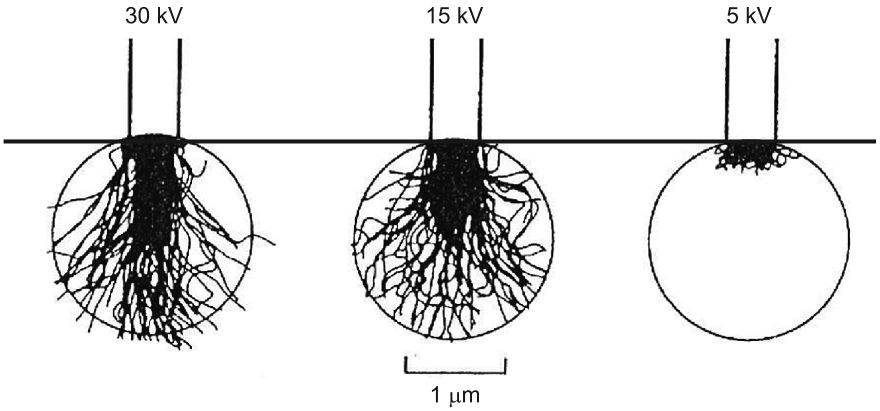

Fig. 2. Depth of beam penetration into the material at different accelerating voltages [1]

To obtain high levels of radiation characteristic of the sample at the optimum ratio of peak to background (Fig. 1, pp. 3 and 4), the energy of electrons bombarding the specimen must exceed double the *ionization potential* of the atoms in the specimen [5, 7]. Thus, for samples of unknown composition, only the first measurement of the spectrum beam voltage of 25 kV [7] will allow the recording of the emission lines of the EDS spectrum for energy up to 10 keV.

The primary electron *penetration depth* (Fig. 2) depends on the energy and density of the material. For example, the electron scattering area at 30 kV for a specimen of iron ($\rho = 7.874 g/cm^3$, $Z = 26$) reaches a depth of 3.1 μm, and at 5 kV – a depth of 0.16 μm. SEM is capable of generating beam voltages of values from 0.3 kV to 30 kV. The Monte Carlo

simulation indicates that the X-ray *emitting region* is in the order of 2–5 μm, which means that the micro-volume of the analyzed specimen is derived only from the subsurface layers of the material [7].

2.2. X-rays emission

The Bohr model of the atom shows the atoms of chemical elements as a quantized system which can exchange energy only in portions of the permitted amount. The name of the series of emission in the EDS spectra corresponds to the sign of the atomic inner shell, from which accelerated electrons of the primary beam strike away stationary electrons (Fig. 3). The excitation energy levels of the L and M lines are lower than for the K series (E_M max.~3 keV), hence the introduction of the electron holes in the K shell simultaneously precipitates the emissions from lines K_α, K_β and K_γ [5]. The probability of each transition is different, which results in the individual lines measured having different intensities. Spectral lines marked K_α are the strongest, thus the quantitative EDS spectrum analysis is carried out conventionally using the K series. The energy of the characteristic X-ray emission of the K series ranges from 0.185 keV for boron ^{5}B to tens of kilo-electron-volts for heavy elements [4].

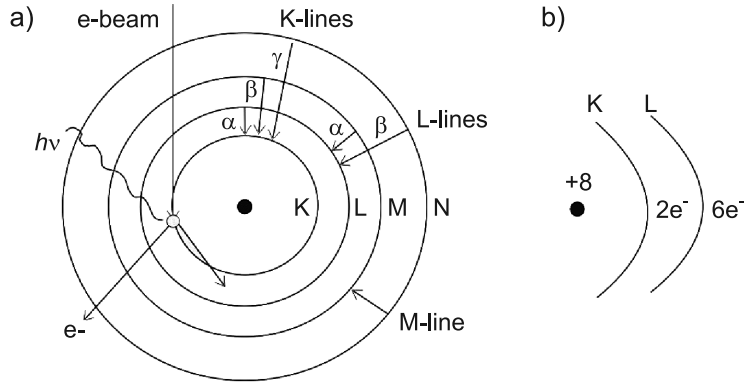

Fig. 3. Model of the atom: a) spectral lines designation; b) oxygen atom (O^8) [5]

One can see from this that the analysis of heavier elements must be carried out after the L series, as the K series of the spectrum will not be excited at the maximum SEM beam voltage of 30 kV; e.g. for uranium ^{92}U: $E_{K\alpha} = 98.43$ keV, $E_{L\alpha} = 13.61$ keV and $E_{M\alpha} = 3.17$ keV.

The full range of the characteristic radiation energy of elements (from 0.120 keV to 120 keV) is due to the conversion of wavelength (λ = 0.1 Å – 100 Å) to photon energies of electromagnetic X-radiation by the well-known equation [1]:

$$E = hc / \lambda e = 12.396 / \lambda \tag{2}$$

where:

- c – light velocity in vacuum (3×10^8 m/s);
- h – Planck's constant (6.62×10^{-34} J·s);
- e – electron charge (-1.6×10^{-19} C).

The system of spectral lines is unique and characteristic for each element and therefore, can be used to study the chemical composition of micro-samples. It should be noted that the atoms from ^{5}B to ^{10}Ne have only two shells filled with electrons (Fig. 3b), i.e. emissions only from the K series. The excitation energy of the K series for the light elements is very small (max. 1 keV), i.e. all peaks are gathered in the low resolution portion of the spectrum, where peaks from ^{11}Na and upward (for L series) and from ^{39}Y and upward (for M series) are imposed. Determination of the percentage concentration of light elements by EDS is also troublesome because of the intense absorption of X-ray emission inside the sample, and thereby, the ZAF correction factor is much larger than one.

2.3. Features of an EDS detector

A standard EDS detector exhibits the highest detection efficiency for K_α lines with an approximate energy range from 3 keV to 20 keV. The emission quanta of lower energies are absorbed by the detector window, whereas the high-energy emissions pass without registration, which is reflected in the so-called 'escape peaks' (ESP) (see Fig. 1, p. 2). The measurement error of ESP does not usually exceed 10%.

The main element of an EDS detector is a single crystal silicon wafer, doped with lithium ions (Fig. 4) [6]. The detector is placed between two electrodes, to which is applied a voltage of opposite signs. Under the influence of the electric field of the *p-n* transition, lithium ions in the detector Si(Li) diffuse into the crystal surface (thus called a silicon drift detector) [6]. When penetrating into the detector, the X-ray photons produce electron--hole pairs by ionization a silicon wafer. To create a pair of carriers in a silicon crystal, an average photon energy level of only 3.5eV is required; hence, the semiconductor detector is highly sensitive and accurate in the registration of X-ray energy impulses. The total charge produced by a single photon is integrated over the electrodes and passed on through the electronics of the spectrometer to the computer.

The Si(Li) detector's resolving power is limited by the background residual currents induced by the Compton scattering to around 135–150 eV. Thermally induced transitions of electrons into the conduction band of the Si(Li) crystal can cover the maxima of quanta absorption, caused by the photo-electric effect. To reduce this effect, the crystal detector is placed in a tank of liquid nitrogen and continuously cooled to a temperature of –196°C.

The EDS detector is located close to the specimen surface and therefore captures the X-ray photons of different energies at the same time, which results in a high

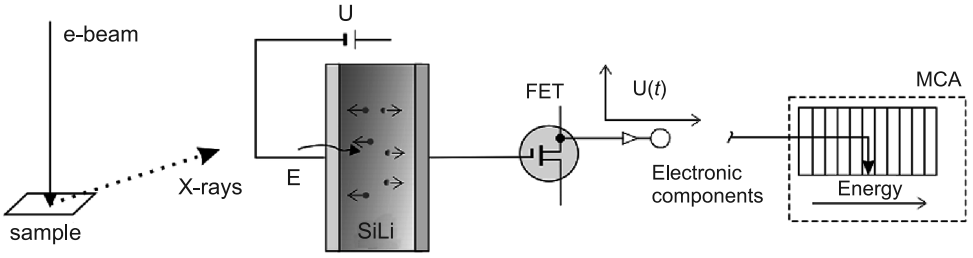

Fig. 4. Principle of the energy dispersive spectrometer with Si(Li) crystal [6]

counting rate. The counting of X-ray quanta could be described as the Poisson's process, wherein, the peak intensity measurement accuracy depends only on the total time of the measurement [4]. The typical time sufficient to collect an EDS spectrum ranges from 10 s to 100 s [7]. In practice, time restrictions are important because of the increasing contamination of the specimen. During electron bombardment, carbon, which is a product of the polymerization of hydrocarbons transmitted from the oil-rotary pump to the vacuum column, is deposited in the area under analysis.

3. Experimental examples

The study was performed with scanning electron microscopy (SEM) using the HITACHI S-3400N variable-pressure electron microscope with a tungsten filament, equipped with the *ThermoScientific*® EDS detector and the *Noran System 7* (NSS) analytical software.

Before placing the sample into the microscope, it must be thoroughly cleared of dirt adhered to the surface, and if the material is non-conductive – the entire surface must be coated with a transparent thin layer of gold or carbon. It is not recommended to investigate rusted, etched, porous or rough specimens using SEM, due to the possible distortion of the EDS analytic results. Reliable results can be obtained by preparing a flat and smooth specimen surface that is perpendicular to primary-electron beam by means of, for example, metallographic methods [3]. The test specimen can be observed in a wide range of magnifications, from about 10× to 100.000×, using the detection of scattered electrons (SE or BSE). The working distance (WD) has to be set to about 10 mm. The transition to the EDS spectrum detection mode occurs when an electron beam is either stationary or scanning. S*econdary electrons* (SE) detectors are used for topographic imaging of the surface and *backscattered electrons* (BSE) detectors, for *Z*-contrast imaging.

An important condition for realization of the measurement of the spectrum is the beam current stability [18], which should be guaranteed for about four hours of tungsten filament heating. Prior to analysis, the system requires the establishment of a database (project name), cooling of the EDS detector and determination of microscope settings, i.e. the accelerating voltage, the beam current, the image magnification and the WD. After correct positioning the electron beam and the activation of the measuring equipment, the energy dispersion spectrum of the all elements present in the test microprobe is accumulated in the system memory and is displayed on the computer monitor.

The NSS system automatically identifies peaks, scanning through all elements of the periodic table, with the exception of the peaks selected 'off' manually or automatically (without the first four [19]: hydrogen, helium, lithium and beryllium). The EDS spectrum consists of a relatively small number of lines – this makes a qualitative spectral analysis sufficiently fast and accurate. The chemical composition of the investigated samples is determined using standardless analytical algorithms, where the element concentrations are normalized to 100%. The components of ZAF provide intensity correction due to the impact of X-ray emission on the sample materials excitation (Z), the probability of absorption (A), and secondary fluorescence (F) at a constant angular set of the detector relative to the specimen.

3.1. Standardless semi-quantitative analysis

The point analysis of the elemental composition was performed with the electron beam at a fixed position. An example of standard EDS analysis was shown for a steel mesh taken from a mechanical water filter used in domestic installations (Fig. 5). Such a filter retains solid particles, such as sand and rust. Unlike other filters tested, on which white-yellow precipitates appear, in this instance, no pollution could be observed with the naked eye. At relatively low magnifications, the images in the detection of secondary electrons (SE) exhibit an excellent depth of field. One can show the weave mesh and measure the thickness of the wire (which has an estimated thickness of about 250 μm) using an automatic zoom scale, shown in the menu bar of the image.

The mesh was oriented in such a way as to focus the electron beam in the center of a cross-section of the cut wire (Fig. 5). Electron beam accelerating voltage was 15 kV and the counting time of the spectrum was 30 s.

Figure 6 shows the dispersion of the energy spectrum of X-rays from the selected point (micro-area) of the sample. Distinct characteristic peaks of K_α and L series for iron ^{26}Fe, chromium ^{24}Cr and nickel ^{28}Ni are clear for specialists that the material investigated is a stainless steel [8]. Precision of measurement is increased by the procedures for the automatic search of peaks (Fig. 1, p. 3). For example, Figure 6 includes both the emission intensity and the theoretical position of the chromium spectral lines which are saved in the analytical data base of the EDS spectrometer. However, the accuracy of quantitative analysis depends on systematic errors of the spectral modeling (Fig. 1) entering the final results. Before calculations of the ZAF, correction of equation (1) is needed, both the position and width of each peak undergo rigorous mathematical analysis, such as deconvolution of the Gaussian curve (Fig. 1, pp. 5 and 6). Results of the concentration measurement of the elements are presented in tabular form (Tab. 1). The list of the analyzed elements is created automatically on the basis of all the peaks labeled as ‘identified’ by the NSS, or labeled manually (e.g. selecting the option ‘peak-off’ of carbon).

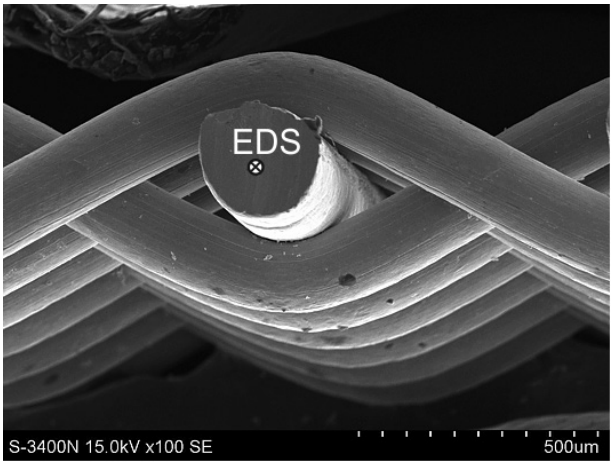

Fig. 5. Wire cross-section with selected point of spectral analysis, 100×

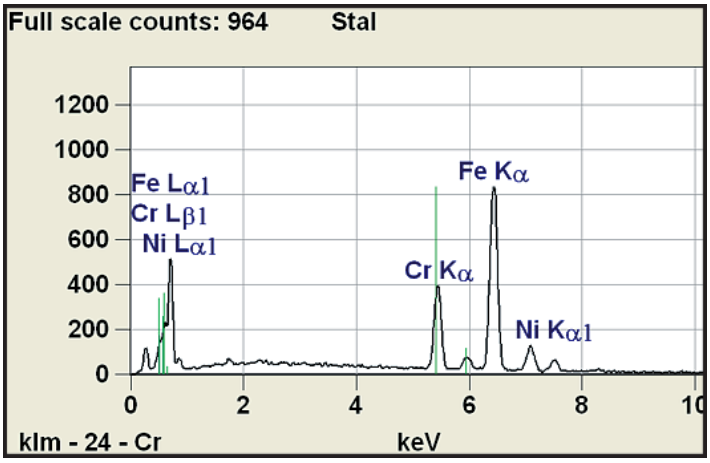

Fig. 6. Energy dispersive spectrum of stainless steel (experimental)

Table 1

Results of EDS analysis of stainless steel investigated

Element	K-Ratio	Z	A	F	ZAF	Wt. %	Wt. % Error	Atom %
Fe K	0.71	1.002	1.019	0.992	1.012	72.54	+/– 1.11	71.86
Cr K	0.21	0.999	1.006	0.879	0.884	18.59	+/– 0.44	19.78
Ni K	0.08	0.990	1.065	1.000	1.054	8.87	+/– 0.96	8.36
Total						100.00		100.00

A standardless EDS analysis of the chemical elements in the filter mesh showed that it is made of stainless steel type AISI 304, formerly called 18/8 (containing 18 wt.% Cr and 8 wt.% Ni). This steel is widely used, it is an austenitic stainless steel, resistant to electrochemical corrosion, it is strong, ductile and weldable and has a reduced content of carbon up to 0.03% C [8].

3.2. Chemical calculations based on stoichiometry

The EDS qualitative analysis can be performed with an electron scanning beam. The smaller the surface area of a scanning beam, the larger the specimen image magnification. Figure 7 shows the cross-section of the layer of *Zinalium*® with a thickness of about 70 μm [9], applied for external protection against the corrosion of buried ductile iron pipes. It has been observed from systematic microscopic studies of pipe sections that a zinc base coating is separated from the ductile iron substrate by a layer of iron oxide with a thickness of approximately 60–80 μm [10, 11]. The aim of the EDS analysis was to investigate the origin of the scale. Approximately 500–700 times magnification is the minimum required to distinguish the different structural layers in the specimen.

To be able to center the beam carefully within the analyzed micro-region, very careful preparation of the metallographic micro-section is required for the quantitative analysis of structurally heterogeneous materials. Errors in the measurement of the intensity of the spectrum, caused by any unevenness of the specimen surface, would be difficult to estimate. For example, the surface convexity of 0.1 μm can reduce the value of the measured intensity by 5–7% (due to local absorption increase, thus the ZAF correction) [6]. Therefore, any analysis of a single point EDS measurement may not be representative of the entire specimen.

EDS spectra were collected from different locations on a homogeneous specimen, where each single scan area was 10 × 10 μm^2. Analyzed areas are marked much darker in the SE image (Fig. 7), because the increase of the spectrum recording time under a focused beam leads to carbon layer deposition. When considering the spatial resolution of X-ray

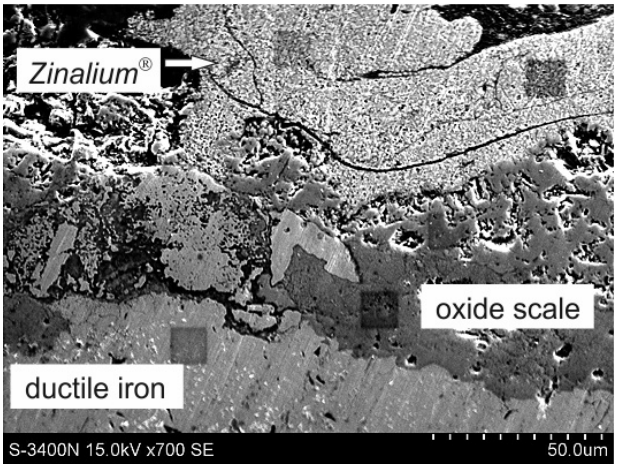

Fig. 7. Cross-section of the coating and carbon-contaminated areas of microanalysis, 700×

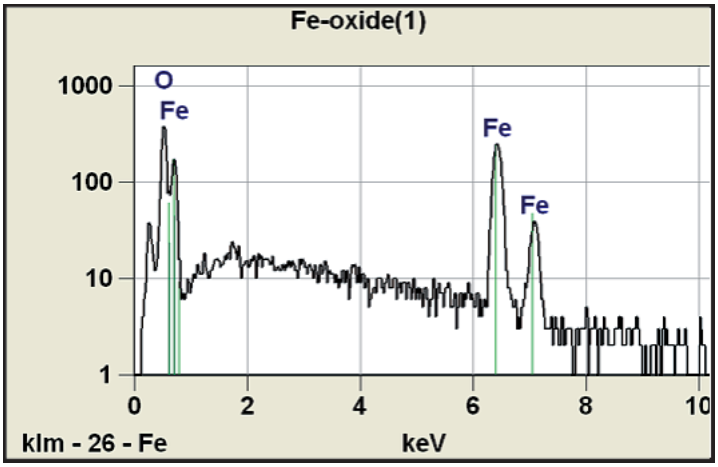

Fig. 8. Energy dispersive spectrum of the sub-coating oxide scale (logarithmic)

emissions, the inelastic electron scattering zone should be considered (Fig. 2) to ensure, that the analyzed micro-area does not extend to the border of two different microstructure components. The spectrum in Figure 8 (in logarithmic intensity scale) comes from a homogeneous area of the sub-coating oxides. The peak from carbon at 0.28 keV was excluded from the analysis because it was not representative for the specimen. Table 2 shows that the iron is combined with oxygen in the ratio of 7:3. Using simple chemical formulas (the atomic weights of elements in one molecule of iron oxide) [12], the Fe_2O_3 compound was identified. The actual standards [13] do not require the removal of the oxide layer, which is a product of the heat treatment of the ductile iron castings, on the surface of the pipes. Results from microscopy investigations of the *Zinalium*® coating raise question about the effectiveness of metal spraying as a means of the corrosion protection of pipes because the coarse-crystalline oxide substrate shows evidence of poor adhesion to the pipe surface [14].

Table 2

Results of EDS analysis of the undercoating oxide scale

Element	K-Ratio	Z	A	F	ZAF	Weight %	Atom %
O K	0.25	0.849	1.680	0.998	1.422	30.80	60.84
Fe K	0.75	1.092	0.996	1.000	1.088	69.20	39.16

3.3. Studies of sample homogeneity using x-ray maps[1)]

In addition to the heterogeneity of the distribution of the microstructure components, other components can be hidden under the surface of the specimen, thus affecting the EDS result. Therefore, the quantitative analysis of the elemental composition should be preceded by studies of the homogeneity of the specimen volume analyzed. Just as scanning electron images, one could obtain pictures of the relative distribution of the concentration of chemical elements on the samples surface using the EDS technique (Fig. 9). To this end, the energy analyzer is set on a selected line of the X-ray spectra, while the scanning primary-electrons beam is synchronized with the computer speed, so this enables the imaging of the element localization on the monitor [4].

The transmitted signals form maps of the element distribution, with higher image brightness corresponding to areas of high element concentration. The mass-sensitivity of EDS analysis substantially depends on the ratio of peak signal to emission background. Obtaining maps of the element distribution is possible only for concentrations of over 1% [7] because peaks from trace elements are extremely difficult to separate from the background (Fig. 9, O-K map). For concentrations below few tenths of a percent, peak intensity is higher than the background intensity only about 30–50% [6]. Errors in the cut-off of a background level may result from the different background intensity on the left and on the right side of the peak (see Fig. 8). Therefore, for measurements of the background level, the dependency of the intensity of the continuous spectrum from

[1] Elemental mapping was performed during Hitachi Workshop in the Warsaw University of Technology, October 2011.

the atomic number is usually applied [6]. Figure 9 contains an SE image of a multilayer sample (named ‘Grey’), as well as the corresponding maps of the distribution of chemical elements on the scanned surface. The metal specimen surface oxidizes easily in air (before the specimen is placed in a vacuum), hence the ‘noise’ signals from a thin oxide layer (see O-K map). The Si-K map shows that the silicon is uniformly distributed in the ductile iron (in iron-rich area, see Fe-K map). Moreover, the epoxy layer contains large amount of Ca (see Ca-K map) and uneven Si distribution. The aluminum layer has a variable thickness of about 10 µm to 75 µm (see Al-K map).

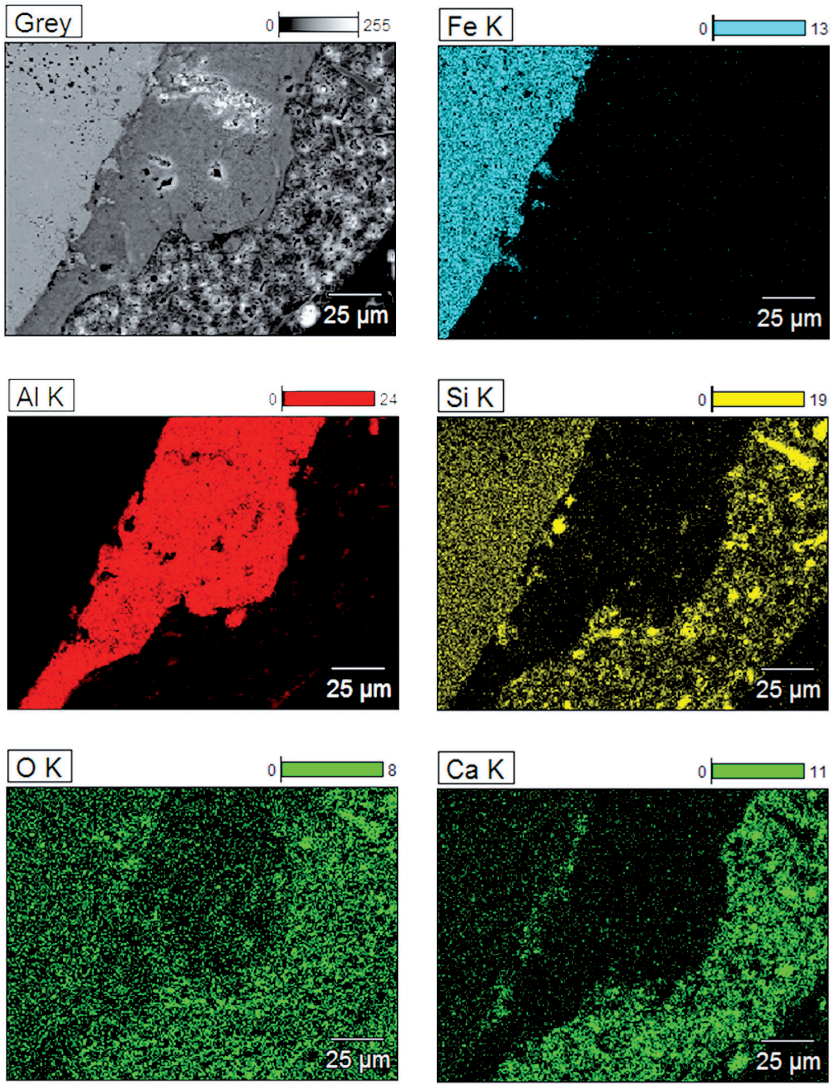

Fig. 9. Map of element distribution in cross-section of the multilayer

Because of the low spatial resolution of X-rays (emission zone of about 2–5 μm), the mapping procedures do not provide enough quantitative information, such as that obtained via point EDS analysis. However, each map can be represented in a different color, which is useful when extracting the location of an element in multi-constituent specimens (like cement mortars). Mapping[1)] is also used for imaging the chemical gradients on the cross-section of the specimen, such as element depth depletion far from the surface boundary.

3.4. Imaging of the atomic number distribution

Establishing of the „quasi-chemical" contrasts on the scanning images in SEM, the so-called *Z*-contrast, is possible by detecting the backscattered electrons from the specimen (BSE). These are electrons of the primary beam, which scatter elastically almost perpendicularly to the sample surface (no loss of kinetic energy) due to the braking force caused by the Coulomb field of the atomic nuclei. Figure 10 demonstrates the usefulness of Z-contrast for the qualitative comparison of the chemical composition of similar samples of materials.

Fig. 10. Sediments of different composition imaged in Z-contrast, 25×

In the BSE image, sediments taken from different measuring points (labeled as no. G1 and no. g31) have been compared. Measuring point no. G1 is located in the central part of the Reservoir Goczałkowice. The sediment is dominated by clay fraction of the soil (Fig. 11), while the concentration of iron amounts 34 mg Fe per gram of dry weight [15]. Measuring point no. g31 is located on the south-eastern side of the reservoir, in the pumping area of Frelichów, where iron is a pollutant in the natural water environment [16]. The sediment is dominated by sand fraction of the soil [15]. The iron content in that measuring point was 140 mg Fe per gram of dry weight.

The observed *Z*-contrast is due to the fact, that the material containing the heavier elements will scatter more BSE electrons and thus looks brighter. Therefore, the interpretation

of the BSE image is as follows: in Z-contrast, sediment no. g31 is revealed as a bright component due to the higher concentration of ^{26}Fe, because iron is an element heavier than silicon ^{14}Si, which in turn is the main component of the sediment no. G1.

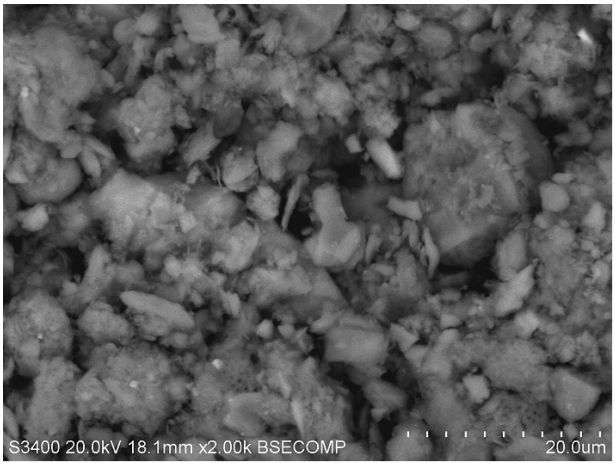

Fig. 11. Magnified image indicating the fineness of the investigated sediment, 2000×

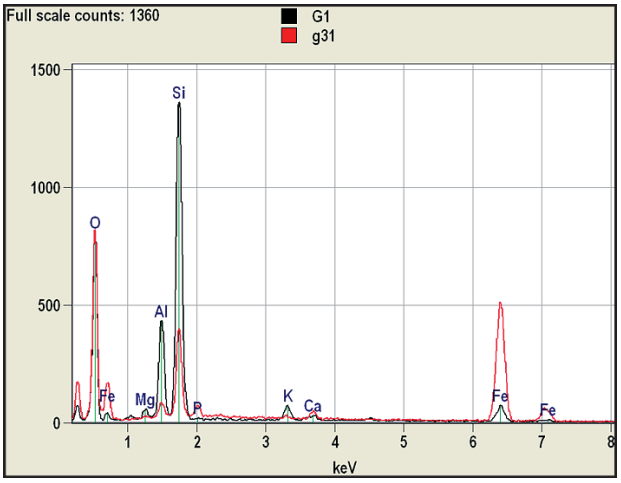

Fig. 12. Comparison of the energy dispersion spectra of two sediments

Table 3

Results of EDS analysis of the sediment samples

Specimen Nr	Chemical composition, Wt %							
	Na	Mg	Al	Si	P	K	Ca	Fe
G1	1.46	1.59	15.27	61.77	0.90	4.67	1.44	12.90
g31	0.23	0.39	2.84	15.49	2.60	0.36	1.37	77.21

The summary of the EDS spectra collected from each area separately confirms these observations (Fig. 12). The analysis was carried out over areas of around 50 × 50 μm^2 at an accelerating voltage of the beam 20 kV. Monte Carlo simulations have shown that for a primary beam energy of 20 kV, the scattering depth of the BSE electrons into a specimen reaches about 1 μm [7]. It is known that a quantitative analysis of sediments by EDS technique may not be very accurate due to the complex composition of these kinds of samples and their high fineness [1, 18]. Only chemical elements with an atomic number $Z \geq 11$ can be included into the calculations of element concentrations (Tab. 3).

For sediment no. G1, intense characteristic peaks pertaining to aluminum silicates and small quantities of iron have been recorded. Sediment no. g31 contains mainly iron-silicon, but most of the elements detected were present in trace quantities (0.2–1.0% by weight). EDS quantitative analysis may be considered only as an estimate, since the errors in the correction ZAF for any 'powder' specimen, even with exclusion of light elements analysis (e.g. oxygen ^{8}O), are quite large [1, 7].

4. Conclusions

More than half of the research tasks are limited to the qualitative analysis of the elemental composition of solids with the objective of answering the question of what elements are in the sample, instead of performing a quantitative analysis. The demand for quantitative EDS is high. However, most research problems require knowledge of the structure of the material and careful preparation of the EDS analysis. In general, the accuracy of calculated concentrations of individual elements is affected by the accuracy of the relative intensity of all the elements in the specimen (by adjusting ZAF). Basically, one operates a hypothetical composition of the sample, i.e. without light elements or dependence on stoichiometry, and equates results of the spectrum measurements to 100% of the total composition.

The EDS quantitative research method cannot be considered as routine like other spectroscopy-chemical methods [17]. The analysis reliability depends on the operator's skills, the diligent execution of the experiment and the correct problem formulation. It is pertinent to note that energy dispersive spectroscopy (EDS) is effective only for a specific class of materials containing heavy elements, and in a concentration above the limit of detection [17–19]. Due to the methodological difficulties of the various stages of the quantification analysis of the chemical composition, to carry out specific measurements on a scanning electron microscope with the EDS technique, it is the equivalent of complex research work.

This work was realized in the frame of the research activity of the Institute of Water Supply and Environmental Protection, Department of Environmental Engineering, Cracow University of Technology (No. Ś-3/440/2013/DS).

References

[1] Goldstein J.I., Newbury D.E., et al., *Scanning electron microscopy and x-ray microanalysis*, Kluwer Academic/Plenum Publishers, New York 2003.

[2] Zhigang R. Li (ed.), *Industrial applications of electron microscopy*, Marcel Dekker, Inc., New York & Basel 2003.

[3] Wassilkowska A, Dąbrowski W., *Zastosowanie mikroskopii elektronowej do badania rur żeliwnych – część I – Struktura wykładziny z zaprawy cementowej*, Gaz, Woda i Technika Sanitarna, 4, 2012, 154-159.

[4] Barbacki A.(Ed.), *Mikroskopia elektronowa*, Wydawnictwo Politechniki Poznańskiej, Poznań 2003.

[5] Szummer A.(ed.), *Podstawy ilościowej mikroanalizy rentgenowskiej*, Wydawnictwo Naukowo-Techniczne, Warszawa 1994.

[6] Кальнер В.Д., Зильберман А.Г., *Практика микросондовых методов исследования металлов и сплавов*, Издательство Металлургия, Моссква 1981.

[7] Żelechower M., *Wprowadzenie do mikroanalizy rentgenowskiej*, Wydawnictwo Politechniki Śląskiej, Gliwice 2007.

[8] PN-EN 10088-1. Stale odporne na korozję, część 1: Gatunki stali odpornych na korozję, 2007.

[9] ZINALIUM PAM Technologies, Materiały: *ZINALIUM Saint-Gobain*, Edycja 2010-12.

[10] Wassilkowska A., Dąbrowski W., *Zastosowanie mikroskopii elektronowej do badania rur żeliwnych – część II – Zabezpieczenia zewnętrzne oparte na cynkowaniu*, Gaz, Woda i Technika Sanitarna, 5, 2012, 206-211.

[11] Wassilkowska A., Dąbrowski W., *Mikroskop elektronowy – narzędzie do oceny jakości rur żeliwnych i powłok ochronnych*, Instal 7/8, 2012, 63-66.

[12] Matusewicz E., Matusewicz J., *Chemia*, Wydawnictwa Szkolne i Pedagogiczne, Warszawa 1989.

[13] PN-EN 545. Rury, kształtki i wyposażenie z żeliwa sferoidalnego oraz ich złącza do rurociągów wodnych – Wymagania i metody badań, 2010.

[14] Wassilkowska A., Dąbrowski W., *Wątpliwości co do ochrony rur żeliwnych przez cynkowanie*, Instal, 10, 2013, 66-71.

[15] Iwanicka K., Czaplicka-Kotas A., Ślusarczyk Z., Szostak A., *Miedź w środowisku wodnym zbiornika Goczałkowice*, Gaz, Woda i Technika Sanitarna, 2, 2014, 75-78.

[16] Czaplicka-Kotas A., Ślusarczyk Z., Zagajska J., Szostak A., *Analiza zmian zawartości jonów wybranych metali ciężkich w wodzie Jeziora Goczałkowickiego w latach 1994–2007*, Ochrona Środowiska 4, 32, 2010, 51-56.

[17] BS ISO 22309. Microbeam analysis – Quantitative analysis using energy-dispersive spectrometry (EDS) for elements with an atomic number of 11 (Na) or above, 2011.

[18] Holton I., *Is Energy-Dispersive Spectroscopy in the SEM a substitute for Electron Probe Microanalysis?*, Microscopy and Analysis, 141, 2012, S4-S7.

[19] Burgess S., Xiaobing Li, Holland J., *High spatial resolution energy dispersive X-ray spectrometry in the SEM and the detection of light elements including lithium*, Microscopy and Analysis, 6, 2013, S8-S13.

TECHNICAL TRANSACTIONS | **CZASOPISMO TECHNICZNE**
CHEMISTRY | CHEMIA
1-Ch/2014

DOROTA ZIĘTEK*

DIFFUSED PHASE TRANSITION IN POLYCRYSTALLINE $(Ba_{0.70}Pb_{0.30})(Ti_{0.70}Sn_{0.30})O_3$

ROZMYTA PRZEMIANA FAZOWA W POLIKRYSTALICZNYM $(Ba_{0.70}Pb_{0.30})(Ti_{0.70}Sn_{0.30})O_3$

A b s t r a c t

In this paper, the method of manufacturing solid solution $(Ba_{0.70}Pb_{0.30})(Ti_{0.70}Sn_{0.30})O_3$ (BP30TS30) is presented. Dielectric spectroscopy and scanning electron microscopy methods were applied to investigate the influence of doping by Pb and Sn on the physical properties of $BaTiO_3$ (BT). It is shown that Pb and Sn substitutions change the temperature of phase transitions, their character and the maximum value of electric permittivity.

Keywords: *Ferroelectric ceramics*, *perovskite structure*, *barium titanate*, *diffused phase transition*

S t r e s z c z e n i e

W artykule przedstawiono metodę otrzymywania stałego roztworu $(Ba_{0.70}Pb_{0.30})(Ti_{0.70}Sn_{0.30})O_3$ (BP30TS30). Badania przeprowadzone za pomocą spektroskopii dielektrycznej i skaningowej mikroskopii elektronowej miały na celu sprawdzenie wpływu domieszkowania jonami ołowiu i cyny na własności $BaTiO_3$ (BT). Wykazano, iż domieszki Pb i Sn zmieniają zarówno temperaturę przemian fazowych, ich charakter, jak i maksymalną wartość przenikalności elektrycznej.

Słowa kluczowe: *ceramika ferroelektryczna*, *struktura perowskitu*, *tytanian baru*, *rozmyta przemiana fazowa*

* M.Sc. Eng. Dorota Ziętek, Institute of Physics, Pedagogical University, Cracow.

1. Introduction

Perovskite type ferroelectric materials have many technical applications. They are very popular due to the variety of their physical properties. The main advantages of these kinds of materials are high values of electric permittivity, polarization, electromechanical coefficients and short switching times. The simplest structure and composition among perovskite type (ABO_3) ferroelectrics has barium titanate $BaTiO_3$ (BT). Moreover, it is the most studied ferroelectric material in recent times [1]. Figure 1 shows the cubic structure of BT, however, depending on the temperature, this material can exist in four different crystalline phases.

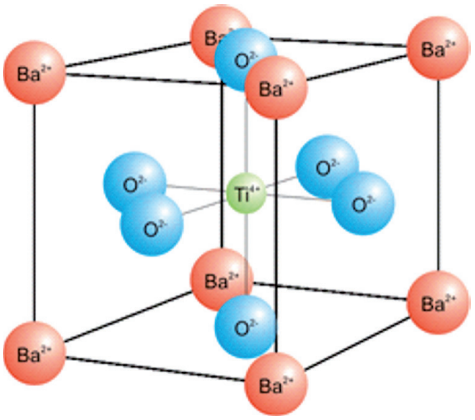

Fig. 1. Cubic structure of $BaTiO_3$

There are three phase transitions which can be observed during the cooling of $BaTiO_3$ [2]:

– T_c = 403 K transition from cubic phase (Pm3m) to tetragonal phase (P4mm),
– T_1 = 288 K transition from tetragonal phase to orthorhombic phase II (Amm2),
– T_2=183K transition from orthorombic phase to rhombohedral phase (R3m).

The cubic phase is paraelectric, but other phases are ferroelectric. Many kinds of solid solutions with various technical applications can be obtained by doping BT with different ions. The physical properties of these solutions depend on the substitution type and its concentration. One of the most important applications of perovskite type ferroelectric materials is FRAM (ferroelectric random access memory) made from thin films of PZT. This kind of memory has many advantages such as: low power usage; fast write performance; a huge number of write-erase cycles. PZT ceramics [3] might also be used in the production of micro-switches, different kinds of sensors, components of piezoelectronics, electromechanical transducers, ultrasound generators, high voltage transformers and echo--sounders [4]. Other electronic components are multilayer capacitors based on BT.

BT can be doped by Pb and Sn ions. Earlier studies of $PbBaTiO_3$ solid solution showed that an increase of Pb concentration leads to an increase in the paraelectric – ferroelectric (PE-FE) phase transition temperature [5]. In the case of $Ba(Ti_{1-y}Sny)O_3$, an increasing Sn

concentration causes a decrease of the phase-transition temperature value [6-11]. It is expected, while investigating BP30TS30, that both of the substitutions have an influence on its physical properties. An influence of substitutions in sublattices A and B was observed in compounds based on BT such as $(Ba_{0.90}Sr_{0.10})(Ti_{1-y}Sn_y)O_3$, $(Ba_{1-x}Sr_x)(Ti_{1-x}Zr_x)O_3$ [12], $Ba(Ti_{1-2x}Fe_xNb_x)O_3$, $Ba(Ti_{1-x}Hf_x)O_3$ [13]. This influence also appears in solutions obtained by a mechanochemical method [14, 15].

2. Experimental Method

Polycrystalline samples of BT and BP30TS30 were prepared by using synthesis from the following powders: BaC_2O_4, PbC_2O_4, TiO_2 and SnO_2. The purity of these reagents was 99.99%. Appropriate amounts of the components were grained in a ball mill for 2 hours. The mixture was then dried and a sample was formed using a tablet maker, under an uniaxial pressure of 0.3 GPa. Tablet synthesis was made in Nabertherm L 5/13/B180 muffle stove at 1273 K for 1 hour. The samples were then re-milled, formed and sintered at 1573 K for 1 hour. The obtained disc-like pellets, with a diameter of 8 mm and thickness ranging from 1.5 mm to 2 mm, were then covered with silver electrodes.

Microstructural investigations of BT and BP30TS30 samples were made using the Jeol JSM-6610F scanning electron microscope. The composition of the samples was checked using the EDS (Energy-Dispersive X-Ray Spectroscopy) analyzing method. Dielectric measurements were carried out using an Alpha-AN High Performance Frequency Analyzer system together with a cryogenic temperature control system – Quatro Cryosystem and WinDETA Novocontrol software. Dielectric properties of the samples were measured in a wide frequency range from 0.1 Hz to 10 MHz. Nitrogen gas was used as a heating and cooling agent.

3. Results and Discussion

Figures 2–4 show f SEM photomicrographs of BT and BP30TS30 samples.

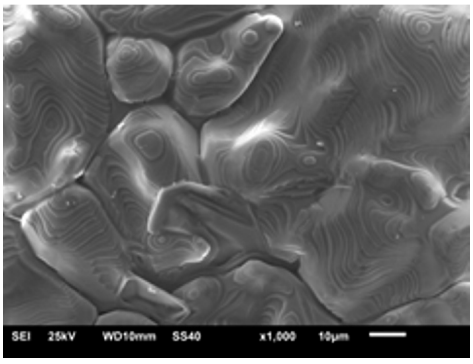

Fig. 2. SEM image for BT

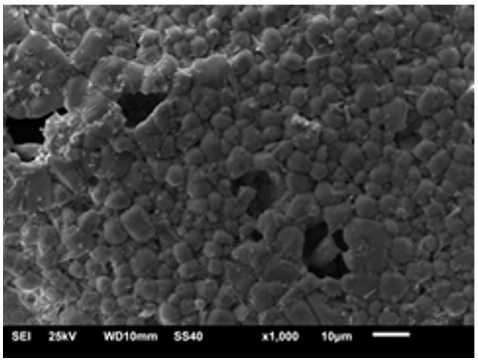

Fig. 3. SEM image for BP30TS30

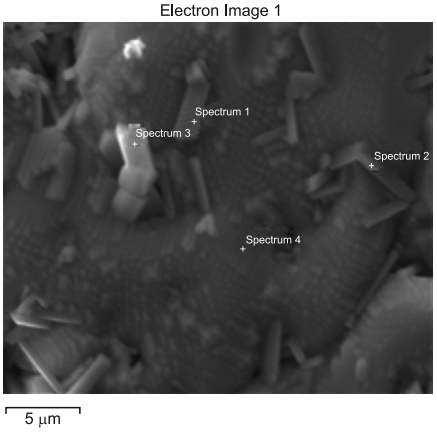

Fig. 4. SEM image for BP30TS30

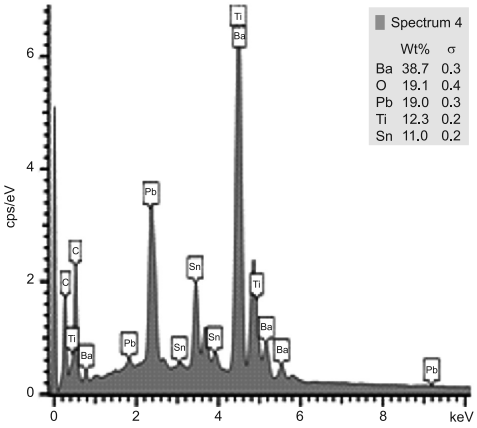

Fig. 5. EDS spectrum for BP30TS30

One can observe that grains in BP30TS30 are much smaller than grains in pure BT (Fig. 2, 3). A structure of BP30TS30 with well-defined grain borders can be clearly seen in the SEM photomicrograph (Fig. 4).

The EDS analysis results, shown in Figure 5, confirm that BP30TS30 sample contains only: Ti, Ba, Pb and Sn atoms. Carbon sputtered on the sample surface during its preparation can also be seen in EDS spectrum because of the specimen preparation mode.

Fig. 6 and 7 show the temperature dependence of the real part of electric permittivity for BT and BP30TS30 respectively.

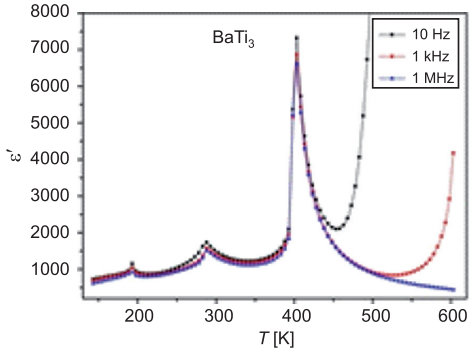

Fig. 6. Temperature dependence of the real part of electric permittivity for BT

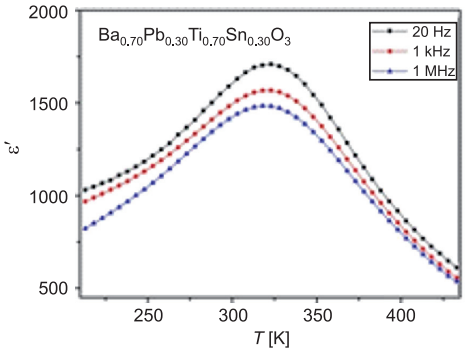

Fig. 7. Temperature dependence of the real part of electric permittivity for BP30TS30

In Fig. 6 there are three strong ε'(*T*) peaks corresponding to the BT structural transitions which were described earlier. At 403 K, one can see a sharp phase transition from the paraelectric phase to the ferroelectric phase. The further lowering of the temperature shows two different phase transitions at 288 K and 188 K. In the case of BP30TS30, one can notice only one broad peak at about 320 K. In BP30TS30, containing the same percentage

value of both Sn and Pb atoms, there is a shift of the PE-FE transition temperature to lower temperatures than in BT. This means that an influence of Sn ions on the phase transition character is stronger than Pb ions. The observed temperature T_m, corresponding to the maximum value of the real part of permittivity ε_m, does not depend on the frequency of the applied electric field. It indicates rather diffused phase transition. The degree of phase transition diffusion can be derived from the following expression:

$$\frac{1}{\varepsilon} \cdot \frac{1}{\varepsilon_m} = A(T - T_m)^{\gamma} \tag{1}$$

where:

- ε – the real part of electric permittivity,
- ε_m – the maximum value of the real part of electric permittivity,
- A – a constant (for $\gamma = 1$ an inverse of the Curie-Weiss constant/coefficient),
- T – a temperature,
- T_m – the temperature of occurring the maximum value of electric permittivity,
- γ – a coefficient with value from 1 to 2, a value close to 1 denotes sharp phase transition, but close to 2 denotes diffused phase transition.

In order to determine a gamma coefficient value, a logarithm of both sides of the equation (1) should be taken:

$$\log\left(\frac{1}{\varepsilon} - \frac{1}{\varepsilon_m}\right) = \log A + \gamma \log(T - T_m) \tag{2}$$

When $\log\left(\frac{1}{\varepsilon} - \frac{1}{\varepsilon_m}\right)$ is plotted as a function of $\log(T - T_m)$, the gamma coefficient is a sloping straight line.

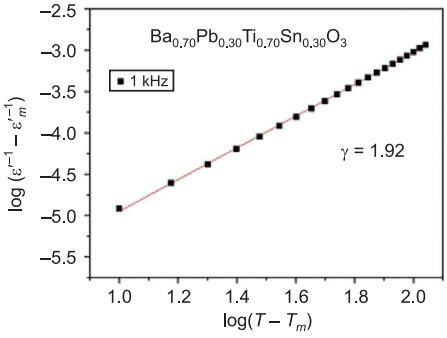

Fig. 8. A dependence of $\log\left(\frac{1}{\varepsilon} - \frac{1}{\varepsilon_m}\right)$ from $\log(T - T_m)$ for BP30TS30

The obtained value of the gamma coefficient is 1.92, so it is close to 2. This means that the phase transition in BP30TS30 is strongly diffused.

4. Conclusions

Experimental results confirmed that non-ferroelectric Sn ions in sublattice B have a very strong destructive influence on the created crystallographic structure. Ferroelectric Pb ions in sublattice A had a very small influence on crystallographic structure. Doping BT by the same amount of Sn substitutions leads to a strongly diffused phase transition across a wide range of temperature. This fact is important for designing devices with stable values of dielectric properties across a wide range of temperature.

The author would like to thank Prof. Czesław Kajtoch and Dr. Wojciech Bąk for their helpful discussions.

References

[1] Kajtoch C., *Dilatometrische und dielektrische Anomalien bei den Phasenumwandlungen in* $Ba(Ti_{1-x}Sn_x)O_3$, Ann. Physik, vol. 2, 1993, 335-338.

[2] Surowiak Z., *Elektroceramika ferroelektryczna*, Wydawnictwo Uniwersytetu Śląskiego, Katowice 2004.

[3] Zarycka A., Zachariasz R., Czerwiec M., Ilczuk J., *Struktura i właściwości elektryczne ceramiki PZT otrzymywanej metodą zolowo-żelową*, Ceramika/Ceramics, 2005. Papers of the Commission on Ceramic Science, Polish Ceramic Bulletin Polish Academy of Science, Kraków Division, Polish Ceramic Society.

[4] Nogas-Ćwikiel E., *Otrzymywanie proszków ceramicznych do kompozytów ceramiczno-polimerowych dla detektorów piroelektrycznych*, Uniwersytet Śląski, Katowice 2012.

[5] Mitsui T., Marutake M., Sawaguchi E., *Landolt-Bornstein Numerical Data and Functional Relationships in Science and Technology*, Group III, Vol. 9, Springer–Verlag Berlin–Heidelberg––New York, 197.

[6] Bąk W., Kajtoch C., Starzyk F., *Dielectric properties of* $BaTi_{1-x}Sn_xO_3$ *solid solution*, Materials Science and Engineering B100, Vol. 9, 2003, 9-12.

[7] Kajtoch C., *Dielectric properties of* $Ba(Ti_{1-x}Sn_x)O_3$ *ceramics in the paraelectric phase*, Ceramics International, Vol. 37, 2011, 387-391.

[8] Kajtoch C., Bak W., Garbarz-Glos B., *Study of the phase transition in polycrystalline* $(Ba_{0.90}Pb_{0.10})(Ti_{0.90}Sn_{0.10})O_3$, Condensed Master Physics, 2014.

[9] Kajtoch C., *Time dependences of dielectric constant in* $BaTi_{0.95}Sn_{0.05}O_3$, Ferroelectrics, Vol. 133, 1992, 193-198.

[10] Kajtoch C., *Dipolar polarization in* $Ba(Ti_{1-x}Sn_x)O_3$, Ferroelectrics, Vol. 172, 1995, 465-468.

[11] Kajtoch C., *Glass-like transformation in* $Ba(Ti_{0.70}Sn_{0.30})O_3$, Ferroelectrics, Vol. 192, 1997, 335-337.

[12] Kajtoch C., Bąk W., Garbarz-Glos B., Stanuch K., Tejchman W., Mroczka K., Czeppe T., *Influence of Sr and Zr substitution on dielectric properties of* $(Ba_{1-x}Sr_x)(Ti_{1-x}Zr_x)O_3$, Ferroelectrics 2014.

[13] Garbarz-Glos B., Bąk W., Molak A., Kalvane A., *Microstructure, calorimetric and dielectric investigation of hafnium doped barium titanate ceramics*, Phase Transitions, 86, 2013, 917-925.

[14] Dulian P., Bąk W., Wieczorek-Ciurowa K., Kajtoch C., *Controlled mechanochemical synthesis and properties of a selected perovskite-type electroceramic*, Materials Science Poland, Vol. 31(3), 2013, 462-470.

[15] Dulian P., Wieczorek-Ciurowa K., Bąk W., Kajtoch C., *Możliwości wytwarzania zaawansowanej elektroceramiki na bazie tytanianu baru metodą mechanochemiczną*, Czasopismo Techniczne (Technical Transactions), Wyd. Politechniki Krakowskiej, Vol. 9-M/2012, Z. 26, 57-65.

CONTENTS

TREŚĆ